ENHANCEMENT OF THERMAL CONDUCTIVITY
USING MAGNETITE (FE$_3$O$_4$) AND SILVER (AG) NANOPARTICLES

by

Merve Yüksel

Submitted to the Institute of Graduate Studies in Science&Engineering

in partial fulfillment of

the requirements for the degree of

Master of Science

Faculty of Engineering and Architecture

Yeditepe University

2010

ENHANCEMENT OF THERMAL CONDUCTIVITY
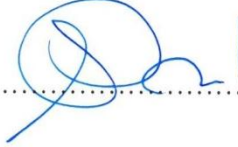## USING MAGNETITE (FE$_3$O$_4$) AND SILVER (AG) NANOPARTICLES

APPROVED BY:

Assist. Prof. Seyda Bucak   ....

(Supervisor)

Prof. İ. Fahir Borak   ....

Assoc. Prof. Mustafa Çulha   ....

DATE OF APPROVAL: 03 / 09 / 2010

ACKNOWLEDGMENTS

ABSTRACT

ENHANCEMENT OF THERMAL CONDUCTIVITY USING MAGNETITE (FE$_3$O$_4$) AND SILVER (AG) NANOPARTICLES

Traditional heat transfer fluids such as water, oil and ethylene glycol mixtures were proven to be inherently poor heat transfer fluids by previous studies in this research area. However, in many high-technology industries, the most significant issue is to achieve the miniaturization of heat transfer devices on one hand and the increase in heat flux on the other. The usual enhancement techniques for heat transfer can hardly meet these challenges. Because of this, nanofluids are prepared by dispersing nanometer-sized solid particles in these traditional heat transfer fluids to increase the thermal conductivity and therefore the heat transfer performance. In this study, the mechanism of thermal conductivity enhancement of fluids in the presence of silver and magnetite nanoparticles is investigated. Colloidal silver with large surface area and high electrical and thermal conductivity and magnetite nanoparticles with superparamagnetic properties under applied external magnetic fields have attracted attention to study the thermophysical property enhancements. In order to achieve this, these metallic nanoparticles of known size, shape and concentration are synthesized and solubilized in polar and nonpolar solvents to obtain different nanofluids. Synthesized hydrophilic and hydrophobic silver and magnetite nanoparticles are found to have hydrodynamic diameters in considerable nanometer ranges and to be highly stable using Dynamic Light Scattering (DLS) and Transmission Electron Microscopy (TEM). Crystal structures of both nanoparticles are verified by X-Ray Diffraction (XRD) studies. The next step after characterization of nanoparticles is the measurement of thermophysical properties such as density, viscosity and thermal conductivity for all obtained nanofluids. Overlapping with the most previous studies, viscosity and density of base fluids indicate enhancements upon addition of nanoparticles. Thermal conductivity results vary depending on the type of dispersing medium. In nonpolar medium, thermal conductivity is found to increase with increasing the particle fraction; in contrast to that in polar medium, it is found to decrease for the same type of particle.

ÖZET

TERMAL İLETKENLİĞİN GÜMÜŞ VE MAGNETİT NANOPARÇACIKLAR KULLANILARAK ARTTIRILMASI

Geçmiş ısı transferi araştırmalarında, geleneksel olarak kullanılan su, yağ ve etilen glikol gibi sıvıların ısı aktarımını iyi ölçüde sağlayamadıkları kanıtlanmıştır. Fakat, birçok yüksek teknoloji endüstrisinde dikkate alınması gereken en önemli sorun bir taraftan ısı aktarımını sağlayan cihazların boyutlarının küçülmesini sağlamak diğer yandan da ısı akımını arttırmaktır. Alışılagelmiş ısı akışını iyileştirme teknikleri bu sorunları çözme konusunda başarısız olmaktadır. Bu yüzden, termal iletkenliği ve ısı transfer performansını arttırabilmek için, nanometre boyutunda sentezlenen katı parçacıklar geleneksel olarak ısı transferinde kullanılan sıvıların içinde dağıtılıp nano sıvılar hazırlanmaktadır. Bu çalışmada, gümüş ve magnetit nanoparçacıkların varlığında termal iletkenliğin artış mekanizması incelenmiştir. Geniş yüzey alanı ve yüksek elektrik ve termal iletkenliği olan, kolloid yapıdaki gümüş ve manyetik alan etkisi altında superparamanyetik özellik gösteren magnetit nanoparçacıklar termofiziksel özelliklerin araştırılmasında büyük ilgi çekmektedir. Bu amaçla, belirli boyut, şekil ve konsantrasyonda metal nanoparçacıklar sentezlenmiş, polar ve apolar solventlerde çözülmüş ve nanosıvılar elde edilmiştir. DLS ve TEM analizleri sonucunda sentezlenen hidrofilik ve hidrofobik gümüş ve magnetit nanoparçacıkların boyutlarının büyük ölçüde istenilen aralıklarda olduğu görülmüştür. İki nanoparçacığın da kristal yapıda oldukları XRD çalışmalarıyla kanıtlanmıştır. Karakterizasyon çalışmalarından sonraki aşamada, elde edilen nanosıvıların yoğunluk, viskozite ve termal iletkenlik ölçümleri yapılmıştır. Önceki araştırmaların çoğu ile örtüşecek şekilde, saf sıvıların viskozite ve yoğunluk değerleri nanoparçacıkların eklenmesi ile artış göstermiştir. Termal iletkenlik sonuçları nanoparçacıkların dağıtıldıkları sıvı ortamlarına göre farklılık göstermiştir. Apolar sıvı ortamında, termal iletkenliğin parçacık miktarıyla arttığı, buna karşın polar ortamda aynı miktar ve aynı tipteki parçacık için azaldığı gözlemlenmiştir.

TABLE OF CONTENTS

LIST OF FIGURES

LIST OF TABLES

LIST OF SYMBOLS

a	Radius of heat wire (m)
A	Area (m^2)
A	Absorbance
c	Spring constant ($kg.m^2/s^2$)
	Specific heat ($J/(^oC.kg)$)
d	Interplanar Spacing (m)
f	Frequency (Hertz)
Gr	Grashof Number
h	Convective heat transfer coefficient ($W/m^2.^oC$)
H	Magnetic Field
I_0	Intensity of reference beam
I	Intensity of sample beam
k	Thermal Conductivity ($W/(m.^oC)$)
	Boltzmann's constant ($J/^oC$)
l	Length (m)
m	Mass (kg)
M_s	Saturation magnetization (emu/g)
n	Empirical Shape Factor
Nu	Nusselt number
Pr	Prandtl Number
r	Radius (m)
R_H	Hydrodynamic Radius (m)
Ra	Rayleigh Number
Q	Convective Heat Transfer (J)
t	Time (s)
T	Temperature (^oC)
V	Volume (m^3)
x	Distance (m)

	Temperature coefficient of resistivity (1/K)
	Coefficient of volume expansion (1/K)
λ	Thermal Conductivity (W/(m.^{o}C))
ε	Molar absorptivity
θ	Diffraction angle (^{o})
μ	Viscosity (cP)
ρ	Density (kg/m^3)
	Mathematical constant Pi (3.14)
	Volume fraction

LIST OF ABBREVIATIONS

Ag NP	Silver Nanoparticle
DC	Direct Current
DLS	Dynamic Light Scattering
MWCNT	Multiwalled Carbon Nanotube
PAO	Poly-α-Olefin
PCS	Photon Correlation Spectroscopy
rpm	Rotate per minute
SEM	Scanning electron microscopy
QELS	Quasi-elastic light scattering
TEM	Transmission electron microscopy
THW	Transient heat wire
UV-VIS	Ultra violet visible
VSM	Vibrating Sample Magnetometer
XRD	X-Ray Diffraction
bf	Base fluid
eff	Effective
nf	Nanofluid
p	Particle
	Fluid

1. INTRODUCTION

Modern nanotechnology provides great opportunities to produce materials in nanometer scales applicable in several engineering areas. Nanofluids are new class of materials which can interestingly transfer heat in a more efficient way compared to conventional fluids.

It is evident that solid form metals possess very high thermal conductivities. Suspending these metallic or nonmetallic powder form particles in traditional heat transfer fluids such as water, ethylene glycol or engine oil display significantly enhanced thermal conductivities relative to those of traditional heat transfer fluids. However, the use of micron sized particles in these suspensions suffer from many drawbacks as clogging in flow passages, erosion and fouling. Nanoparticles appear therefore to be perfectly suited for applications in which fluid flow takes place, because of their high stability and large surface area which eliminates the sedimentation. Therefore, several studies have been performed thorugh the years to have an insight to enhancement mechanisms using nanoparticles. Now, it is well known that generally heat transfer is enhanced by the addition of nanoparticles.

The primary objective of the present study is to investigate experimentally the mechanism of thermal conductivity enhancement of several fluids in the presence of silver and magnetite nanoparticles. Ag NPs having large surface area and high electrical and thermal conductivity and magnetite nanoparticles with superparamagnetic properties under applied external magnetic fields have attracted the attention to study the thermophysical property enhancements. In order to achieve this, these metallic nanoparticles of known size, shape and concentration are synthesized and solubilized in polar and nonpolar solvents to obtain these nanofluids. The results from this research are expected to provide a better understanding of the mechanism of thermal conductivity enhancement, and thus provide guidance in designing nanofluids with high performances as new kind of heat transfer fluids.

General information about heat transfer, nanofluids and their synthesis routes, and finally thermophysical properties such as viscosity, density and thermal conductivity are given in the theoretical background section to provide a basic illustration of whole concept. In the next chapter (Chapter 3), materials used in the synthesis routes and characterization methods are expressed. Magnetite and silver synthesis procedures and the characterization of obtained nanoparticles are discussed in more detail in Chapters 4 through 7. Finally thermophysical properties of silver and magnetite nanofluids are tabulated and general discussions are given.

2. THEORETICAL BACKGROUND

2.1. HEAT TRANSFER

Heat transfer is the science that predicts the energy transfer taking place between material bodies because of a temperature difference driving force. Heat is transported by the transfer of energy of motion between adjacent solid, liquid or gas molecules from the high temperature region to the low temperature region. [1]

There exist three types of heat transfer; conduction, convection and radiation. The conduction is the transfer of heat energy by direct contact of particles of matter. In the physical mechanism of conduction in liquids, higher-energy molecules collide with lower-energy molecules and transfer heat. Conduction mechanism in fluids or solids follows the basic equation written as Fourier's law:

$$\text{—} \qquad \text{—} \tag{2.1}$$

where q_x is the heat transfer rate in the x direction in Watts (W), A is the cross-sectional area normal to the direction of flow of heat in m^2, T is the temperature in K and x is the distance in m. The positive specific constant k is called the thermal conductivity of the material having the units of Watts per meter per Celsius degree (W/m.^{o}C). [2]

On the other hand, convection is the transfer of heat through a fluid, either gas or liquid, in the presence of bulk fluid motion. The fluid motion enhances heat transfer in terms of bringing parts of a fluid into contact being at different temperatures. Therefore, it is evident that heat transfer increases as the fluid velocity increases. Depending on the fluid motion, convection is classified as natural (free) and forced. In forced convection, the fluid is forced to flow over a surface or in a pipe by external means such as a pump or fan. In natural convection, the fluid motion is caused by natural means such as the buoyancy effect. [3]

Convection heat transfer is expressed by means of the Equation 2.2,

$$\tag{2.2}$$

where h is the convection heat transfer coefficient, $W/m^2.^oC$; A_s, the heat transfer surface area, m^2; T_s, the surface temperature, ^oC; , the temperature of the fluid sufficiently far from the surface, ^oC. Generally, the conductive and convective heat transfer can be grouped together. At the boundary or surface within a fluid, the ratio of convective heat transfer to conductive heat transfer is defined with the dimensionless Nusselt number:

$$— \tag{2.3}$$

where k is the characteristic thermal conductivity of the fluid, L is the characteristic length and h is the convective heat transfer.

Heat transfer mainly involves various dimensionless numbers besides the Nusselt number. The dimensionless Reynolds number is the key point to determine the flow regime in forced convection which represents the ratio of inertial forces to viscous forces acting on the fluid. On the other hand flow regime in natural convection is governed by the dimensionless Grashof number, which represents the ratio of the buoyancy force to the viscous forces acting on the fluid and provides information about the fluid flow type as laminar or turbulent. [3]

Natural convective heat transfer correlations are usually expressed in the form;

$$— \tag{2.4}$$

where Ra is the Rayleigh number, product of the Grashof and Prandtl numbers and Pr is the Prandtl number, the ratio of momentum diffusivity to thermal diffusivity: [3]

$$— \tag{2.5}$$

2.2. THERMAL CONDUCTIVITY

Many industrial processes like heat exchangers, refrigerators, automobiles, power plants, microelectronics etc. involve the transfer of heat over a finite fluid medium by means of a flowing fluid in either laminar or turbulent regime. [4]

The characteristic properties of fluids have to be analyzed in order to determine their heat transfer contributions. Thermal conductivity is the key point in heat transfer analyses, which is an intrinsic property of a material indicating its ability to conduct heat.

Table 2.1. Thermal Conductivity of Common Materials at 300 K [5]

Material	Thermal Conductivity, W/mK
Aluminum Oxide	30
Air	0.024
Copper	401
Gold	310
Iron	80
n-Heptane	0.140
n-Hexane	0.124
Silver	429
Water	0.609

It is well known that at room temperature, metals in solid form possess an order-of-magnitude higher thermal conductivity than fluids. Even oxides such as alumina (Al_2O_3), which are good thermal insulators compared to metals such as copper, have thermal conductivities higher than water. Therefore, fluids containing suspended solid particles are expected to display significantly enhanced thermal conductivities relative to those of conventional fluids for instance ethylene glycol, hexane, heptane or water. [6]

Advances in different areas of technology have necessitated developing heat transfer systems being small in size, light mass and having high performances. Further experiments

in this research area focused therefore, on the synthesis of various types of particles and their suspensions in conventional base fluids for studying the thermal conductivity enhancements. However, dispersion of milli- and micrometer-sized solid particles is susceptible to rapid settling of the particles or sedimentation, clogging and erosion of pipes and flow channels and increased pressure drop in the fluid. [7]

For that reason, over the last decades, scientists and engineers have attempted to develop fluids, which offer better cooling or heating performance for a variety of thermal systems compared to conventional heat transfer fluids. Applying nanotechnology to thermal engineering, the novel concept of a "nanofluid" was coined at Argonne National Laboratory of USA by Choi in 1995. [8] The effective thermal conductivities of nanofluids containing nanoparticles with varying concentrations, materials and sizes dispersed in different base fluids have been experimentally investigated. [9]

Maxwell was one of the first to analytically investigate the mechanism of heat conduction through suspended particles. A very dilute suspension of spherical particles was considered in Maxwell's studies and an approximation was obtained applicable only to mixtures having low particle volume concentrations. Since Maxwell's initial investigation, a number of extensions have been carried out taking various factors into account related with the measurement of effective thermal conductivity. [4]

2.3. NANOFLUIDS

As previously mentioned, in contrast to traditional heat transfer fluids, a new class of materials "nanofluids" are developed, which are stable colloidal suspensions containing low (<1 per cent) volume fraction of ultra-fine solid particles in nanometric dimensions (one billionth of a meter) dispersed in conventional heat transfer fluids. [10]

In fact, the conventional coarse-grained particles used in heat transfer fluids previously had many disadvantages such as settling, and clogging in channels and abrasion in heat transfer system surfaces, because of their large sizes and significantly higher masses. On the other hand, these new kinds of nanofluids offer a dramatic enhancement in

conductivity of the fluid without the above-mentioned problems encountered in dispersing coarse particles. [10]

The nanoparticles are small, therefore gravity becomes less important and chances of sedimentation are also less, making the nanofluids more stable. Besides the anomalously high effective thermal conductivity and microchannel cooling without clogging, miniaturized systems in the design of smaller and lighter heat exchanger systems, large savings in pumping power and improved heat transfer and stability should be also mentioned as benefits of nanoparticles. Another reason to use nanoparticles is their large surface area. As the heat transfer takes place at the surface of the particles, the relatively larger surface areas of nanoparticles compared to micro particles, provide significantly improved heat transfer capabilities. In addition, particles finer than 20 nm carry 20 per cent of their atoms on their surface, making them available for thermal interaction. [9]

Various nanoparticles, such as multi-walled carbon nanotubes (MWCNT), fullerenes, metal oxides (copper, silicon, iron etc…), silver or gold are dispersed in different base fluids to produce nanofluids for enhancing thermal conductivity. In most of the studies, distilled water, ethylene glycol, oil, silicon oil or poly-α-olefin oil (PAO) are used as base fluids. [11]

2.4. NANOPARTICLE PROPERTY EFFECTS ON THERMAL CONDUCTIVITY

Thermal conductivity enhancement of a nanofluid can be affected by various parameters such as particle volume concentration, particle material, particle size, particle shape, base fluid material, temperature, additive, and acidity. Each of these eight parameters will be considered separately in the next section.

2.4.1. Effect of Particle Material and Particle Size

The particle size is an important parameter in the enhancement of thermal conductivity. Decreasing the particle size down to nanoscale increases not only the surface area relative to volume but also generates some nanoscale mechanisms in the suspensions.

According to previous studies, the effective thermal conductivity of nanofluids increases with decreasing particle size. [9]

However, the effect of particle material on the enhancement of thermal conductivity depends on the specific type of the particle. For particles having relatively low thermal conductivity, there is essentially no effect on the thermal conductivity enhancement, on the other hand for higher conductivity particles the situation changes. [4]

Yu *et al*., compared the results for thermal conductivity enhancement of various nanofluids such as Al_2O_3 (15 nm), Cu (10 nm) and Fe (10 nm)/ethylene glycol. The metal particles produce the same enhancement as the nonmetallic (oxide) particles but at much lower volume concentrations. When the metal particle volume concentration was increased to 2.5 per cent, the thermal conductivity of the nanofluid was seen to be 115 per cent above ethylene glycol. [4]

Chon and Kihm experimentally measured the thermal conductivity of nanofluids containing nanoparticles of different sizes. Al_2O_3 (47 nm)/water nanofluids gave a larger increase in thermal conductivity compared to the Al_2O_3 (150 nm)/water nanofluids. [12]

2.4.2. Effect of Volume Fraction

Nanofluids exhibit much higher thermal conductivities than their base fluids even when the concentrations of suspended nanoparticles are very low. The general trend is that the thermal conductivity enhancement increases with increasing particle volume concentration. Several studies on the enhancements of nanofluid thermal conductivity confirm also with this assumption. [9]

Eastman *et al*. reported the first results on the enhanced effective thermal conductivity of nanofluids. By dispersing Al_2O_3 and CuO nanoparticles in water, 29 per cent and 60 per cent increase in thermal conductivity was achieved respectively for a nanoparticle volumetric loading of 5 per cent. [13]

Wang *et al*. reported a significant 17 per cent increase in the thermal conductivity for a loading of 0.4 vol. per cent of 50 nm sized CuO nanoparticles in water. [14]

Patel *et al*. used gold and Ag NPs to prepare water and toluene-based nanofluids. Their results showed that at room temperature, the conductivity of Au/toluene nanofluid was enhanced by 4-7 per cent for a very low particle loading of 0.005-0.011 per cent, whereas the enhancement for Au/water nanofluid was about 3.2-5 per cent again for a very small concentration of 0.0013-0.0026 per cent. The reason for such high thermal conductivities was the small size of nanoparticles and high thermal conductivity of particle materials. [15]

Patel *et al*. also studied the citrate-reduced Ag (60-70 nm)/water nanofluid with a particle loading of 0.001 vol. per cent resulting in a thermal conductivity enhancement ratio of 1.030. [15]

Zhu *et al*. prepared Fe_3O_4 (10 nm)/water-based nanofluids and measured their thermal conductivity by the transient heat wire method. For the nanoparticle volume fraction of 0.04, a 38 per cent increase was found. Zhu *et al*. ascribed such anomalously high thermal conductivity to the nanoparticle alignment in clusters. [16]

2.4.3.   Effect of Temperature

In general, the thermal conductivity of nanofluids is more temperature sensitive than that of the base fluid. The general trend shows that the thermal conductivity increases with increased temperature. [4]

Das *et al*. supported this general trend by investigating water-based Au (10-20 nm)/water nanofluids. Using the transient heat wire technique, nanofluids stabilized with citrate showed thermal conductivity enhancements of 5-21 per cent in a temperature range of 30-60°C at a very low particle volumetric loading of 0.00026 per cent. Das *et al*. concluded that chemical effects came into play in determining the extent of energy transfer in nanofluids. [15]

Mintsa *et al*. presented the influence of temperature and nanofluid particle volume fraction on effective thermal conductivity in their studies using Al_2O_3 (36 nm)/water and CuO (29 nm)/water nanofluids. Between 20°C and 40°C, an average increase in thermal conductivity was noted of approximately 15 per cent for each type of nanofluid. Mintsa *et al*. explained the result for the enhancement of thermal conductivity with temperature by Brownian motion. [17]

Yang and Han measured the thermal conductivity of suspensions of Bi_2Te_3 (20 x 170 nm) nanorods in hexadecane by using the 3ω-wire method. They observed a slightly decrease in the thermal conductivity with increasing temperature in contrast to the trend observed in nanofluids containing spherical particles. This contrary trend was claimed to be due to the particle aspect ratio. [18]

To sum up, nanofluids are new class of advanced heat transfer fluids engineered by dispersing nanoparticles smaller than 100 nm in diameter in conventional heat transfer fluids providing inherently higher thermal conductivities because of their stabilities and large surface area to volume ratios. Depending on their synthesis method, size distribution, stability etc., nanoparticles affect the enhancement of thermal conductivities of these fluids to high extents.

2.5. PRODUCTION OF NANOPARTICLES AND NANOFLUIDS

Modern fabrication technology allows the fabrication of materials at the nanometer scale. Preparation of nanofluids is the first key step to investigate the heat transfer performance of nanofluids. The synthesis method, synthesis conditions, choice of precursors, reducing and stabilizing agents are all determining points how a nanoparticle will behave characteristically. A nanofluid does not mean a simple mixture of solid nanoparticles with a liquid. Special techniques are developed for good dispersions of nanoparticles in liquids or directly producing stable nanofluids. [4]

An unavoidable problem associated with the synthesis of nano-sized particles is their instabilities over longer periods of time. The main reason of these unstable nanofluids is

the tendency of such small particles to form agglomerates in order to reduce their energy associated with the high surface area to volume ratio. Moreover, naked metallic nanoparticles are chemically highly active, and are easily oxidized in air, resulting generally in loss of dispersity and stability. [19]

For many applications it is thus crucial to develop protection strategies for preventing the agglomeration and obtaining stable colloidal solutions. These strategies comprise coating with organic species, including surfactants or polymers, or coating with an inorganic layer, such as silica or carbon. Depending on the desired application, these protecting shells can be used not only as stabilizers also as various ligands. [19]

Nanoparticles suspended in nanofluids are obtained from different materials, and their fabrication techniques can be classified into two broad categories: top-down and bottom-up. [4] The first method "top-down approach", involves the division of solid particles into smaller portions. This approach may involve milling or attrition, chemical methods, and volatilization of a solid followed by condensation of the volatilized components. On the other hand, the second one "bottom-up approach", which is far more popular in the synthesis of nanoparticles, involves the condensation of atoms or molecular entities in a gas phase or in solution. Both approaches can be further classified into other main categories: [20]
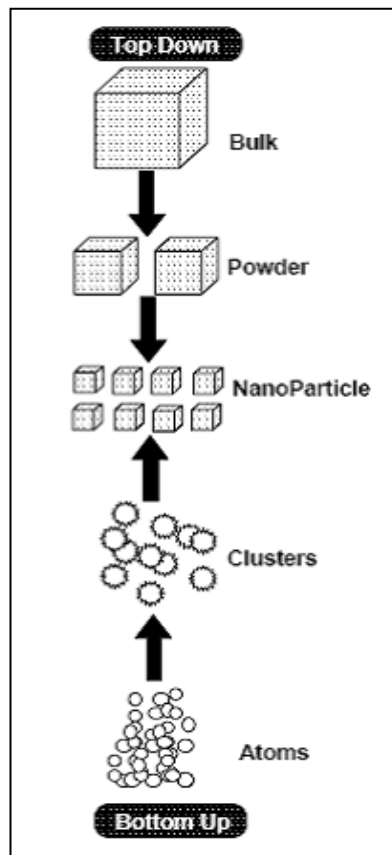
Figure 2.1. Schematic Representation of the Building up of Nanostructures [21]

2.5.1. Mechanical Milling Technique

High energy ball milling of powder form particles as a method for materials synthesis has been developed as an industrial process to successfully produce new alloys and phase mixtures in 1970's. This powder metallurgical process allows the preparation of alloys and composites, which cannot be synthesized via conventional routes. [22]

In nanomaterials research, this "top-down" technique is well used to fine-tune the grain sizes of the materials in nanoscale. The milling material, milling time and atmospheric medium are the main parameters affecting the process of ball milling. The approach can be used to produce nanoparticles from materials that do not readily lend themselves to other techniques like inert-gas condensation or chemical precipitation. [23]

2.5.2. Inert-Gas Condensation Technique

Inert-gas condensation approach is mainly used to produce metallic and metal oxide nanoparticles under inert gas atmospheres to avoid the nanoparticle oxidation. A reactive oxygen atmosphere is used in conjunction with the inert-gases to produce metal oxide ceramic nanoparticles. It involves evaporation of a solid metal followed by rapid condensation to form nanosized clusters, which can settle in the form of a powder. Final particle size can be controlled varying the parameters such as temperature, gas environment and evaporation rate. The main advantage of this approach is low contamination levels compared to other techniques. [23]

Another variation of the vapor condensation technique is the chemical vapor deposition (CVD) generally used to make films. In a typical synthesis, both liquid and gas forms of a substance are put into a reactor. Depending on several parameters such as gas-to-liquid ratio, temperature and length of time, different particle shapes can be created and controlled. [23]

2.5.3. Chemical Precipitation Technique

The most widely used chemical nanoparticle synthesis technique consists of a growth of nanoparticles in a liquid medium composed of various reactants. Comparing the chemical techniques with condensation techniques, chemical methods are generally better to control the final shape of the particles. The approaches do not require high costs, produce higher volumes. However, contamination from the precursor chemicals and undesirable surface coatings are the main disadvantages. [23]

There are several sub routes in chemical precipitation techniques. Generally, direct synthesis involves the preparation of nanoparticles under conditions appropriate for the nanoparticle nucleation and growth. Generally, metal ions are reduced and the precipitated solid particles are further coated with surfactant molecules offering stability and increased control over nanoparticle size, polydispersity and modifying surface reactivity. Obtained nanoparticles can be further dispersed in required base fluids. [24]

2.5.4. Green Nanoscience

The most recent approach to produce nanoparticles is the green chemistry approach. Green chemistry is the utilization of a set of principles reducing or eliminating the use or generation of hazardous substances in the design, manufacture, and application of chemical products. The 12 principles of green chemistry originally defined by Anastas and Warner are applied to the design of a wide range of chemical products and processes with the aims of minimizing chemical hazards to health and the environment, reducing waste, and preventing pollution. [24]

Table 2.2. Green Chemistry Approach Principles [24]

Green Chemistry Principles	
P1.	Prevent waste
P2.	Atom economy
P3.	Less hazardous chemical synthesis
P4.	Designing safer chemicals
P5.	Safer solvents/reaction media
P6.	Design for energy efficiency
P7.	Renewable feedstocks
P8.	Reduce derivatives
P9.	Catalysis
P10.	Design for degradation/Design for end of life
P11.	Real-time monitoring and process control
P12.	Inherently safer chemistry

The preparation of nanoparticles within a green context poses interrelated challenges in terms of maintaining product structure, shape and size dispersity, functionality, purity and stability. While employing greener methods whenever possible, such as the particle size and dispersity controls during the nanoparticle synthesis may reduce purification requirements by eliminating the need for extensive separations. [24]

2.6. SPECIAL SYNTHESIS OF HEAT TRANSFER NANOFLUIDS: MAGNETITE AND SILVER NANOFLUIDS

Many syntheses of nanoparticles have been developed in recent years, in an effort to produce structures that have specific forms and functions relevant to a given application. Intended to enhance the heat transfer performances of nanofluids, synthesis of iron oxide and Ag NPs are presented in the next section in more detail because of characteristic conductivity properties of silver and iron metals.

2.6.1. Silver Nanofluid Synthesis Methods

Silver (Ag) is a noble metal with an inert chemical reactivity in its bulk form and is listed below hydrogen in the activity series of metals. [25]

Ag NPs have attracted considerable interest in the past few decades, from chemical industry and medicine due to unique properties, such as high thermal conductivity, high resistance to oxidation, and antibacterial activity. Among these characteristic properties, the antibacterial activity of Ag NPs is influenced mainly by the size of the particles. Thus, Ag NPs having small sizes and without agglomeration are preferable generally for industrial applications. [26]

Many methods, including chemical reduction method and polyol process have been developed for the synthesis of Ag NPs. Chemical reduction method has been widely studied among these methods, due to its advantages of yielding nanoparticles without agglomeration, high yield, and low preparation cost. [26] The chemical reduction method involves the reduction of silver by a reducing agent in the presence of a suitable stabilizer to protect the growth of silver particles from aggregation.

Song et al. investigated the particle size and degree of aggregation of Ag NPs prepared by chemical reduction synthesis route using UV-VIS absorption spectrophotometer. Stable Ag NPs were obtained with water-soluble stabilizer SDS, a strong reducing agent $NaBH_4$ and silver nitrate as the silver content. [26]

Hiramatsu and Osterloh found that borohydride reducing agents are unnecessary for the synthesis of nanomaterials in larger size regimes. Silver-amine stabilized particles with core diameter ranges of 8-32 nm for silver (Figure 2.1) were synthesized in a simple scalable preparation method where silver acetate was refluxed with oleylamine in an organic solvent. Other reducing agents are not necessary, since amines are capable of reducing silver. The particle size is determined primarily by the reflux temperature associated with each solvent: hexanes (bp: 69°C) yield 8.5 nm particles, while the use of toluene (bp: 110°C) and 1,2 dichlorobenzene (bp:181°C) results in 12.7 nm and 32.3 nm particles, respectively. [27]
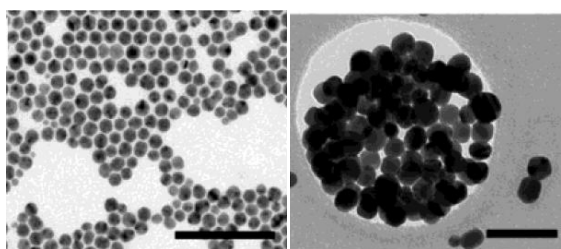
Figure 2.2. TEM images of Ag nanoparticle samples
(Left: 12 nm Ag nanoparticle from hexane, right: 32 nm Ag from 1,2 dichlorobenzene) [27]

Hu *et al*. reported a modified polyol process for the synthesis of highly water-soluble silver nanocrystals with uniform and tunable sizes ranging from several nanometers to ~20 nm. The use of polyacrylic acid as the surfactant, in place of polyvinylpyrrolidone (PVP) in the conventional polyol process, significantly limits the growth of silver nanocrystals, prevents the interparticle aggregation and fusion, and leads to a uniform population of samples with high water solubility. The size of nanocrystals can be conveniently tuned by controlling the reaction time, the concentration and chain length of the polymeric surfactants, and the reaction temperature. [28]

Yin *et al*. reported a simple and convenient procedure based on the Tollen's process for the preparation of Ag NPs with a relatively narrow size distribution between 20-50 nm. The starting reagents were similar to those commonly used in the electroless deposition of silver: three separate aqueous solutions (silver (silver nitrate), activator (sodium

hydroxide), and reducer (formaldehyde and sorbitol) solutions). Only under appropriate conditions, mixing of these reagents was able to generate stable aqueous dispersions of silver colloids. [29]

Songping *et al*. investigated the preparation of ultrafine silver powder with chemical reduction method. The reaction of $AgNO_3$ with the reducing agent ascorbic acid and gum arabic as the dispersion agent gives ultrafine silver powder having narrow size distribution. The silver powder having excellent dispersibility and different size was prepared through different pH value or different dosage surfactant. [30]

Alvarez-Puebla *et al*. explored new methods of synthesis of silver nano-colloids using amino acids as reducing agents. The goal of the study was to fabricate nanostructures with controllable surface charge (zeta potential) that may allow optimizing the adsorption of target molecules for ultrasensitive analysis using surface enhanced Raman scattering (SERS). [31]

Dong *et al*. investigated the growth of Ag NPs by the citrate reduction of silver nitrate under the range of pH from 5.7 to 11.1. A stepwise reduction method, in which the nucleation and growth processes were carried out at high and low pH, was proposed for the syntheses of spherical Ag NPs. [32]

Lee *et al*. proposed a reduction method for preparation of different kinds of silver sols by using silver nitrate and sodium citrate. [33]

AL-Thabaiti *et al*. reported kinetic data for the silver nitrate-ascorbic acid redox system in presence of three surfactants (cationic, anionic and nonionic). The Ag NPs are spherical and of uniform particle size, and the average particle size is about 10 and 50 nm, respectively, for SDS and CTAB. [34]

Medina-Ramirez *et al*. proposed a facile green chemistry synthetic route for synthesizing Ag NPs. The reaction occurred at ambient temperature. Different reducing agents and advanced instrumentation techniques were used. [35]

Pillai and Kamat investigated the role of citrate ions in the synthesis of spherical and anisotropic Ag NPs. Citrate reduction of silver ions yields large Ag NPs having a size distribution between 60 – 200 nm, wide range of morphologies depending upon the reaction conditions. [36]

2.6.2. Magnetite Nanofluid Synthesis Methods

The synthesis of magnetic nanoparticles has received increased attention as the possibility of creating functional materials became more apparent such as heat transfer reagents, and medical imaging enhancers. [24]

Magnetic nanoparticles (including the Fe_3O_4 magnetite, the α-Fe_2O_3 hematite, the γ-Fe_2O_3 maghemite, FeO, ε-Fe_2O_3 and β-Fe_2O_3) have unique magnetic properties such as superparamagnetism and high coercivity. [37]

Discussing the properties of magnetic particles, there exist generally three main types of magnetic behavior in nature; paramagnetism, in which the unpaired electrons are randomly arranged; ferromagnetism, in which the unpaired electrons are all aligned; and antiferromagnetism, in which the unpaired electrons line up in opposite directions to one another as shown in the Figure 2.3. [38]
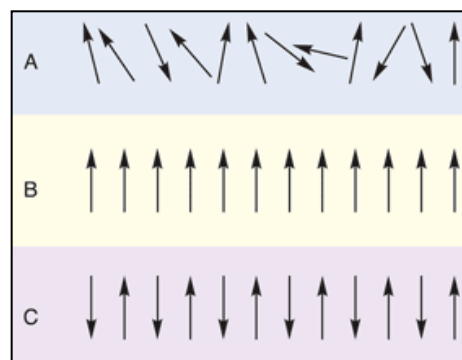
Figure 2.3. Types of magnetism

(A) Paramagnetism, (B) Ferromagnetism, (C) Antiferromagnetism [38]

Paramagnetism is a form of magnetism that occurs only in the presence of an externally applied magnetic field. Unlike ferromagnets, such as iron or nickel, which can form permanent magnets or are attracted to magnets, paramagnets do not retain any magnetization in the absence of an externally applied magnetic field. Thus the magnetization of paramagnetic materials is proportional to the applied field and the total magnetization drops to zero when the applied field is removed. [39]

Another group of magnetic materials are the superparamagnetic materials that show induced magnetic behavior. They are generally characterized by their saturation magnetization values at very strong fields. Each particle behaves as a single magnetic domain. If a magnetic field is applied, the particles will align producing a net moment. This behavior is characteristic of paramagnetic materials, but the difference is that each nanoparticle has a great net moment, so the saturation of magnetization occurs at very strong fields of several Teslas. [40]

Magnetic iron oxide nanoparticles have a large surface-to-volume ratio and therefore possess high surface energies. Consequently, they tend to aggregate so as to minimize the surface energies. The naked iron oxide nanoparticles have high chemical activity, and are easily oxidized in air (especially magnetite), generally resulting in loss of magnetism and dispersibility. Therefore, providing proper surface coating to keep the stability of magnetic iron oxide nanoparticles is very important. These strategies comprise grafting of or coating with organic molecules, including small organic molecules or surfactants, polymers, and biomolecules, or coating with an inorganic layer, such as silica, metal or nonmetal elementary substance, metal oxide or metal sulfide. [40]
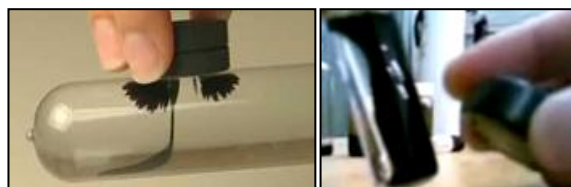
Figure 2.4. Magnetic Nanofluid and its Response to a Magnet [41]

Especially, during the last few years, many publications have described efficient synthetic routes to shape-controlled, highly stable magnetic nanoparticles with narrow size distribution. Several popular methods including co-precipitation, thermal decomposition and/or reduction, micelle synthesis, hydrothermal or sonochemical synthesis, and laser pyrolysis techniques can all be directed at the synthesis of high-quality magnetic nanoparticles. [19]

2.6.2.1. Co-Precipitation Method

The most conventional method for obtaining iron oxides (either Fe_3O_4 or γ-Fe_2O_3) from aqueous Fe^{2+}/Fe^{3+} salt solutions is co-precipitation by the addition of a base under inert atmosphere at room temperature or at elevated temperatures. The size, shape, and composition of the magnetic nanoparticles strongly depend on the type of salts used (e.g. chlorides, sulfates, nitrates), the Fe^{2+}/Fe^{3+} ratio, the reaction temperature, the pH value and ionic strength of the media. [40]

The experimental challenge in the synthesis of Fe_3O_4 by co-precipitation lies in control of the particle size and thus achieving a narrow particle size distribution. Particles prepared by co-precipitation unfortunately tend to be rather polydisperse. It is well known that a short burst of nucleation and subsequent slow controlled growth is crucial to produce particles with narrow size distribution. Controlling these processes is therefore the key in the production of narrow size distributed iron oxide magnetic nanoparticles. [19]

Recently, significant advances in preparing magnetite nanoparticles, of different sizes, have been made by the use of organic additives as stabilization and/or reducing agents. The effects of several organic anions, such as carboxylate and hydroxy carboxylate ions, on the formation of iron oxides have been studied extensively. However, recent studies showed that oleic acid is the best candidate for the stabilization of Fe_3O_4. [19]

On the other hand, Kang *et al.* reported a synthesis method for uniform and narrow size distributional Fe_3O_4 nanoparticles (the diameter of nanoparticles was 8.5 ± 1.3 nm) by co-precipitation without surfactants. [40]

2.6.2.2. Thermal Decomposition Method

Magnetic nanocrystals with smaller size can be synthesized through the thermal decomposition of organometallic compounds including metal acetylacetonates [$Fe(acac)_3$ (acac=acetylacetonate)], carbonyls, $Fe(cup)_3$ (cup=N-nitrosophenylhydroxylamine), or $Fe(CO)_5$ in high-boiling organic solvents containing stabilizing surfactants such as fatty acids, oleic acid or hexadecylamine. [40] The ratios of the starting reagents, the reaction temperature, reaction time and aging periods are crucial for the precise control of the size and morphology of magnetic nanoparticles. [19]

Sun and Zeng have reported a general decomposition approach for the synthesis of size-controlled magnetite nanoparticles based on high temperature ($265^{o}C$) reaction of $Fe(acac)_3$ in phenyl ether in the presence of alcohol, oleic acid, and oleylamine. With the smaller magnetite nanoparticles as seeds, larger magnetite Nanoparticles of up to 20 nm in diameter can be synthesized and dispersed into nonpolar solvent by seed-mediated growth method. The as-synthesized Fe_3O_4 nanoparticle assemblies can be transformed easily into γ-Fe_2O_3 nanoparticles by annealing at high temperature ($250^{o}C$) and oxygen for two hours. This representative procedure was applied in this study to synthesize (Fe_3O_4) magnetite nanoparticles highly dispersible in hydrophobic solvents. [42]

Hyeon *et al*. reported a synthesis of highly crystalline iron nanoparticles without size-selection process by the thermal decomposition of iron pentacarbonyl in the presence of oleic acid at $100^{o}C$. The resulting iron nanoparticles were transformed to γ-Fe_2O_3 nanocrystallites with narrow size distribution by controlled oxidation using trimethylamine oxide as a mild oxidant. Particle size can be varied from 4 to 16 nm by controlling the experimental parameters. [43]

Although the thermal decomposition method has many advantages for producing particles with a narrow size distribution, it has the big disadvantage that the resulting nanoparticles are generally only dissolvable in nonpolar solvents. [40]

2.6.2.3. Microemulsion Synthesis Method

Microemulsion is a thermodynamically stable isotropic dispersion of two immiscible phases (water and oil) under the surfactant present, the surfactant molecules may form a

monolayer at the interface between the oil and water, with the hydrophobic tails of the surfactant molecules dissolved in the oil phase and the hydrophilic head groups in the aqueous phase. In this sense, microemulsion and inverse micelles route can be employed for obtaining the shape- and size-controlled iron oxide nanoparticles. [40]

Vidal-Vidal *et al*. have reported the synthesis of maghemite nanoparticles having narrow size distribution by the microemulsion method. The spherical shaped particles, capped with a monolayer coating of oleylamine (or oleic acid), show a narrow size distribution of 3.5 ± 0.6 nm, are well crystallized and have high saturation magnetization values. [44]

Chin and Yaacob reported the synthesis of magnetic iron oxide nanoparticles (less than 10 nm) via w/o microemulsion method. Particles produced by microemulsion technique were smaller in size and were higher in saturation magnetization. [45]

However, one drawback of this synthesis procedure is the aggregation of the produced nanoparticles despite the presence of surfactants. [40]

2.6.2.4. Hydrothermal Synthesis Method

The microemulsion and thermal decomposition methods for synthesizing iron oxide nanoparticles usually lead to complicated processes or require relatively high temperatures. As an alternative, hydrothermal synthesis includes various wet chemical technologies of crystallizing substance in a sealed container from the high temperature aqueous solution (generally in the range from 130 to 250°C) at high vapor pressure (generally in the range from 0.3 to 4 MPa). The hydrothermal synthesis is prone to obtain the highly crystalline iron oxide nanoparticles. [40]

Wang *et al*. have reported a one-step hydrothermal process to prepare highly crystalline Fe_3O_4 nanopowders without using the surfactants. The obtained nanoscale Fe_3O_4 powder with a size of approximately 40 nm) is synthesized at 140°C. [46]

On the contrary, Zheng *et al*. reported a hydrothermal route for preparing Fe_3O_4 nanoparticles with diameter of ca. 27 nm in the presence of a surfactant, sodium bis(2-

ethylhexyl)sulfosuccinate (AOT). The magnetic properties of the nanoparticles exhibited a superparamagnetic behavior at room temperature. [47]

Li *et al*. reported a generalized hydrothermal method for synthesizing a variety of different nanocrystals based on the strategy of a general phase transfer and separation mechanism occurring at the interfaces of the liquid, solid, and solution phases present during the reaction. As an example, Fe_3O_4 and $CoFe_2O_4$ nanoparticles have been synthesized in very uniform sizes of about 9 and 12 nm, respectively. [19]

Li *et al*. also reported a synthesis of hydrophilic, single-crystalline ferrite microspheres by hydrothermal reduction. A mixture, consisting of $FeCl_3$, ethylene glycol, sodium acetate, and polyethylene glycol, was stirred vigorously and the solution was heated to 200^oC. In this way, ferrite spheres were obtained with sizes in the range of 200-800 nm. [19]

Moreover, hydrothermal treatment is one of the successful ways of growing crystals for iron oxide nanoparticles. Recently Daou *et al*. have reported that the magnetite particles with an average size of 39 nm and good monodispersity have been synthesized by co-precipitation at 70^oC from ferrous Fe^{2+} and ferric Fe^{3+} ions by a $N(CH_3)_4OH$ solution, followed by hydrothermal treatment at 250^oC. [49]

2.6.2.5. Sonochemical Synthesis Method

As a competitive alternative, the sonochemical method has been extensively used to generate novel materials with unusual properties. The chemical effects of ultrasound arise from acoustic cavitation, that is, the formation, growth, and implosive collapse of bubbles in liquid. These extreme conditions were beneficial to form the new phase, and have a shear effect for agglomeration, which is prone to prepare nanoparticles with narrow size distribution. This method has been applied for the synthesis of various nanocomposites, and its versatility has been successfully demonstrated in iron oxide nanoparticles preparation [40]. For instance, magnetite nanoparticles can be simply synthesized by sonication of iron(II)acetate in water under an argon atmosphere.

Vijayakumar *et al*. reported a sonochemical synthetic route for preparing the pure nanometer-size Fe_3O_4 powder with particle size of ca. 10 nm. The prepared Fe_3O_4 nanoparticles are superparamagnetic. [49]

Ultrasonic irradiation of a volatile organometallic precursor, $Fe(CO)_5$, in octanol with polyvinylpyrrolidone (PVP) under oxygen free argon atmosphere produced a black colloidal solution having 3-8 nm size iron particles in the polymer matrix. [50]

Recently Pinkas *et al*. [51] developed a sonochemical synthetic method for preparing the amorphous nano-scale iron oxide by sonolysis of $Fe(acac)_3$ under Argon gas with a small amount of added water. Such surface modified ultrasmall (1–2 nm) nanoparticles exhibit an unrecorded low magnetic transition temperature of about 25 K, below this temperature they behave as highly magnetically disordered systems with a high contribution of the surface anisotropy.

Table 2.3. Summary and Comparison of the Nanoparticle Synthetic Methods [19]

Synthetic Method	Synthesis	Reaction Temp. (^{o}C)	Reaction period	Solvent	Size distribution	Shape Control/ Yield
Co-precipitation	Very simple, ambient conditions	20-90	Minutes	Water	Relatively narrow	Not good/high
Thermal decomposition	Complicated, inert atmosphere	100-320	Hours-days	Organic compund	Very narrow	Very good/high
Microemulsion	Complicated, ambient conditions	20-50	Hours	Organic compund	Relatively narrow	Good/low
Hydrothermal Synthesis	Simple, high pressure	200-250	Hours, ca. days	Water, ethanol	Very narrow	Very good/ medium

2.7. THERMOPHYSICAL PROPERTIES

2.7.1. Density

Density is a physical property of matter that expresses a relationship of mass to volume. The density of a material (usually represented by the Greek symbol ρ) is defined as its mass (m) per unit volume (V). It is mainly a measure of how closely a matter is packed together. It is generally expressed as:

$$—$$

(2.6)

It is important to remember, though, that this relationship is not just about how closely packed together the atoms of an element or molecules of a compound are, it is also affected by the atomic mass of an element or compound. Since different substances have different densities, density measurements are a useful means for identifying substances.

Density, as an intensive property of matter, expressed generally as grams per milliliters (g/ml) and grams per cubic centimeter (g/cm^3). Mass is the amount of matter contained in an object and is commonly measured in units of grams (g). Volume is the amount of space taken up by a quantity of matter and is commonly expressed in cubic centimeters (cm^3) or in milliliters (ml) (1cm^3 = 1 ml). [52]

2.7.2.   Viscosity

Viscosity, defined by the equation of Newton, is the ratio of the shearing stress to the velocity gradient in a fluid. It generally states that the resulting shear of a fluid is directly proportional to the force applied and inversely proportional to its viscosity. [53]

$$— \quad —$$

(2.7)

Viscosity has the units of the pascal second [Pa·s], which is rarely used in scientific area compared to the common viscosity unit of dyne second per square centimeter [dyne·s/cm^2], also called as poise (P).

Viscosity is a measure of a fluid's resistance to flow. In order to characterize materials according to their rheological properties, viscosity analyses must be performed. However, there exist some parameters affecting viscosity measurements of a sample, which should be taken into consideration. One of these parameters affecting the viscosity of a fluid is the temperature. Generally, viscosity has a trend to decrease with increasing temperature. The motion of molecules in a fluid increases as temperature increases and the amount of time spend in contact with their nearest neighbors decreases. Thus, as temperature increases, the average intermolecular forces decrease resulting in much lower viscosities.

Among the other parameters affecting the viscosity, there exist variables related to the test fluid which are dependent on the rheological properties of the fluid, and instrument variables which include the rheometer design and the spindle geometry system. Fluids have different rheological characteristics that can be described by rheometer measurements. There are two categories of fluids, Newtonian and Non-Newtonian fluids. Newtonian fluids have the same viscosity at different shear rates (different RPM's) and Non-Newtonian fluids have different viscosities at different shear rates (different RPM's). Most fluid viscosities are found to be Non-Newtonian, in other words shear rate dependent. [53]

In the investigation of thermophysical properties of nanofluids, the significance of investigating the viscosity of nanofluids should also be emphasized. Viscosity is as critical as thermal conductivity in engineering systems that employ fluid flow. Pumping power of a system is proportional to the pressure drop, which in turn is related to fluid viscosity.

Masuda *et al*. measured the viscosity of suspensions of dispersed ultra-fine TiO$_2$ (27 nm) particles in water. At a volumetric loading of 4.3% increased the viscosity of water by 60%. [54]

Wang *et al.* observed that the effective viscosity of Al_2O_3 (28 nm)/ DIW-based nanofluids was increased by about 86% for a 5 vol% of nanoparticles. They also found an increase of about 40% in viscosity of ethylene glycol at a volumetric loading of 3.5% of Al_2O_3 nanoparticles. [55]

At a given shear rate, Ding *et al.* observed that the viscosity of nanofluids increased with an increasing CNT concentration and decreasing temperature. This suggests that nanofluids can offer better fluid flow performance due to higher shear rate at the wall, which results in low viscosity. [56]

Kang *et al.* investigated the viscosity of silver nanofluids prepared by ultrasound vibration. The viscosity of the silver nanofluid was measured by viscometer (Brookfield DV II+LV) and showed an enhancement up to 10% for 0.4 vol% of silver particles. [57]

2.7.3.   Thermal Conductivity Measurement

Different steady-state techniques exist to measure the effective thermal conductivity of fluids, for instance the "transient hot-wire (THW)" method, temperature oscillation technique, and the 3ω-wire method.

In order to measure the absolute thermal conductivity of powders, the transient heat wire technique was first suggested by Stalhane and Pyk in 1931. Since that time, many researchers have modified the method to make it more accurate. [6] Such as Nagasaka and Nagashima performed thermal conductivity measurements of electrically conducting liquids by considering the electrical insulation layer effect on heat transfer. No significant negative effect of insulation was found. [6]

Besides the THW technique, there exist several methods as mentioned before to determine the effective thermal conductivity of nanofluids; however these techniques are not as accurate as the THW method. The temperature oscillation technique measures the thermal diffusivity and derives the thermal conductivity from this measured value and the

volumetric specific heat of sample. The 3ω-wire method is similar to THW and uses a metal wire suspended in a liquid. A sinusoidal current at frequency ω passes through the metal wire and generates a heat wave at frequency 2ω, which is deduced by the voltage component at frequency 3ω. The method is more suitable to measure temperature-dependent thermal conductivity. [9]

Besides, the THW method has proven to be one of the most accurate techniques for determining the thermal conductivity of a fluid, because the advantage of this method lies in its almost complete elimination of the effects of natural convection, whose unwanted presence results in problems for measurements made with a steady-state apparatus. In addition, this method is very fast relative to other techniques and the design of the hot-wire apparatus is also very simple. [6]

The principle of the hot-wire method is based on ideal, constant heat generation source, an infinitely long and thin continuous line, dissipating the heat into an infinite test medium. [58] In practice, the ideal case is approximated with a finite long wire suspended symmetrically in a liquid in a vertical cylindrical container where the wire serves both as heating element and as thermometer. [6]

While the wire is electrically heated, the change in resistance of the wire, thus its temperature, is measured as function of time using a computerized data acquisition system. [58] The mathematical model to approximate is an infinite-line source of heat suspended vertically in an infinite medium. The method is called transient, because the power is applied abruptly and briefly. The working equation is based on a specific solution of Fourier's law: [6]

$$ \qquad \underline{\qquad} \quad \underline{\qquad} \tag{2.8}$$

where T(t) is the temperature of the wire in the fluid at time t, T_{ref} is the temperature of the cell, q is the applied electric power, k is the thermal conductivity, K is the thermal diffusivity of the fluid, a is the radius of the wire, and ln C =g, where g is Euler's constant.

Finally, the thermal conductivity (T_c) value is determined from the heating power and the slope of temperature change in logarithmic time. [58]

$$\rule{3cm}{0.4pt} \quad \rule{0.8cm}{0.4pt} \tag{2.9}$$

where T_2-T_1 is the temperature rise of the wire between times t_1 and t_2. From the temperature coefficient of the wire's resistance, the temperature rise of the wire can be determined by the change in its electrical resistance as the experiment progresses. [6]

Despite the advantages of the transient hot-wire method, it is impossible to measure the thermal conductivity of electrically conducting fluids because current flows through the liquids, the heat generation of the wire becomes ambiguous, and polarization occurs on the wire's surface. Therefore, this method is restricted to electrically nonconducting fluids such as noble gases and organic liquids. [6]

Therefore, Nagasaka and Nagashima (1981) have attempted to expand the transient hot-wire method to measure electrically conducting liquids using a platinum wire, whose resistance/temperature relationship is well known over a wide temperature range, coated with a thin electrical insulation layer. As the nanofluids are likely to be electrically conducting (metallic nanoparticles and the suspending fluid such as water are electrically conducting materials), the expanded transient hot-wire method has been adopted in these experiments. [6]

Briefly, nanofluids are produced by dispersing nanometer-scale solid particles into liquids such as water or oils. Among the nanoparticle production methods, mostly preferred one is the chemical precipitation technique, also used in the present study to synthesize stable magnetite and Ag NPs. As mentioned before, hydrophobic or hydrophilic nanoparticles, unlike conventional particles, reduce the friction and improve heat transfer. To verify experimentally the effects of nanoparticle material, size and volume fraction on the enhancement of nanofluid thermal conductivity, the primary objective of the present study is to investigate the behavior of various nanofluids using different thermophysical property measurement techniques.

In the following sections of this study, the materials used in the syntheses, the measurement equipments and techniques will be explained in further details. The
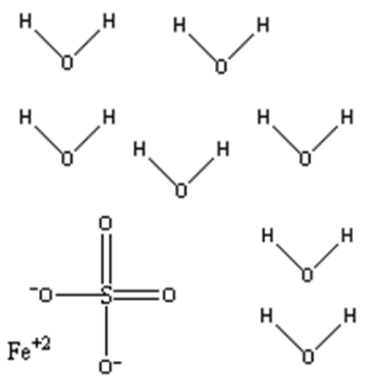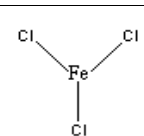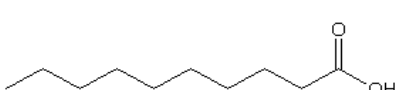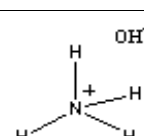
experimental results showing the enhancements of thermophysical properties of density, viscosity and thermal conductivity will be tabulated.
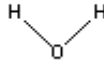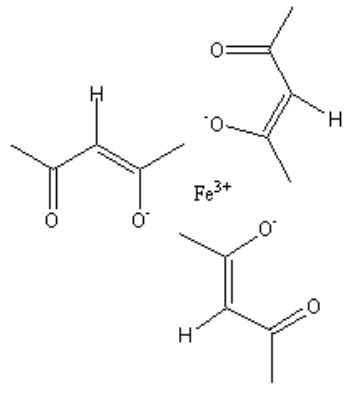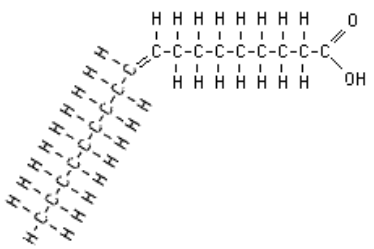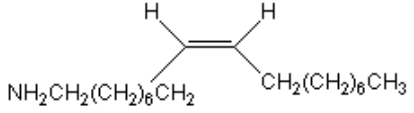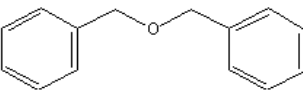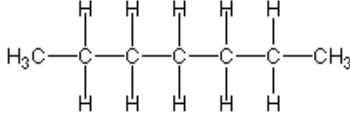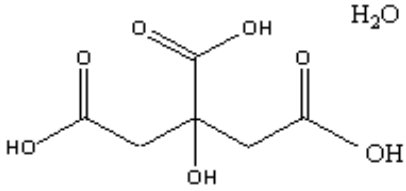
3.   MATERIALS AND METHODS

In this section, various chemicals used to synthesize different types of magnetite and Ag NPs, either hydrophobic or hydrophilic are summarized in Tables 3.1 and 3.2. Short information about characterization techniques such as dynamic light scattering, transmission and scanning electron microscopy, x-ray diffraction and UV-VIS spectrophotometry are summarized and various instruments to measure the thermophysical properties (density, viscosity and thermal conductivity) of nanofluids are described in more detail.

3.1. CHEMICALS

Table 3.1. Chemicals used in the Synthesis of Magnetite Nanoparticles

Chemical name	Formula	Structure	Provider	Purity
Iron (II) sulfate hepta hydrate	$FeSO_4.7H_2O$		Riedel-de Haen	90%
Iron (III) Chloride	$FeCl_3$		Riedel-de Haen	97%
Capric Acid	$C_{10}H_{20}O_2$		Fluka	98%
Ammonium Hydroxide	NH_4OH		Riedel-de Haen	99%

Water	H_2O		-	-
Ferric Acetylacetonate	$C_{15}H_{21}FeO_6$		Fluka	97%
1,2 – Tetradecanediol	$CH_3(CH_2)_{11}CH(OH)CH_2OH$		Aldrich	90%
Oleic Acid	$C_{18}H_{34}O_2$		Riedel-de Haen	99%
Oleylamine	$C_{18}H_{37}N$		Fluka	70%
Dibenzylether	$C_{14}H_{34}O_2$		Merck	Pure
Heptane	C_7H_{16}		Lab-Scan	95%
Citric Acid	$C_6H_8O_7$		Sigma Aldrich	99%
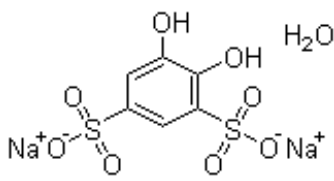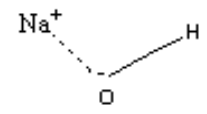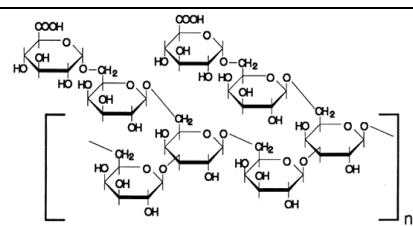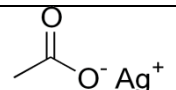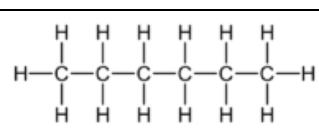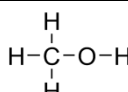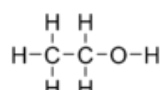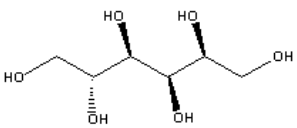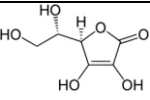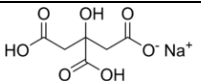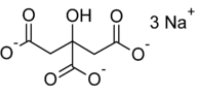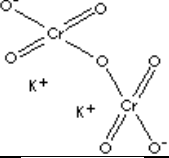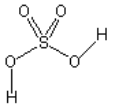
Tiron	$C_6H_4Na_2O_8S_2$		Riedel-de Haen	98.5%
Hydrochloric Acid	HCl	H—Cl	Merck	98.5%
Sodium Hydroxide	NaOH		Fluka	99%

Table 3.2. Chemicals used in the Synthesis of Ag NPs

Silver nitrate	$AgNO_3$		Fluka	99.5%
Gum Arabic	$(C_6H_{10}O_5)_n$		Merck	Pure
Silver acetate	$AgC_2H_3O_2$		Sigma-Aldrich	99.9%
Sodium borohydride	$NaBH_4$		Merck	98.0%
Hexane	C_6H_{14}		Riedel-de Haen	95%s
Methanol	CH_3OH		Emboy	99.9%
Ethanol	C_2H_5OH		LabKim	99.8%

Formaldehyde	CH_2O		Fluka	37%
D-Sorbitol	$C_6H_{14}O_6$		Alfa Aesar	Pure
Poly Vinyl Alcohol	$(C_2H_4O)_x$		Fluka	Pure
L-Ascorbic Acid	$C_6H_8O_6$		Sigma-Aldrich	Pure
Gelatin	N/A	N/A	Sigma-Aldrich	From fish skin
Sodium Citrate (mono)	$C_6H_7NaO_7$		AppliChem	99%
Sodium Citrate (tribasic dihydrate)	$C_6H_5Na_3O_7 . 2H_2O$		Riedel – de Haen	99%
Potassium dichromate	$K_2Cr_7O_7$		Merck	Pure
Sulfuric Acid	H_2SO_4		Riedel – de Haen	95-97%

3.2. CHARACTERIZATION TECHNIQUES

The size and shape of colloidal particles are the most important characteristics to determine the behavior of colloidal suspensions. Colloidal suspensions often exhibit a wide range of particle sizes and shapes. For some purposes it may be enough to know the minimum or maximum, or the average particle size value, but in many cases it is necessary to have knowledge of the distribution, that is the number of particles in each size range. [59]

There exist various methods to determine the size and shape of colloidal particles. Since each method interacts with the particles in a different way, different results can be

obtained from different methods. Structural information can be acquired most commonly by light scattering, high resolution imaging through microscopy and by electron diffraction.

3.2.1.   Dynamic Light Scattering

Dynamic Light Scattering (DLS) also known as Photon Correlation Spectroscopy (PCS) or Quasi-Elastic Light Scattering (QELS) is one of the most popular methods used to determine the size of particles and molecules typically in the submicron range. Typical applications of dynamic light scattering are the measurement of the size and size distribution of particles, emulsions and molecules dispersed or dissolved in a liquid such as proteins, polymers, micelles, carbohydrates, nanoparticles, colloidal dispersions, emulsions, micro-emulsions. [60]

In this study, both types of synthesized nanoparticles, magnetite and silver in hydrophobic and hydrophilic conditions were examined through dynamic light scattering for their size and size distributions. Generally, the obtained result is the measured DLS radius which is the radius of a hypothetical hard sphere that diffuses with the same speed as the particle under examination.

The idea behind the dynamic light scattering is to estimate how much particle motion is occurring by measuring the signal at a certain instant in time and then comparing it with signals obtained at later times. By multiplying the initial signal by the one obtained at a number of later times and summing the result, it can be obtained how highly correlated the signal is. [59]

Therefore, the measured data in an experiment is the correlation curve providing all of the information regarding the diffusion of particles within the sample. The diffusion coefficient (D) is calculated by fitting the correlation curve to an exponential function. The hydrodynamic radius (R_H) is then calculated from the diffusion coefficient using the Stokes-Einstein equation, where k is the Boltzmann constant, T is the temperature,   is the medium viscosity, and   is the frictional coefficient for a hard sphere in a viscous medium.

$$\overline{\quad}\quad\overline{\quad\quad\quad} \tag{3.1}$$

There exist a number of commercial instruments taking advantage of this technique. The Zetasizer Nano series instruments provides the ability to measure the characteristics of particles or molecules in a liquid medium such as the particle size, zeta potential and molecular weight over a wide range of concentrations. The instrument performs size measurements using the dynamic light scattering technique and measures Brownian motion by relating this to the size of the particles. Brownian motion is the random movement of particles in a liquid due to the bombardment by the molecules that surround them and this speed of movement is used to determine the size of the particles. [61]

Table 3.3. Zetasizer Nano Series Specifications [61]

Zetasizer	Size range (diamater)	Size range for Zeta potential (diameter)	Molecular weight range
Nano S	0.6nm to 6µm	–	1000 to 2×10^7 Daltons
Nano Z	–	5nm to 10µm	–
Nano ZS	0.6nm to 6µm	5nm to 10µm	1000 to 2×10^7 Daltons
Nano S90	1nm to 3µm	–	10,000 to 2×10^7 Daltons
Nano ZS90	1nm to 3µm	5nm to 10µm	10,000 to 2×10^7 Daltons

This technique is principally based on illuminating the spherical particles in the solution with a light beam such as a laser and analyzing the intensity fluctuations in the scattered light. [61]
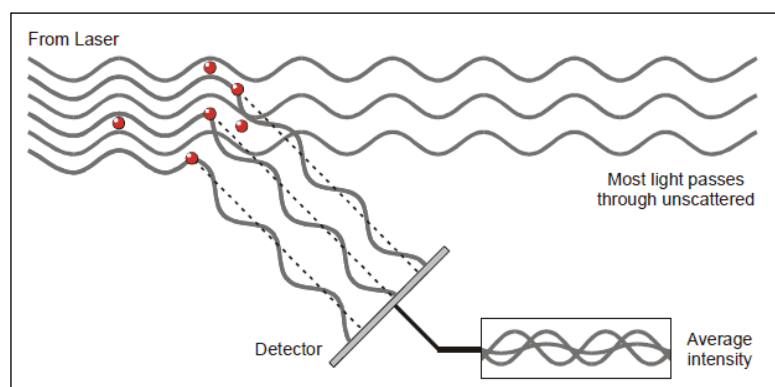
Figure 3.1. Illustration of the scattered light falling on the detector [61]

The scattered light has an intensity which fluctuates at a rate that is dependent upon the size of the particles. For example smaller particles are "kicked" further by the solvent molecules and move more rapidly. Analysis of these intensity fluctuations yields the velocity of the Brownian motion and hence the particle size using the Stokes-Einstein relationship. [62]
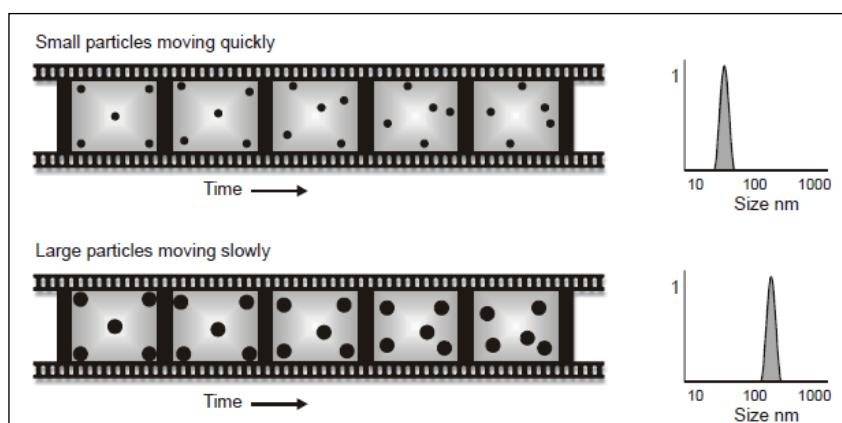
Figure 3.2. Particle size and Brownian motion dependency [61]

3.2.2.   Electron Microscopy

Nanoparticles can be characterized before and after dispersion in liquids. Evaluation of particle size before dispersion in liquids is carried out using electron microscopy techniques. Electron microscopes can be divided into two main types: transmission and

scanning electron microscopes. Both microscopes are scientific instruments that use a beam of highly energetic electrons to examine objects on a very fine scale.

Electron microscopes were developed due to the limitations of light microscopes having 500x or 1000x magnification and a resolution of 0.2 micrometers. In the early 1930's this theoretical limit had been reached and there was a scientific desire to see the fine details of the interior structures of organic cells (nucleus, mitochondria...etc.) which required higher magnification. [63]

The Transmission Electron Microscope (TEM) was the first type of Electron Microscope to be developed and is patterned exactly on the Light Transmission Microscope except that a focused beam of electrons is used instead of light to "see through" the specimen. It was developed by Max Knoll and Ernst Ruska in Germany.

The first Scanning Electron Microscope (SEM) debuted in 1942 with the first commercial instruments around 1965. Its late development was due to the electronics involved in "scanning" the beam of electrons across the sample. [63]

Transmission Electron Microscopy (TEM) is a well known technique for imaging solid materials at atomic resolution. The design of a transmission electron microscope (TEM) is analogous to that of an optical microscope. However, in a TEM high-energy (>100 kV) electrons are used instead of photons and electromagnetic lenses instead of glass lenses. [64]

Briefly, the electron beam is produced by thermionic emission from a tungsten cathode, C and is accelerated towards an aperture in the anode, A, [64] passing through an electron-transparent sample and a magnified image is formed using a set of lenses. This image is projected onto a fluorescent screen or a CCD camera. [64]

This device depends for its operation on the wave nature of the electron and the fact that electric and magnetic fields of suitable geometry are able to function like lenses to refract, deflect, and focus an electron beam. The ultimate limit of resolution of an electron microscope is determined by the wavelength of the electron. [59] The use of visible light

limits the lateral resolution in an optical microscope to a few tenths of a micrometer, on the other hand much smaller wavelength of electrons allows for a resolution of 0.2 nm in a TEM. [64]
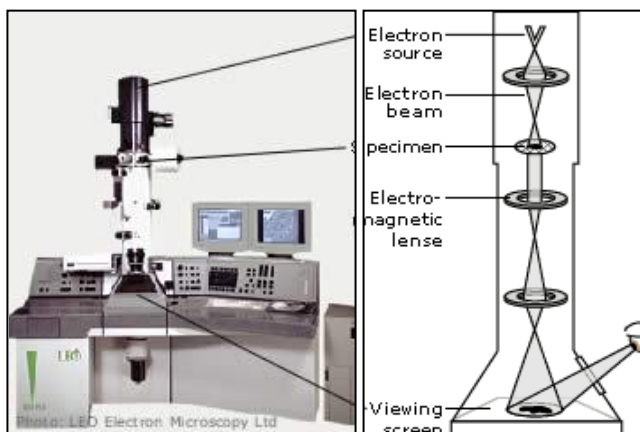
Figure 3.3. Transmission Electron Microscopy Equipment Parts [65]

As a result of the interaction of the electron beam with the specimen, some energy is transferred from the electrons to the sample. The excitation and de-excitation of atoms and molecules in the sample allow the chemical analysis.

Image contrast is obtained by interaction of the electron beam with the sample. In the resulting TEM image denser areas and areas containing heavier elements appear darker due to scattering of the electrons in the sample. This contrast depends on the orientation of a crystalline area in the sample with respect to the electron beam. As a result, in a TEM image of a sample consisting of randomly oriented crystals each crystal will have its own grey-level. In this way one can distinguish between different materials, as well as image individual crystals and crystal defects. [64]

In order to characterize the magnetite and Ag NPs in this study, FEI Company Tecnai G2 F30 which is a service of National Nanotechnology Research Center (UNAM) was used. The corresponding technical data is given in the Table 3.4 below:

Table 3.4. Technical data for TEM - FEI Tecnai G2 F30 [66]

TEM Magnification Range	60x – 1000 kx
Maximum Diffraction Angle	$\pm 12^{o}$
TEM Point Resolution	0.20 nm
Information Limit	0.14 nm

Figure 3.4. Transmission Electron Microscope FEI - Tecnai G2 F30 [66]

Comparing the images of both techniques, Scanning and Transmission Electron Microscopy, it is apparent that TEM methods offer an improvement in resolution over the SEM. In the present study, first of all magnetite and Ag NP samples were characterized by SEM. However, the very small particle sizes of synthesized nanoparticles did not allow visualizing them in every detail. TEM was selected therefore for further characterization of nanoparticles in this study.

3.2.3. X-Ray Diffraction

This study focuses towards the investigation of crystalline structures of synthesized nanoparticles and estimation of their particle sizes using X-Ray diffraction analysis. As all solid matter is divided into two main categories as amorphous or crystalline, nanoparticles in solid form can be easily identified by this technique.

In amorphous structures, the atoms are arranged in a random way similar to the disorder in a liquid. In crystalline structures, the atoms are arranged in a regular pattern, and the smallest three dimensional volume elements describe the crystal. This smallest volume element is called a unit cell. The dimensions of the unit cell are described by three axes h, k, l and the angles between them as alpha, beta, and gamma. [67]

About 95 per cent of all solid materials can be grouped into crystalline category. When X-rays interact with a crystalline substance, a diffraction pattern can be obtained, which is ideally suited for characterization and identification of polycrystalline phases. The X-ray diffraction pattern of a pure substance is, therefore, like a fingerprint of the substance. [67]

X-Ray diffraction involves the measurement of the intensity of X-rays scattered from electrons bound to atoms. Waves scattered at atoms at different positions arrive at the detector. Therefore, the measured intensities yield information about the relative atomic positions. [68]
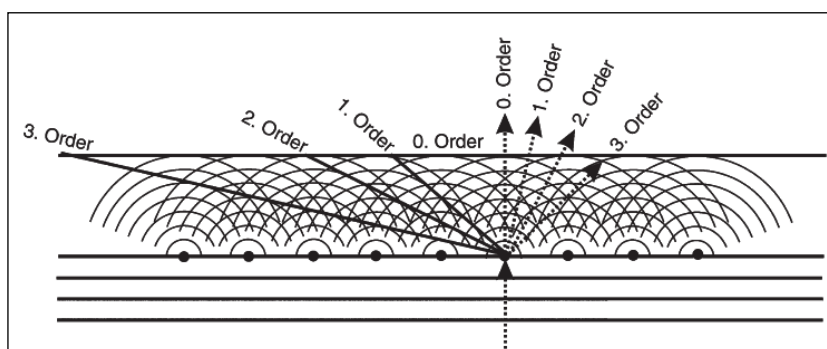
Figure 3.5. X-Ray Diffraction on a Plane [68]

The easiest access to the structural information in powder diffraction is via the well-known Bragg equation, which describes the principle of X-ray diffraction in terms of a reflection by sets of lattice planes. Lattice planes are crystallographic planes, characterized by the index triplet hkl, the so-called Miller indices. Parallel planes have the same indices and are equally spaced, separated by the distance d_{hkl}. Bragg analysis treats X-rays like visible light being reflected by the surface of a mirror, with the X-rays being specularly

reflected at the lattice planes. In contrast to the lower energy visible light, the X-rays penetrate deep inside the material where additional reflections occur at thousands of consecutive parallel planes. From Figure 3.8 the Bragg's equation can be obtained geometrically as:

$$(3.3)$$

where d is the interplanar spacing of parallel lattice planes and 2θ is the diffraction angle, the angle between the incoming and outgoing X-ray beams, λ is the wavelength and n is an integer representing the order of the diffraction peak. [68]
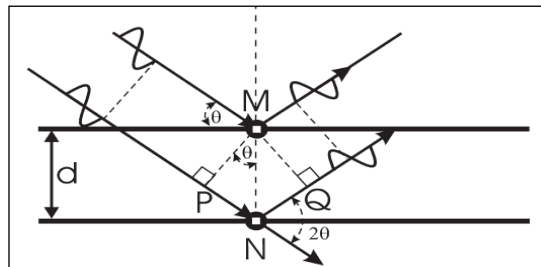
Figure 3.6. Illustration of the geometry used for the simplified derivation of Bragg's Law [68]

X-ray diffractometers consist of three basic elements: an X-ray tube, a sample holder, and an X-ray detector. All diffraction methods are based on generation of X-rays in an X-ray tube or synchrotron radiation. [69] These X-rays are directed at the sample, and the diffracted rays are collected. A key component of all diffraction is the angle between the incident and diffracted rays.
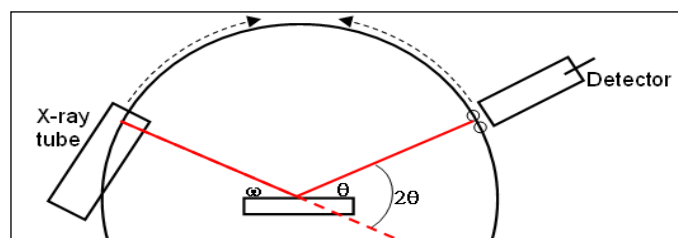
Figure 3.7. X-Ray Diffractometer Working Principle [70]

Similar to microscopy techniques, diffraction methods also require perfectly prepared samples. In powder diffraction method, a mineral is ground up to a fine powder. A powdered mineral sample is placed on a sample stage so that it can be irradiated by the X-ray tube. To detect the diffracted X-rays, an electronic detector is placed on the other side of the sample from the X-ray tube, and it is allowed to rotate to produce angles from 0 to 90°. After a scan of the sample the X-ray intensity can be plotted against the angle 2θ to produce a chart. So, the crystal structure and associated atomic planes can be worked out. [69]
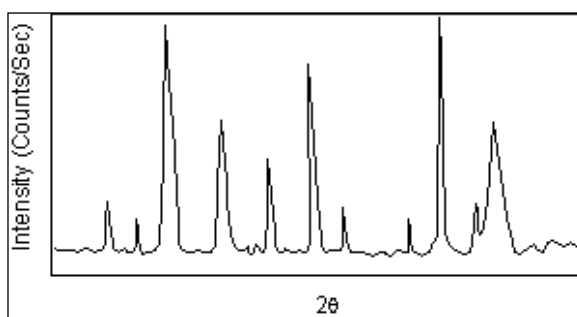
Figure 3.8. Sample X-Ray diffractogram [69]

Since every compound with the same crystal structure will produce an identical powder diffraction pattern, the pattern serves as kind of a "fingerprint" for the substance and thus comparing an unknown mineral with the Powder Diffraction Standards (JCPDS) the unknown sample can be identified. [71]

3.2.4. Vibrating Sample Magnetometer

Samples containing magnetic properties, as in the case of magnetite nanoparticles, can be characterized physically with a vibrating sample magnetometer (VSM). It is used to measure the magnetic behavior of magnetic materials as a function of magnetic field, temperature, and time. VSM has become a widely used instrument for determining magnetic properties of a large variety of materials: diamagnetics, paramagnetics, ferromagnetics and antiferromagnetics in forms of powders, bulk and thin films. [72]

Using a vibrating sample magnetometer the DC magnetic moment can be measured as a function of temperature, magnetic field, angle and time. So, it allows performing magnetization studies. Some of the most common measurements done are: hysteresis loops and saturation magnetization as a function of temperature (thermomagnetic analysis), magnetization curves as a function as a function of angle (anisotropy), and magnetization as a function of time. [72]

Figure 3.9. A typical Vibrating Sample Magnetometer [72]

A VSM operates by first placing the sample to be studied in a constant magnetic field (H). If the sample is magnetic, this constant magnetic field will magnetize the sample by aligning individual magnetic spins, with the field. The stronger the constant field, the larger the magnetization will be. The magnetic dipole moment of the sample will create a magnetic field around the sample. As the sample is moved up and down, this magnetic field is changing as a function of time and can be sensed by a set of pick-up coils. The alternating magnetic field will cause an electric field in the pick-up coils according to Faraday's Law of Induction. This current will be proportional to the magnetization (M) of the sample. As the magnetization increases, the induced current increases also. Using controlling and monitoring software, the system can tell how much the sample is magnetized and how its magnetization depends on the strength of the constant magnetic field. [73]

3.2.5.   UV Spectroscopy

Besides the use of electrons, UV or visible light is also most commonly used to identify an unknown sample. The main difference between certain compounds is their color. In this respect, to determine the relationship between the color and the conjugation of a certain compound, a spectrometer is used analyzing the light reflected from the surface of a solid or passing through a liquid. In the present study, the specific colors of magnetite and silver nanofluids (red brown) enabled to characterize the nanoparticles also by spectrophotometric methods.

Ultraviolet and visible spectrometers have become the most important analytical instrument in the modern day laboratories because of the simplicity, versatility, speed, accuracy and cost-effectiveness. [74]

The working principle of spectroscopic techniques follows a similar route as the one of the microscopy or diffraction. Sample molecules are exposed to light and some of the light energy will be absorbed as the electrons are promoted to higher energy orbital. In a typical spectrometer, a beam of light from a visible or UV light source is separated into its component wavelengths by a prism or diffraction grating. Each monochromatic (single wavelength) beam in turn is split into two equal intensity beams by a half-mirrored device. One beam, the sample beam (colored magenta), passes through a small transparent container (cuvette) containing a solution of the compound being studied in a transparent solvent. The other beam, the reference (colored blue), passes through an identical cuvette containing only the solvent. [74]

The intensities of these light beams are then measured by electronic detectors and compared. The intensity of the reference beam, which should have suffered little or no light absorption, is defined as I_0. The intensity of the sample beam is defined as I. The ultraviolet (UV) region scanned is normally from 200 to 400 nm, and the visible portion is from 400 to 800 nm. [74]

An optical spectrometer records the wavelengths at which absorption occurs. The resulting spectrum is presented as a graph of absorbance (A) versus wavelength. The absorbance of a sample is proportional to the number of absorbing molecules in the spectrometer light beam (e.g. their molar concentration in the sample). For this reason, it is necessary to correct the absorbance value if the spectra of different compounds are to be compared in a meaningful way. The corrected absorption value is called "molar absorptivity", and is particularly useful when comparing the spectra of different compounds and determining the relative strength of light absorbing functions (chromophores). Beer's Law states the molar absorptivity (ε) as:

$$\overline{\qquad} \tag{3.4}$$

where A is the absorbance, c is the sample concentration in moles/liter and l is the length of the light path through the sample in cm. [74]
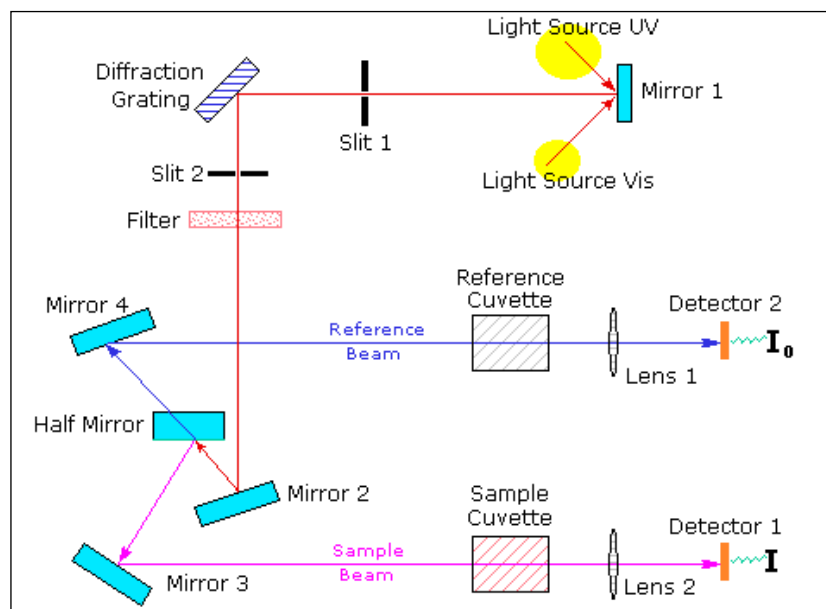
Figure 3.10. Working Principle of UV-VIS Spectrophotometry [74]

3.3. MEASUREMENT OF THERMOPHYSICAL PROPERTIES

3.3.1. Density

Dispersing solid nanoparticles in conventional heat transfer fluids result generally in the enhancements of thermophysical properties such as density, viscosity and thermal conductivity. In this study, these enhancements were analyzed using synthesized magnetite and Ag NPs dispersed in water, hexane and heptane.

In order to measure the densities of various solid, liquid or gas materials experimentally, digital density meters are used. In 1967 the company Anton Paar GmbH presented the first digital density meter for liquids and gases. It was the first instrument to employ the oscillating U-tube principle invented by Dr. Hans Stabinger and Prof. Hans Leopold for density determination. [75]

Figure 3.11. Density meter Anton Paar DMA 4100 [76]

The density range (mass per volume), accuracy and response time generally characterize most of these instruments. In this study, a digital density meter Anton Paar DMA 4100 is used. Below, the technical data is provided in the Table 2.5.

Table 3.5. Technical data for Anton Paar DMA 4100 [76]

Measuring Range	$0 - 3$ g/cm^3
Accuracy	$5\,e^{-5}$
Measuring Temperature	$0 - 90\ ^oC$
Pressure Range	$0 - 10$ bar
Volume of the cell	1 mL
Measuring Time	30 Sec.

In a typical measurement, the sample to be measured is filled into an oscillating hollow, U-shaped glass tube vibrating at a certain frequency. The vibration frequency is related with the mass of the material to be measured and as the mass of the sample increases, the vibration frequency decreases. This frequency is then measured and converted into density. The measuring principle is mainly based on the mass-spring model and the relationship between the oscillation frequency and the sample density can be easily seen by the Equation (3.5):

$$ f = \frac{}{} \tag{3.5} $$

where, f is the oscillating frequency in Hertz, ρ is the density of liquid in kg/m^3, V is the volume of the liquid in m^3, m is the cell mass in kg and c is the spring constant in kg.m^{2}s^{-2}. [77]

By taking into account that volume is highly temperature dependent, the density of a specific substance is also temperature dependent. To measure the density of a sample by changing the temperature, a thermostat is built in the digital density meter controlling the temperature. [77]

3.3.2. Viscosity

Viscosity of a fluid increases as the particle volume concentration increases. To verify this effect, viscosity analyses of synthesized magnetite and Ag NPs dispersed in

water, hexane and heptane were performed using a Brookfield DV-III Ultra Programmable Rheometer, which measures fluid parameters of shear stress and viscosity at given shear rates. The principle of operation of DV-III Ultra is to drive a spindle (which is immersed in the test fluid) through a calibrated spring. The viscous drag of the fluid against the spindle is measured by the spring deflection, which is then measured with a rotary transducer. The viscosity measurement range of the DV-III Ultra (in centipoises or cP) is determined by the rotational speed of the spindle, the size and shape of the spindle, the container the spindle is rotating in, and the full scale torque of the calibrated spring. [78]

Figure 3.12. Brookfield DV-III Ultra Programmable Rheometer [78]

Table 3.6. Rheometer Specifications [78]

Specifications	
Speed Ranges for viscosity tests	0.01 RPM (Increments of 0.01 to 0.99 RPM) 250 RPM (Increments of 1.0 to 250 RPM)
Viscosity Accuracy	+/- 1.0% of full scale range for a specific spindle running at a specific speed
Temperature sensing range and accuracy	+/-1.0^{o}C from -100°C to 150°C +/-2.0^{o}C from +150°C to 300°C

The DV-III Ultra Rheometer is used in conjunction with Brookfield software, RHEOCALC controlling all rheometer functions by the computer. Before readings may be taken, rheometer must be autozeroed. The fluid to be measured (sample) must be in a container. The standard spindle supplied with the DV-III Ultra is designed to be used with a specific sample chamber. The rheometer has the capability of measuring viscosity over a wide range. The process of selecting a spindle and speed for an unknown fluid is by trial and error. An appropriate selection will result in measurements made between 10 and 100 on the instrument per cent torque scale. [78]

3.3.3. Thermal Conductivity Lambda Unit

This study focuses mainly on the enhancement of thermal conductivity of conventional heat transfer fluids such as water, hexane and heptane containing dispersed solid nanoparticles of magnetite and silver. Among the various parameters affecting the thermal conductivity as mentioned in the first section of this thesis, temperature, particle material and particle volume concentration effects were particularly investigated.

The equipment used in this study is a portable Lambda system and uses also the transient hot wire (THW) measurement method. The system mainly enables to determine the thermal conductivity of fluids, powders, gels and fluids containing suspended nanoparticles in a wide temperature range of -30 °C to +190 °C. The temperature range is covered by use of tap water as cooling medium. A cooling water supply of 800 ml/min at a water temperature of +8 °C is sufficient to reach the minimal temperature of -30 °C. The thermal conductivity is measured directly in the sample. The homogeneous temperature control excludes convectional influences. Due to the very high speed of the thermoelectric heating/cooling and the extreme temperature homogeneity short measuring times are achieved. Only small amounts of sample (ca. 50 ml) are sufficient to execute reliable measurements. [79]

Figure 3.13. Thermal Conductivity Equipment [79]

Table 3.7. Thermal Conductivity Equipment Specifications [79]

Specifications	
Measuring Media	Fluids, fluids with nanoparticles, gels, powders
Temperature range	-30 °C* ... +190 °C (-22 °F ... +374 °F),
Resolution/ Accuracy	0.1 °C / 0.1 K
Cooling water temperature LabTemp	+3 °C ... +25 °C (+37 °F ... +86 °F)
Voltage Input	85 V~ ... 264 V~ (47 Hz ... 63 Hz)
Dimensions	LabTemp: 26 x 38 x 16 cm (10 x 15 x 6 in) Lambda: 26 x 38 x 16 cm (10 x 15 x 6 in)

4. SYNTHESIS OF MAGNETITE NANOFLUIDS

Synthesis of magnetite (Fe_3O_4) nanoparticles has long been of great interest because of their technological applications especially in the form of ferrofluids. A ferrofluid is a colloidal suspension of magnetite particles in a liquid medium having unusual properties due to the simultaneous fluid mechanic effects and magnetic effects. [80]

4.1. SYNTHESIS OF MAGNETITE NANOPARTICLES DISPERSED IN WATER PHASES

There exist different methods for synthesizing magnetite nanoparticles soluble in polar base fluids. The chemical precipitation synthesis method is the most commonly used method which aims to produce hydrophilic magnetite nanoparticles using iron sulphate hepta-hydrate and iron chloride anhydrous as the iron content and capric acid as the surfactant.

In a typical synthesis, 40 mL distilled water is first de-aerated by passing nitrogen gas through the reacting medium for twenty minutes in a round bottom flask. At the end of deaeration procedure, required amounts of iron sulphate hepta-hydrate and iron chloride anhydrous are added to the reaction medium under continuous agitation. The color of the solution immediately turns to dark orange. The reacting mixture is then heated up to 70°C at a constant rate. At that temperature, the surfactant solution capric acid in ammonium hydroxide is quickly added and at the same time nitrogen gas is disconnected. As the reaction proceeds, blackening of the solution is observed showing the formation of magnetite nanoparticles. The mixture is further heated up to 80°C and stirred at that constant temperature for half an hour. At the end, the final solution is allowed to cool down to room temperature and magnetite nanofluids are obtained.

Table 4.1. Materials for the Synthesis of Magnetite Nanoparticles in Water

Chemicals	Formula	Amounts (g/ml)
Iron Sulfate Hepta-Hydrate	$FeSO_4.7H_2O$	2.412 g
Iron Chloride (III) Anhydrous	$FeCl_3$	2.82 g
Capric Acid	$C_{10}H_{20}O_2$	2 g
Ammonium Hydroxide	NH_4OH	20 mL
Distilled Water	H_2O	80 mL
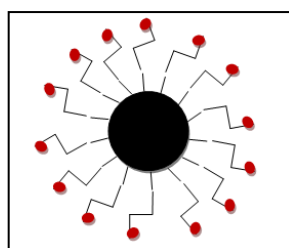
Figure 4.1. Surfactant and magnetite particle prepared by water synthesis method

4.2. SYNTHESIS OF MAGNETITE NANOPARTICLES DISPERSED IN OIL PHASES

The highest demand to use iron oxide nanoparticles for future magnetic nanodevices and biomedical applications lead to practical routes for the synthesis of iron oxide nanoparticles having narrow size distributions with diameters smaller than 20 nm. The synthesis route of hydrophobic magnetite nanoparticles is a more complex and energy consuming method compared to that of hydrophilic magnetite nanoparticles.

This convenient procedure for obtaining Fe_3O_4 nanoparticles with narrow size distribution implies the reaction of a metal precursor with a long-chain alcohol. The synthesis involves high reaction temperatures and a special experimental setup providing N_2 blanket and mercury manometer to control the pressure of the reacting system.

In a typical synthesis, Fe (III) acetylacetonate responsible for the iron content and different surfactants are mixed in a round bottom flask in the solvent dibenzylether. Using different surfactants agglomeration is prevented, the structure of magnetite nanoparticles is controlled and more stable nanofluids are obtained. Under a flow of N_2, the mixture is heated up to 100^oC at a rate of 2.5^oC/min and kept at that temperature for half an hour. Then, this solution is further heated to 180^oC. At this temperature, nitrogen blanket is connected to the round bottom flask in order to apply pressure on the reaction mixture allowing the solution to reach higher temperatures without any reflux taking place. Following this step, all reactions are carried out under N_2 atmosphere.

Then, the mixture is heated up to 200^oC and kept at that temperature for 2 hours and at the end of this time period again it is heated up to 300^oC with the rate of 2.5^oC/min. As a last step, the black-brown solution is kept for an hour at that temperature and finally cooled to room temperature by removing the heat source.
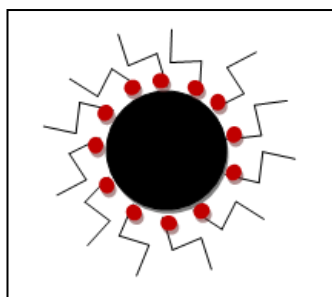
Figure 4.2. Surfactant and magnetite particle prepared by oil synthesis method

Obtained nanofluid is further cleansed by centrifugation in centrifuge tubes containing 6 mL magnetite nanofluid and 7 mL methanol. All samples are centrifuged for 15 minutes at 7500 rpm and black nanoparticles are precipitated out of the solution. In order to obtain clear liquid phase and precipitated magnetite nanoparticles, centrifugation can be repeated 3 or 4 times.

Finally, these solid nanoparticles are left overnight in a vacuum oven for removing the final undesired liquid. With this last step, prepared nanoparticles can be dispersed in any kind of solvent such as oil (hexane or heptane).

Table 4.2. Materials for the Synthesis of Magnetite Nanoparticles in Oil

Chemicals	Formula	Amounts (g/ml)
Iron(III) Acetyl Acetonate	$C_{15}H_{21}FeO_6$	0.706 g
Oleylamine	$C_{18}H_{37}N$	1.69 mL
Oleic Acid	$C_{18}H_{34}O_2$	1.90 mL
1,2 – Tetradecanediol	$CH_3(CH_2)_{11}CH(OH)CH_2OH$	2.3039 g
Dibenzyl ether	$C_{14}H_{34}O_2$	20 mL
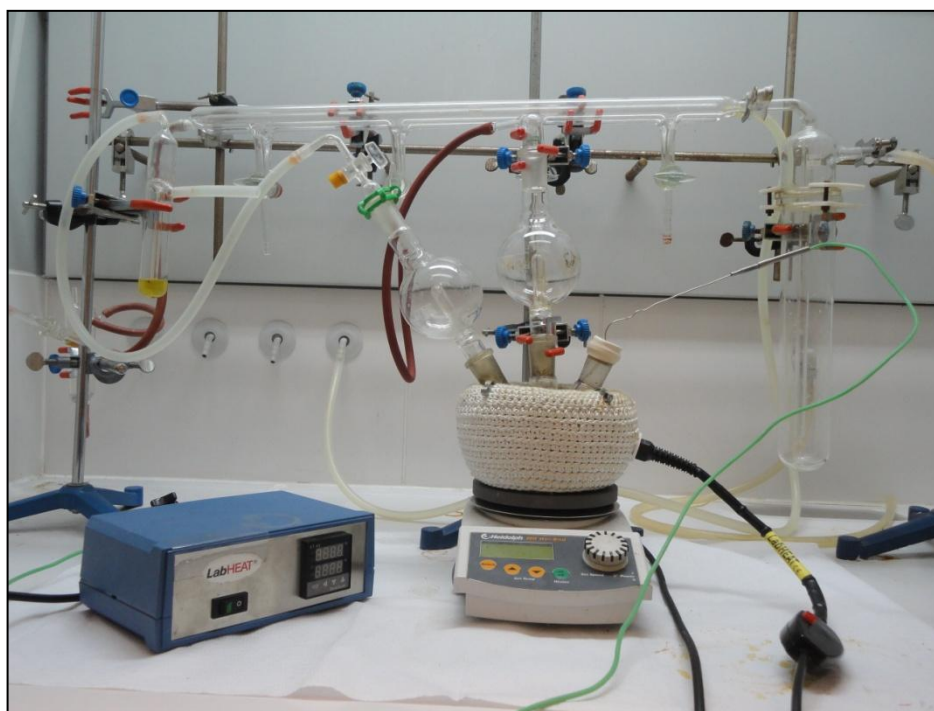
Figure 4.3. Hydrophobic Magnetite Nanoparticle Synthesis Experimental Setup

4.3. TEST FOR DETERMINATION OF IRON CONTENT IN THE MAGNETITE NANOPARTICLES

The magnetic property of a magnetic fluid originates from the magnetite core at the center of each nanoparticle. In order to quantify the amount of magnetite in magnetic fluids, a colorimetric iron analysis technique was developed. By this method, the Fe^{2+} and Fe^{3+} concentrations in solution can be determined, from which the total amount of magnetite in the fluid is calculated. The technique is mainly based on the ability of certain organic compounds to form complexes with the free iron ions in solution. The light absorption of formed iron complex at a certain wavelength is then measured by UV-VIS Spectrophotometry. The organic compound used for this colorimetric technique is 4,5-dihydroxy-1,3-benzenedisulfonic acid, disodium salt, also known as Tiron reagent. This compound forms complexes with Fe^{2+} and Fe^{3+} ions in a ratio of three Tiron molecules to one iron molecule and shows an absorbance at 480 nm. [81]

In a typical Tiron test, 0.1 mL of the concentrated magnetic nanofluid is taken and mixed with 0.4 mL of 37% concentrated HCl in a 25 mL volumetric flask to release the iron into solution as Fe^{2+} and Fe^{3+}. This solution is then heated under a heat gun at approximately $150^{o}C$ for a few seconds until the color of the solution turns to yellow. The hot acidic solution is left at room temperature to cool down and afterwards it is mixed with the proper amount of Tiron solution. After this step, 3 mL from 4 M of sodium hydroxide is added to the final solution to neutralize the acid. Upon the addition of the base, the color change to red is observed. The solution is then diluted using distilled water until the volume of the final solution reaches 25 mL.

The solution can be further diluted by the factor of 8-10 depending on the concentration of the final solution, so that it can be read by the UV-Spectrophotometer at 480 nm. The absorbance value is then inserted into the Equation 4.1 and the concentration is determined with the units of g/mL.

$$ \frac{\quad}{\qquad\qquad} \tag{4.1} $$

Table 4.3. Materials for the Tiron Test

Chemicals	Amounts (g/ml)
Magnetite Nanofluid	0.1 mL
Hydrochloric Acid (37%)	0.4 mL
Tiron Solution	0.083 g/mL
Sodium Hydroxide (4M)	3 mL

5. CHARACTERIZATION OF MAGNETITE NANOPARTICLES

Depending on the chemical identity, magnetic property and polydispersity, magnetic nanoparticles find wide industrial application areas. After the synthesis of magnetite nanoparticles, the next step is therefore to characterize the nanoparticles in terms of their size, size distributions and crystallinity. Magnetite nanoparticles synthesized by the above mentioned techniques are examined by Transmission Electron Microscopy (TEM) and Dynamic Light Scattering (DLS) and X-Ray diffraction (XRD) to obtain structural information.

5.1.Transmission Electron Microscopy (TEM) Analyses

Appropriate sample preparation is a crucial step in the TEM analysis process to obtain well-dispersed particles. Magnetite nanoparticle samples for transmission electron microscopy analysis were prepared by placing a small amount of a very dilute dispersion of nanoparticles on amorphous carbon-coated copper grid and allowing the solvent to evaporate at room temperature. TEM images were obtained on a Philips Tecnai TEM operating at approximately 100 kV. As illustrated in the figures below, images indicate that the obtained hydrophobic and hydrophilic magnetite nanoparticles are nearly spherical.

Hydrophobic nanoparticles have a core diameter of approximately 6 nm and a hydrodynamic diameter of 9.7 nm and the hydrophilic magnetite nanoparticles have a core diameter of 8 nm.
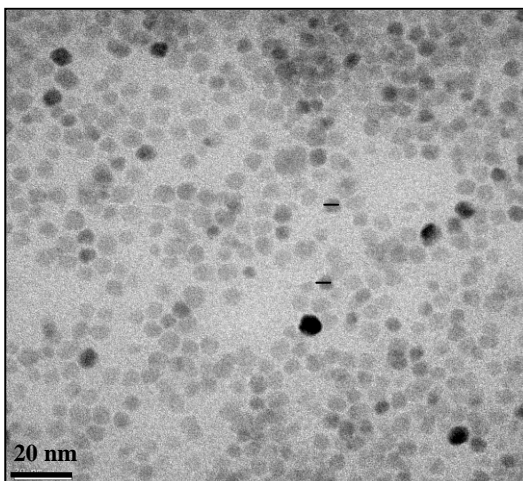
Figure 5.1. TEM image of magnetite nanoparticles prepared by oil synthesis
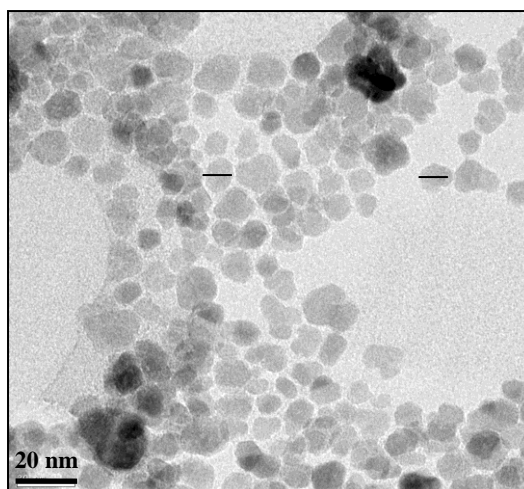
Figure 5.2. TEM image of magnetite nanoparticles prepared by water synthesis

TEM images also indicate that both types of nanoparticles have narrow size distribution without any noticeable agglomeration. The monodispersity is mainly due to the reaction conditions. During the magnetite/oil synthesis procedure, the reacting mixture is gradually heated to 300°C in dibenzyl ether, where direct heating would result in magnetite nanoparticles with wide size distributions.

5.2. DYNAMIC LIGHT SCATTERING (DLS) ANALYSES

In order to determine the radius of small particles in Brownian motion in a solution, dynamic light scattering technique is generally used. Malvern Zeta-Sizer Nano is the device utilized for measuring the size of the nanoparticles in this study. The analysis technique is mainly based on the principle of the particle diffusion speed due to Brownian motion. In a typical measurement, the intensity of the scattering light is measured where a very dilute amount of suspension is placed in a special cuvette and illuminated by laser light. Depending on the size of the particles, the intensities will vary and the particle size will be determined.

Hydrophobic and hydrophilic magnetite particle suspensions are examined for their sizes and size distributions and the corresponding profiles are shown in the figures below as intensity, volume and number percentages versus particle diameters.
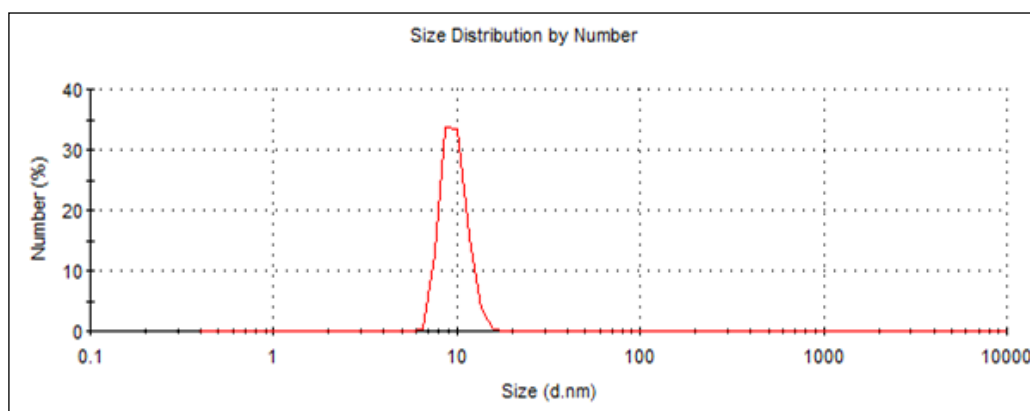
Figure 5.3. Magnetite- Heptane Nanoparticles (9.7 nm)
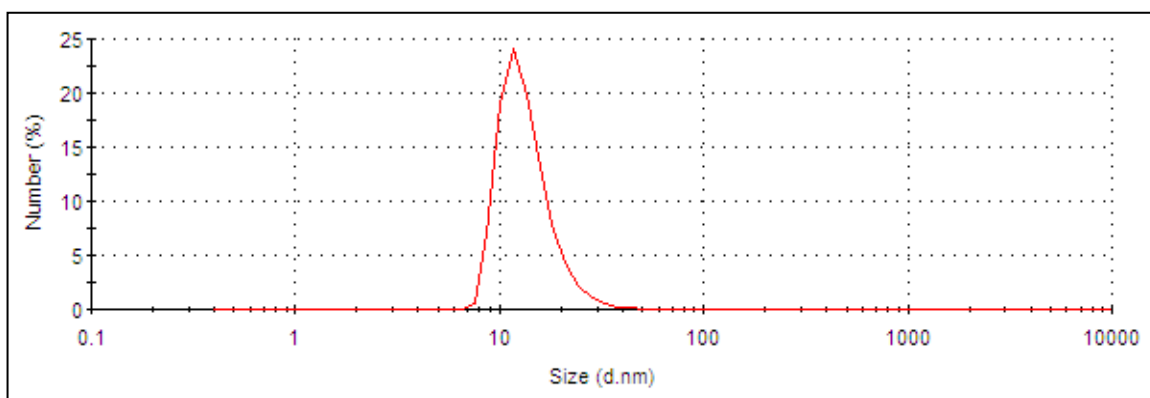
Figure 5.4. Magnetite-Water Nanoparticles (10.14 nm)

5.3. X-RAY DIFFRACTOMETER (XRD) ANALYSES

X-Ray analyses require also a special sample preparation process. Aqueous magnetite nanoparticles were obtained as black precipitates by evaporating water in a freeze dryer. On the other hand, hydrophobic nanoparticles dispersed either in hexane or heptane were obtained as black solid nanoparticles by evaporating the solvents using a rotary evaporator.

According to the X-ray diffractogram for the sample of hydrophobic magnetite nanoparticles shown in the figures below the particles were identified basically as pure magnetite. The position and relative intensity of all diffraction peaks (111, 220, 311, 400, 422, 511, 440, 620 and 533) were indexed as the corresponding standard magnetite powder diffraction data (reference code: JCPDS 01-088-0315) and according to the results it can be concluded that no characteristic peaks of impurities were observed.
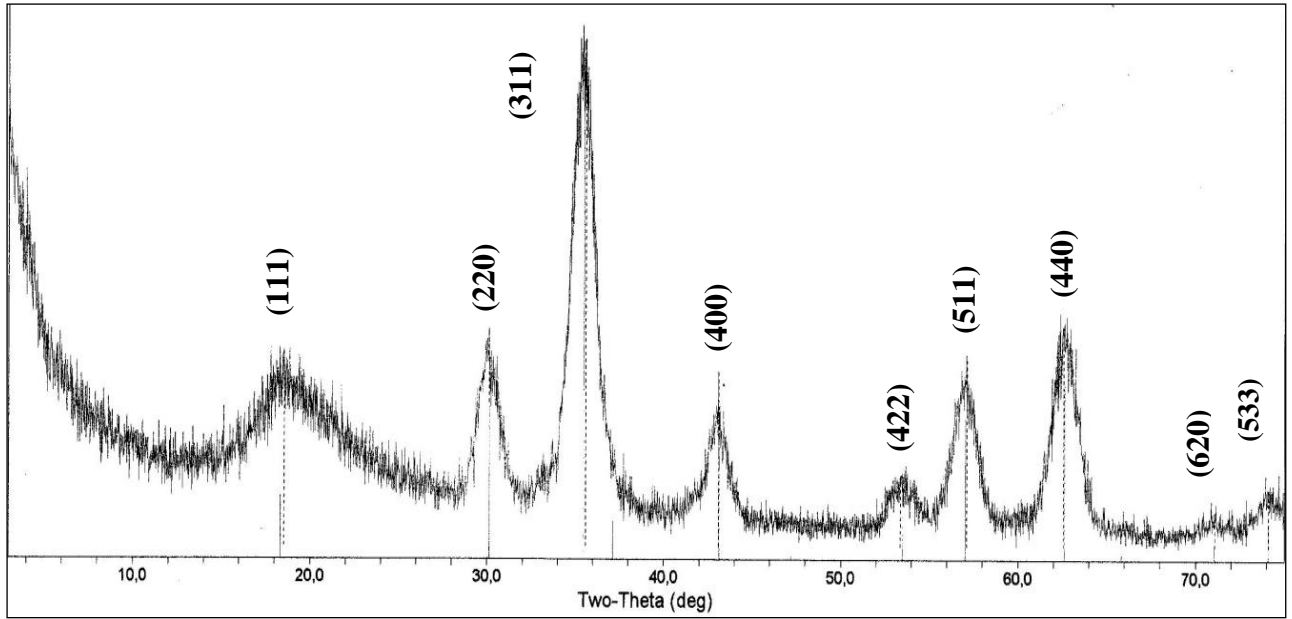
Figure 5.5. Magnetite – Oil X-Ray Diffractogram

5.4. VIBRATING SAMPLE MAGNETOMETER (VSM) ANALYSES
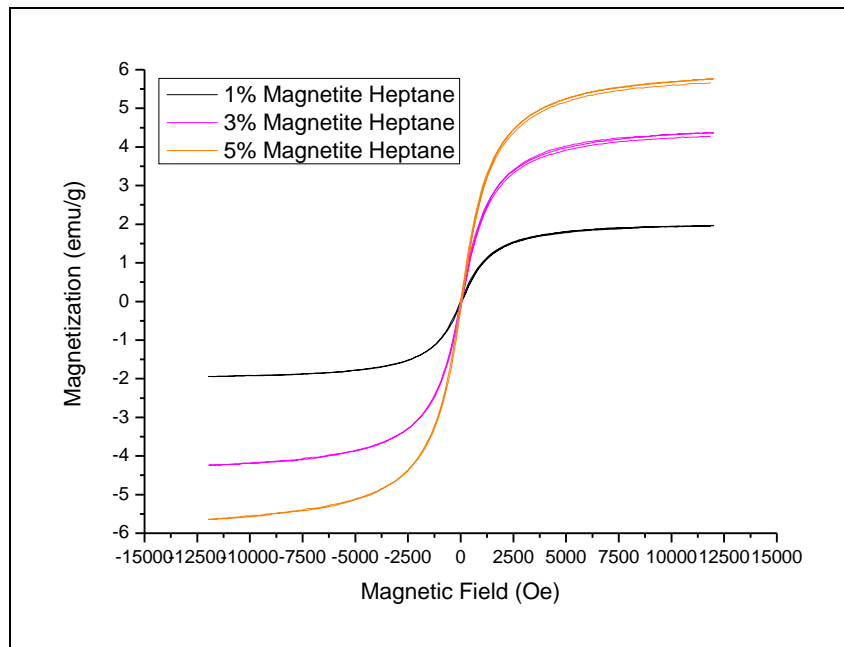
Figure 5.6. Hysteresis loop of the Fe_3O_4 nanoparticles at 296 K

The magnetic properties of Fe_3O_4 samples were analyzed by a vibrating sample magnetometer (VSM). Figure 5.6 shows a typical magnetization curve. The saturation magnetization of synthesized magnetite nanoparticles were found to be equal to approximately 6 emu/g for 5 wt% of magnetite nanoparticles, 4 emu/g for 3 wt% of nanoparticles and 2 emu/g for 1 wt% of magnetite nanoparticles.

The hysteresis loop which is characteristic of the ferrimagnetic behavior is clearly observed in the figure confirming that Fe_3O_4 nanoparticles are characteristic of superparamagnetic properties. From the magnetization curve, it can be also concluded that the saturation magnetization (M_s) of the Fe_3O_4 nanoparticles increase from 2 to 6 emu/g when the concentration of magnetite increases from 1 to 5 wt%, which can be attributed to the increase of weight and volume of magnetite nanoparticles. [82]

Magnetic measurements on all Fe_3O_4 nanoparticles indicate that the particles are superparamagnetic at room temperature, meaning that the thermal energy can overcome the anisotropy energy barrier of a single particle, and the net magnetization of the particle assemblies in the absence of an external field is zero. Under a large external field, the magnetization of the particles aligns with the field direction and reaches its saturation value.

6. SYNTHESIS OF SILVER NANOFLUIDS

Nanoparticles ranging in size from 1 nm to 100 nm show important heat transfer, optical, magnetic, etc. properties that cannot be revealed by the bulk materials. Among the noble metals, Ag NPs have become the focus of intensive research due to their plasmonic and heat transfer applications. The amount of heat passing in unit time through unit surface in a direction to this surface is defined as the thermal conductivity. Pure metallic silver is the highest metal among the others having a thermal conductivity of 406.0 W/mK.

There exists a rich variety of procedures for preparing Ag NPs as stable, colloidal dispersions in water or in organic solvents. Various radiation-, chemical-, photo-, and electro-chemical methods and theories have been used for the preparation and characterization of these nano-sized particles. For the stabilization of these small particles, different types of polymers, ligands, solid matrix and surfactants has been suggested. These synthesized nanoparticles are further dispersed in various base fluids and nanofluids are obtained. Production of these nanofluids becomes a new challenge for the heat transfer fluids since the thermal conductivity of nanofluids are anomalously enhanced at a very low volume fraction of nanoparticles.

6.1. SYNTHESIS OF SILVER NANOPARTICLES THROUGH THE TOLLEN'S PROCESS

A versatile and effective technique for the preparation of finely-dispersed aqueous silver colloids is examined though modified Tollen's process. This synthesis route is environmentally friendly because of non-toxic chemicals used. The fundamental reaction involved in the Tollen's process is:

$$Ag(NH_3)_2^+{}_{(aq)} + RCHO_{(aq)} \rightarrow Ag_{(s)} + RCOOH_{(aq)}$$
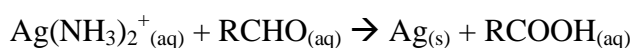
In a typical synthesis, three separate aqueous solutions are prepared (A) silver solution, (B) activator solution, (C) reducer solution. The silver solution contains 24-30% (by weight) silver nitrate and 28-34% ammonium hydroxide. The activator solution

contains 7-12% sodium hydroxide and 6-10% ammonium hydroxide. The reducer solution contains 0.3% formaldehyde and 27-33% sorbitol. These three solutions are prepared daily as fresh solutions. 0.5 mL of the concentrated silver solution A is mixed with 14 mL distilled water and 0.5 mL of the concentrated activator solution B are put into another container and the solution "SAB" is further diluted to 300 mL. In another container, 0.5 mL of the concentrated reducer solution C is measured and also diluted to 300 mL "SC".

0.9 mL of both SAB solution and SC solution are further mixed and diluted to 10 mL with distilled water. The final solution is immersed in a sonication bath and the reaction takes place under N_2 gas atmosphere controlling the temperature and the reaction times. [29]

Table 6.1. Materials for the Synthesis of Ag NPs through Tollen's Process

Chemicals	Formula/Structure	Amounts (g/mL)
Silver Nitrate	$AgNO_3$	3 g
Sodium Hydroxide	$NaOH$	10 g
Formaldeyhde	CH_2O	92 μL
Sorbitol	$C_6H_{14}O_6$	8.25 g
Ammonium Hydroxide	NH_4OH	~ 100 g
Distilled Water	H_2O	~ 600 mL

6.2. SYNTHESIS OF SILVER NANOPARTICLES THROUGH REDUCTION METHOD

Another way to synthesize Ag NPs is the reduction method. The chemical reduction is one of the most frequently applied synthesis method for the preparation of colloidal metal particles, because of its simple operation and simple equipments needed. Dispersions of colloidal silver are prepared by the reduction of mainly silver nitrate, with different reductants in the presence of various stabilizing agents. Commonly used reductants are sodium borohydride, sodium citrate, ascorbic acid, and elemental hydrogen. The reduction mechanism follows the route consisting of three main steps. In the first step, the silver ions (Ag^+) are reduced and silver atoms (Ag^o) are formed followed by agglomeration into

oligometric clusters. These clusters eventually lead to the formation of colloidal silver particles. [83]

6.2.1. Synthesis of Ag NPs through Citrate Reduction Method

The most frequent preparation of Ag NPs is the reduction of silver salts by sodium citrate described by Lee and Meisel. [33]

In a typical synthesis, all glassware is soaked in chromic acid and left overnight to prevent all impurities. The solutions are prepared daily fresh using distilled water. 90 mg of silver nitrate ($AgNO_3$) is dissolved in 500 mL of distilled H_2O and the solution is brought to boiling. A solution containing 1% Sodium Citrate (10 mL) is then added to the boiled reaction medium. The solution is kept on boiling for approximately 1 hour until the volume decreased to 250 mL. [33]

Table 6.2. Materials for the Synthesis of Ag NPs through Citrate Reduction Method

Chemicals	Formula/Structure	Amounts (g/mL)
Silver Nitrate	$AgNO_3$	18 mg
Sodium Citrate (1%)	$C_6H_5Na_3O_7 \cdot 2H_2O$	2 mL
Distilled Water	H_2O	100 mL

6.2.2. Synthesis of Ag NPs through Borohydride Reduction in Polyvinyl alcohol

In a typical synthesis, 0.002 M sodium borohydride ($NaBH_4$) solution is freshly prepared and 30 mL is put to an Erlenmeyer flask placing it in an ice bath on a stirring plate. After 20 minutes of stirring, 2 mL of 0.001 M silver nitrate ($AgNO_3$) is added into the stirring $NaBH_4$ solution at approximately 1 drop per second. As soon as all of the $AgNO_3$ is added, stirring is stopped. The solution immediately turns to yellow indicating the presence of silver colloids. In order to prevent the aggregation of the colloidal solution, enough solid PVA (poly vinyl alcohol) is added slowly to obtain a 4% solution overall. [84]

Table 6.3. Materials for the Synthesis of Ag NPs through PVA Stabilization

Chemicals	Formula/Structure	Amounts (g/mL)
Silver Nitrate	$AgNO_3$	0.005 M – 20 mL
Sodium Borohydride	$NaBH_4$	0.002 M – 60 mL
Poly vinyl alcohol (1%)	$(C_2H_4O)_x$	1% - 10 mL
Distilled Water	H_2O	~ 100 mL

6.2.3. Synthesis of Ag NPs through Borohydride Reduction Dispersed in Gum Arabic

Despite the many applications of Ag NPs, there is little progress in developing a facile green route for the formation of robust metal nanoparticles and metal nanoparticle–polymer composites. The most significant disadvantages of earlier studied methods are the use of toxic surfactants, organic solvents and the polydispersities. Later, the preparation of Ag NPs with water-soluble polymers, gelatin, poly(vinyl alcohol) and methylhydroxyethyl, cellulose are reported.

Over the past decades, green chemistry methods have been applied to design greener nanomaterials by reducing the use of hazardous chemicals. Medina-Ramirez *et al*. have reported a convenient method to achieve stable colloidal solutions of Ag NPs having narrow size distribution using green chemistry methods. The synthesis is carried out at low temperatures using green reducing agents. [35]

In a typical synthesis of hydrophilic Ag NPs, silver powder is obtained through the reaction of silver nitrate ($AgNO_3$) with sodium borohydride ($NaBH_4$), where gum arabic serves as a dispersing agent. First of all, as the procedure is primarily based on a reduction reaction the glassware are soaked in chromic acid and left in it overnight. Then they are all rinsed with distilled water. Silver nitrate and sodium borohydride solutions are prepared freshly before starting an experiment. [35]

The chemical reaction is the sodium borohydride reduction of silver nitrate:

$$AgNO_3 + NaBH_4 - Ag + ½ H_2 + ½ B_2H_6 + NaNO_3$$
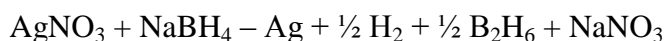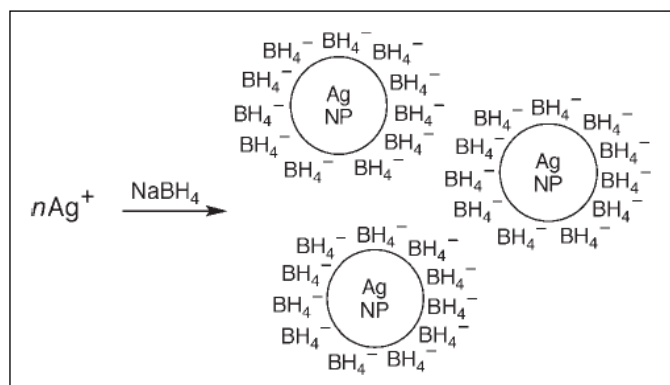
Figure 6.1. Synthesis and Study of Ag NPs [85]

Aqueous Gum Arabic solution (3% (m/v) 50 mL) is stirred in a round bottom flask for 30 min at 60°C. 3.5 mL of 0.1 M $AgNO_3$ solution is then added to it under continuous stirring and the mixture is kept at those conditions for 15 minutes to allow the diffusion of metal ions to the pores of the dispersing agent. 3.5 mL of reducing agent 0.1 M Sodium borohydride is injected into the solution incrementally under continuous agitation. For the formation of Ag NPs, the mixture is heated to 85°C and stirred at that temperature for 3 hours for the hydrolysis of excess dispersing agent.

Obtained colloidal suspension of Ag NPs is further cleansed with absolute ethanol through centrifugation at 7500 rpm for 30 minutes. The supernatant is then removed and centrifugation is repeated two or three times according to the samples obtained.

Table 6.4. Materials for the Synthesis of Ag NPs in Water

Chemicals	Formula	Molarity (M)/ Weight Percentage (%)	Amounts (g/ml)
Silver Nitrate	$AgNO_3$	0.1 M	3.5 mL
Gum Arabic	-	3 wt%	1.5 g
Sodium Borohydride	$NaBH_4$	0.1 M	3.5 mL
Distilled Water	H_2O	-	50 mL

In the synthesis method, instead of gum arabic, gelatin is used as the dispersing agent and also ascorbic acid reduction is followed to study the effects of varying reducing and dispersing agents on the particle size, crystallinity, polydispersity and stability of the nanoparticles. All results are tabulated in the next section.

6.3. SYNTHESIS OF HYDROPHOBIC AG NPS DISPERSED IN HEXANE

In the synthesis for hydrophobic Ag NPs, an inexpensive; versatile and very reproducible method is used. For obtaining very small Ag NPs with low polydispersities, only the following reagents: silver acetate, oleylamine, oleic acid and a solvent are required. [27]

Silver acetate is used as the silver content, the surfactants oleylamine and oleic acid help to reduce silver acetate to Ag NPs. In a typical synthesis, 150 mL hexane is started to reflux in a 250 mL three-neck round bottom flask containing glass beads to provide efficient mixing. The flask is placed in an electrothermal heating mantle so that the reaction can be kept at a constant temperature.

At the same time 3.75 mL oleylamine and 3.75 mL oleic acid are mixed with 150 mg silver acetate (AgOAc), where oleylamine and oleic acid serve as surfactants. The mixtures are injected quickly into the refluxing hexane and three neck round bottom flask is sealed carefully. The reaction proceeds over the course of two days and the size of the Ag NPs can be effectively controlled with the solvent hexane and the growth temperature.

After two days, obtained silver nanofluids are further cleaned by precipitation with methanol in a centrifugation flask at 4500 rpm for 15 minutes. According to properties of solid Ag nanoparticles, centrifugation can be repeated two or three times. Finally, Ag NPs can be dispersed in hexane.
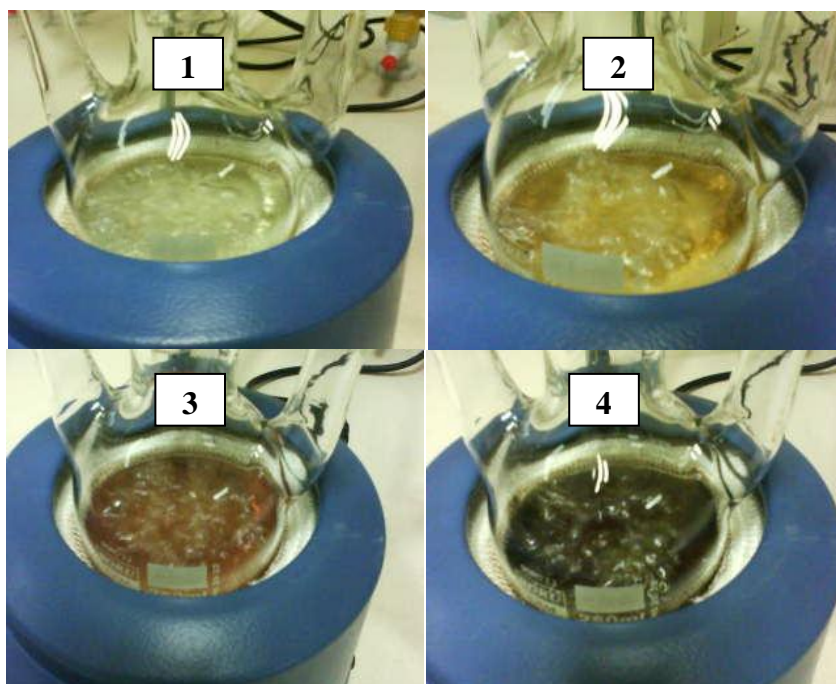
Figure 6.2. Progress of Silver-Hexane Synthesis Reaction with Time

Table 6.5. Materials for the Synthesis of Ag NPs in Hexane

Chemicals	Formula	Amounts (g/ml)
Silver Acetate	$AgC_2H_3O_2$	150 mg
Oleic Acid	$C_{18}H_{34}O_2$	3.75 mL
Oleylamine	$C_{18}H_{37}N$	3.75 mL
Hexane	C_6H_{14}	150

7. CHARACTERIZATION OF SILVER NANOPARTICLES

7.1. SILVER NANOPARTICLES THROUGH TOLLEN'S

Through the Tollen's process, Ag NP dispersions are obtained under sonication. For the specific procedure described in the previous section, the color of the reacting solution changes from clear at the time of mixing, through light brown, brown and finally to yellow-green.

The color changes indicate different stages in the formation of Ag NPs and allow the control of the progress of reaction by means of spectrophotometric analysis. The UV-VIS absorbance spectra were recorded with a Perkin Elmer Lambda 25 spectrophotometer, and quartz cuvettes were used for the measurement. Distilled water was applied as the reference sample to take "blank" spectrum for all measurements.

At different reaction times (13, 23, 35 and 45 min) samples were taken from the reacting solution and analyzed. According to the UV spectra shown in the Figure 7.1, the maximum absorbance peak appears at the same wavelength. For the sample at a reaction time of 13 minutes, the peak corresponds to 435 nm, for the sample at 23 minutes to 440 nm, for the one at 35 minutes to 436 nm and for the sample at 45 minutes corresponds to 437 nm. As the reaction proceeded, Ag NPs were formed, the brown color intensified and the absorbance increased slightly at all wavelengths indicating the increase in the concentration of Ag NPs.
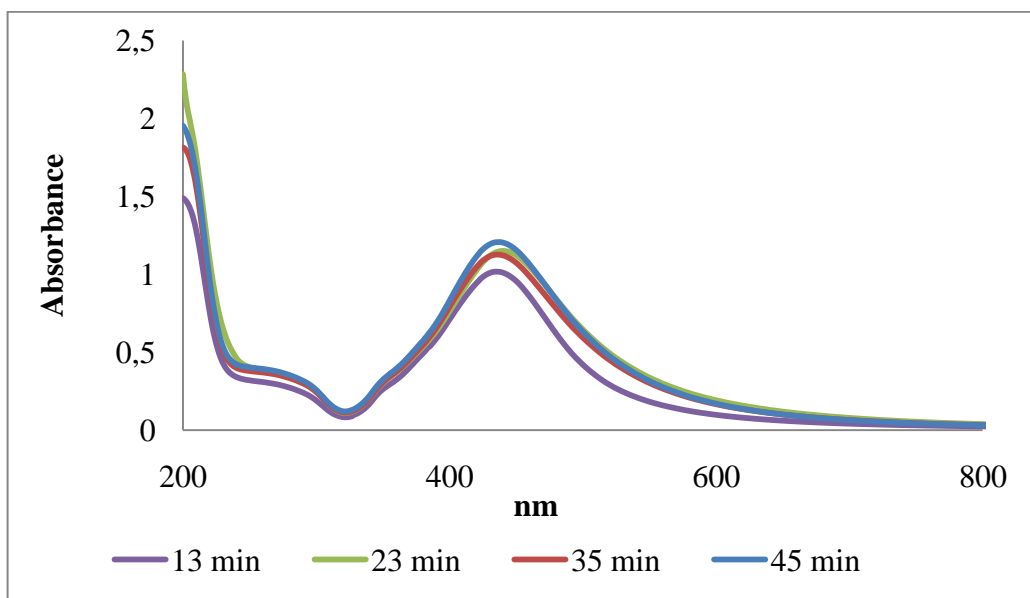
Figure 7.1. UV Spectra for Ag NPs through Tollen's Process

In order to analyze the Ag NP dispersions in terms of their size distributions dynamic light scattering is applied. Figure 7.2 shows relatively narrow size distributions for Ag NP samples at different reaction times. The black line represents the sample at 13 minutes having an average diameter of 38 nm, the green line represents the sample at 23 minutes with 41 nm, the blue line is for the sample at 35 minutes with a size of 42 nm and the red line is for 45 minutes having a diameter of 51 nm. As the reaction time proceeds, the size of the Ag NPs slightly increases.
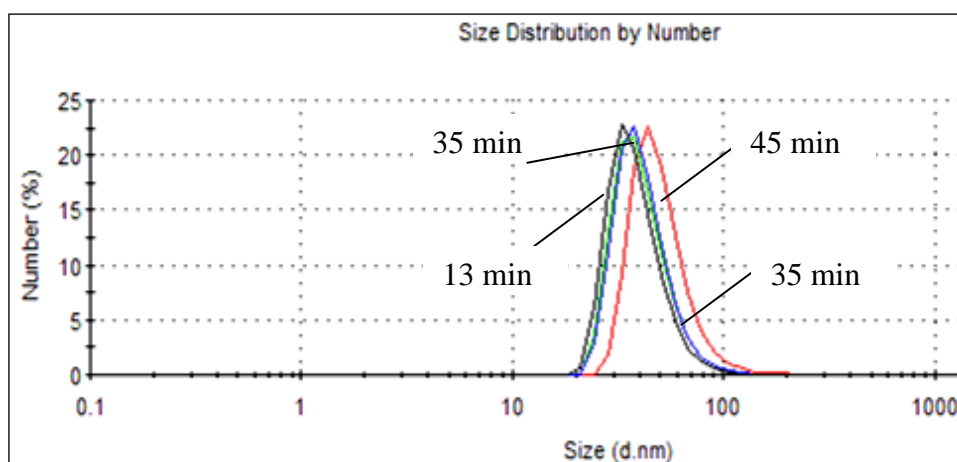
Figure 7.2. Number Average Size Distribution of Ag NPs through Tollen's Process

However, the Ag NP dispersions were not stable and precipitated after several days. Therefore, further studies to characterize and investigate other properties of Ag NPs were omitted. To sum up, the particle size, size distribution, and stability of Ag NP dispersions depend on the temperature of the process, initial silver concentration, pH of the medium, reaction times and intensity of ultrasound. The stability and other properties of the synthesized nanoparticle dispersions can be enhanced by using additional components such as surfactants during the synthesis.

7.2. CITRATE REDUCED AG NPS

In citrate reduction method, Ag NP dispersions were obtained having a greenish yellow color. The color indicates the presence of larger particles resulting in high absorbance values in the long wavelength range. Citrate reduction of silver ions generally yield large Ag NPs having a wide range of morphologies, depending upon the reaction conditions, due to citrate's complexing agent role.

According to dynamic light scattering analysis, diluted Ag NP sample has an average diameter of 318 nm. The large size and broad size distribution of Ag NPs affect the stability of nanofluid. This synthesis is therefore not appropriate for further studies, which requires stable and smaller nanoparticle dispersions.
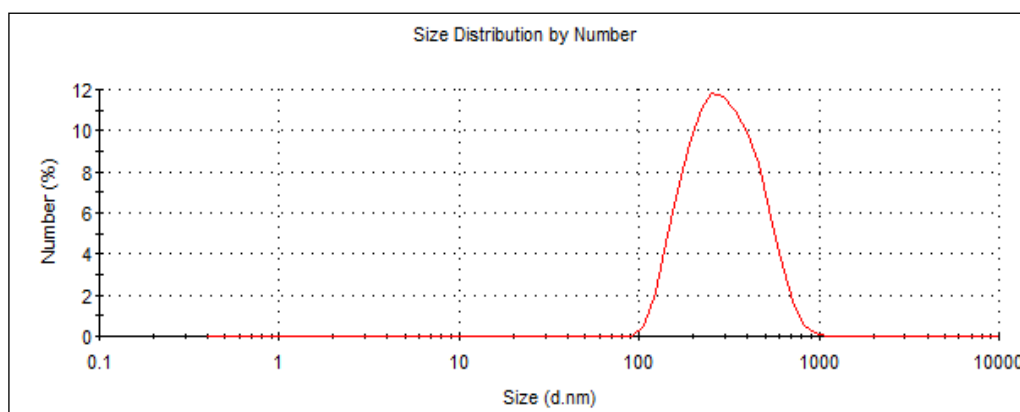
Figure 7.3. Number Average Size Distribution of Ag NPs through Citrate Reduction Process

7.3. POLYVINYL ALCOHOL STABILIZED SILVER NANOPARTICLES

Another synthesis method applied frequently for Ag NP synthesis is the sodium borohydride reduction technique. Sodium borohydride is one of the strongest reducing agents compared to ascorbic acid or sodium citrate. Therefore, it is generally used to obtain nanoparticles with narrow size distributions.

In a typical nanoparticle synthesis process, the type of the surfactant also plays an important role. Poly vinyl alcohol was selected to prevent the agglomeration of nanoparticles and to obtain a more stable dispersion, which is a water soluble synthetic polymer having emulsifying and adhesive properties.

During the synthesis, mixing silver nitrate with the reducing agent, sodium borohydride, a black solution forms immediately. As the reaction proceeds, the color turns to light brown. In order to determine the characteristic properties of Ag NPs synthesized by this method, dynamic light scattering and UV-VIS spectrophotometric analyses were performed.

The size distribution is relatively narrow compared to the synthesized nanoparticles using sodium citrate. However, the average size is still very large at approximately 105 nm.
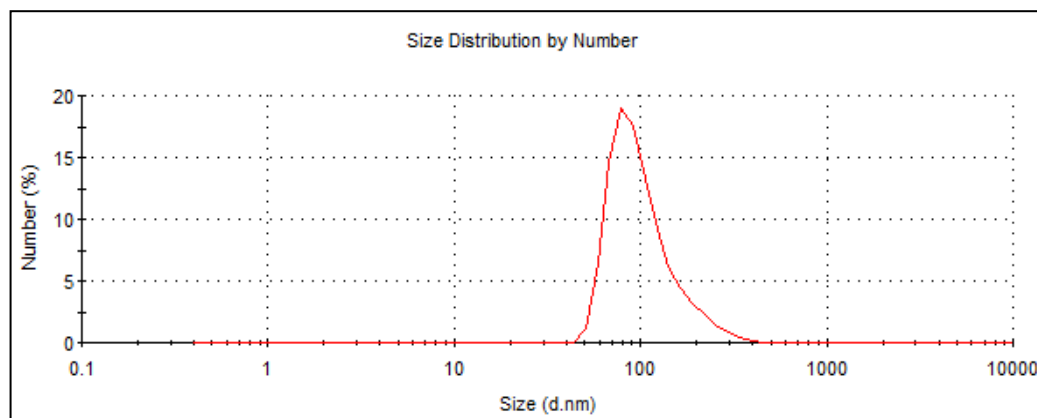
Figure 7.4. Number Average Size Distribution of Ag NPs through PVA Stabilization Process

According to UV spectra, it is evident that Ag NPs have been formed. The maximum absorbance peak can be found at approximately 442 nm.
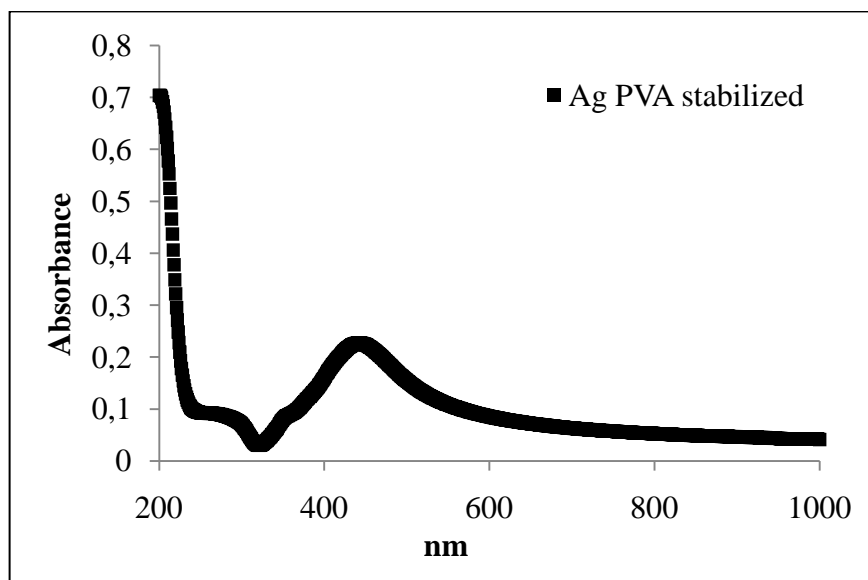
Figure 7.5. UV Spectra for Ag NPs through PVA Stabilization Process

7.4. GELATIN DISPERSED BOROHYDRIDE REDUCED AG NPS

Ag NP synthesis methods applied up to this part were not appropriate for further studies because of limited stabilities and large particle sizes. Nanoparticles have generally the tendency to aggregate in time resulting in decreased concentrations and increased particle sizes. However, the aggregation stability can be enhanced by adding sufficient amounts of surfactants and/or dispersing agents. The additive used in this green synthesis technique was gelatin, which is a colorless solid biological substance derived from animal collagen and used often as gelling agent in food industry.

First of all, a similar synthesis procedure was applied to synthesize stable Ag NPs using gelatin as the dispersing agent instead of gum arabic. Grey colored hydrophilic silver nanofluids were obtained and the particle size and size distribution were investigated by means of dynamic light scattering. According to the result, Ag NPs have an average particle size of 47.84 nm with a relatively narrow size distribution as represented in the

Figure 7.6. Gelatin substantially prevented the aggregation and reduced the average size of nanoparticles.
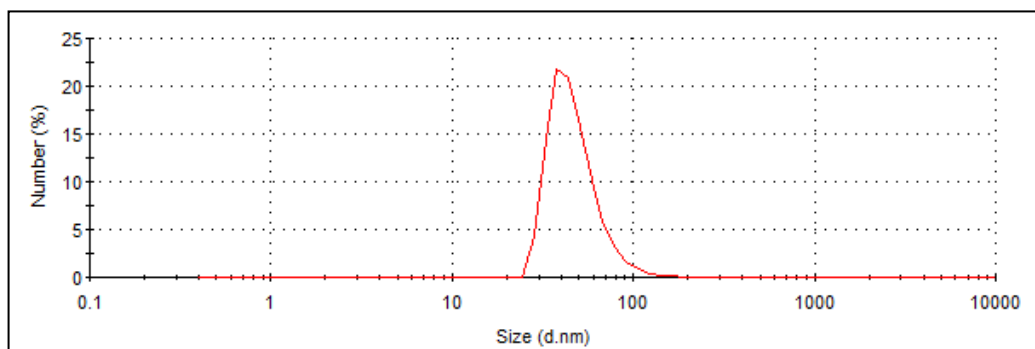
Figure 7.6. Number Average Size Distribution of Ag NPs Dispersed in Gelatin

As the size of the synthesized nanoparticles was in the required range, the particles are further characterized by other methods. To examine the crystallinity and the presence of Ag NPs, silver nanofluid was freeze-dried first and then X-Ray diffraction analysis was performed.

XRD pattern as shown in the Figure 7.7, the particles seemed to be non-crystalline because of the absence of peaks and the noisy structure. Comparing this with the standard one (ICDD-PDF standard file 4-0783) for Ag NPs, between the 2θ diffraction angle of 10-55°, the highest peak around 38-39° could not be observed either. Excess amount of gelatin present in the nanofluid is thought to suppress the appearance of silver in the X-Ray diffractogram.
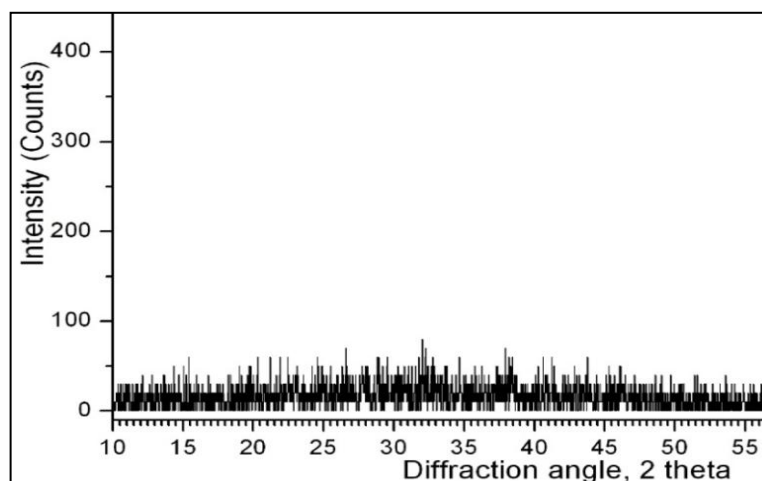
Figure 7.7. X-Ray Diffractogram of Ag NPs Dispersed in Gelatin

In order to avoid this consequence, additionally cleaning procedures were applied such as hydrolysis of the excess amount of gelatin, centrifugation and dispersion in water. However, these cleaning techniques did not result in appropriate samples. Next step to consider in the synthesis of Ag NPs is to find a more suitable dispersing agent.

7.5. GUM ARABIC DISPERSED ASCORBIC ACID REDUCED SILVER NANOPARTICLES

As discussed in the previous part, gum arabic was selected as the dispersing agent to synthesize stable Ag NPs having convenient particle size. In this typical synthesis method, silver nitrate was reduced with ascorbic acid and dispersed in gum arabic. According to UV spectra, it is evident that Ag NPs have been formed. The maximum absorbance peak was found at approximately 441 nm.
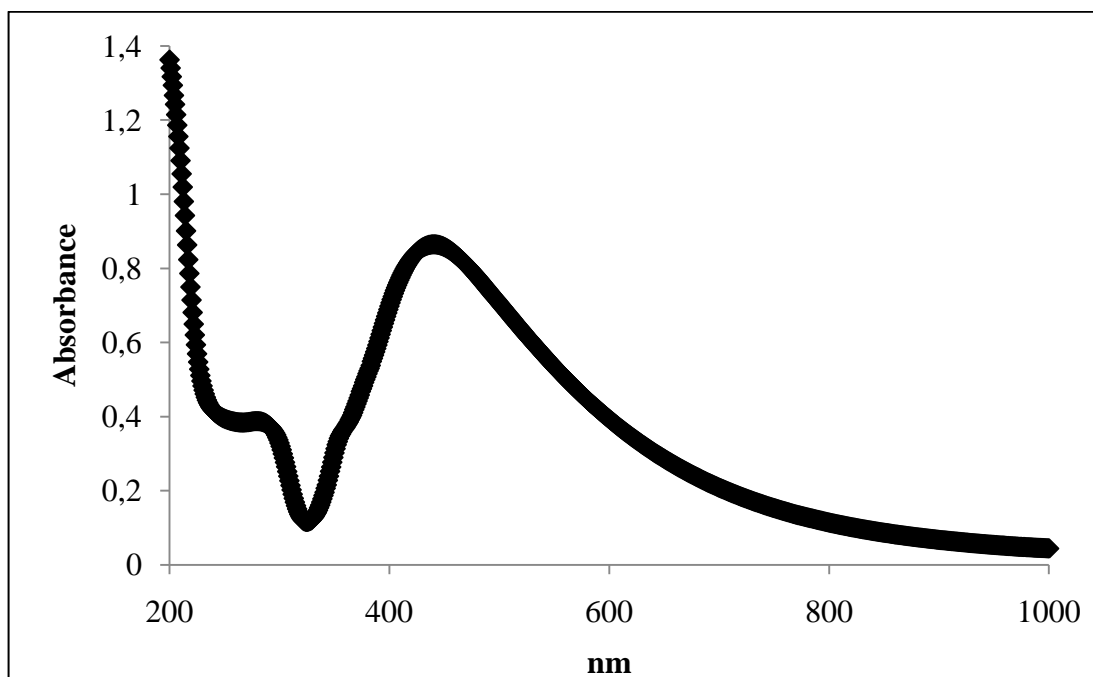
Figure 7.8. UV Spectra for Ag NPs Reduced with Ascorbic Acid

The presence of Ag NPs was confirmed by UV spectrophotometric analysis. The next step in nanoparticle characterization is the dynamic light scattering test. The resulting nanoparticles had an average particle size of 215.8 nm with a broader size distribution. This high value of particle size could be attributed to the type of the reducing agent, which is not a very strong one, leading to the slow hence larger formation of nanoparticles.
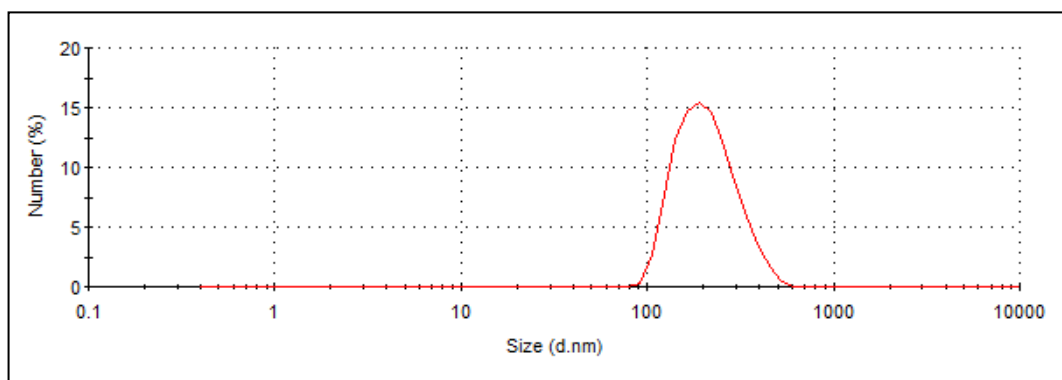
Figure 7.9. Number Average Size Distribution of Ag NPs Dispersed in Gum Arabic

7.6. GUM ARABIC DISPERSED BOROHYDRIDE REDUCED SILVER NANOPARTICLES

Strong reducing agents can easily lose electrons. According to the oxidation potentials, sodium is one of the strongest reducing agents. Hence, sodium borohydride was chosen as the reducing agent for this synthesis.

Figure 7.10. Ag NPs Reduced by Sodium Borohydride
Dispersed in Gum Arabic

Figure 7.11. Freeze-Dried Hydrophilic Ag NPs

Obtained solid silver nanofluid had black-brown color allowing a UV-spectrophotometric analysis to indicate the presence of Ag NPs. The maximum absorbance peak was obtained at 414 nm. Comparing with previous results, absorption peak shifted from 440 nm to 414 nm. This change was due to larger particles requiring lesser energy and hence longer wavelengths.
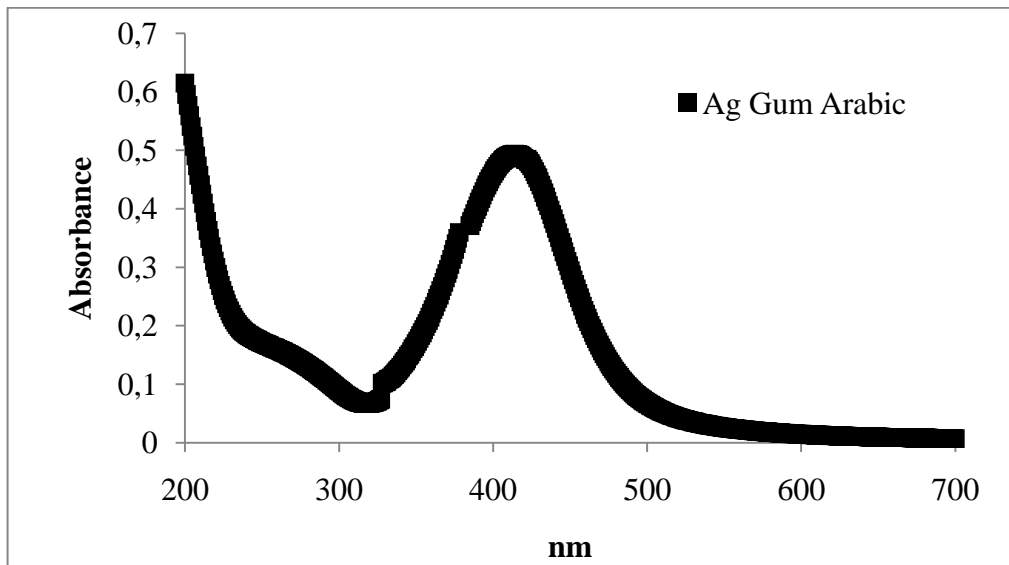
Figure 7.12. UV Spectra for Ag NPs Reduced by Sodium Borohydride

The particle size inference according to UV analysis was verified through dynamic light scattering. The number average size distribution of Ag NPs reduced by sodium borohydride and dispersed in gum arabic was demonstrated in the Figure 7.12. The particle size was approximately 18.64 nm. This result confirmed with the UV analysis that the synthesized nanoparticles were in the required/desired size ranges.
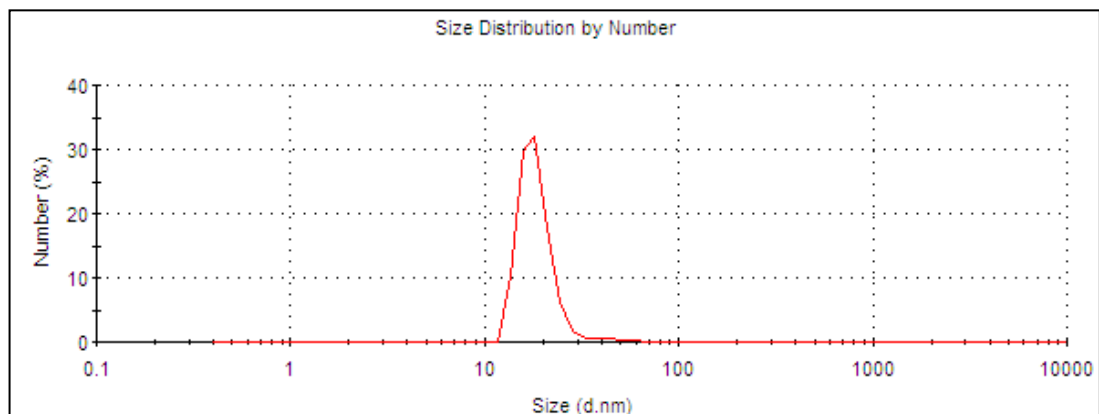
Figure 7.13. Number Average Size Distribution of Ag NPs Reduced by Sodium
Borohydride Dispersed in Gum Arabic

Another important parameter to be considered in nanoparticle synthesis is the stability. Solid nanoparticles homogeneously dispersed in fluids are stabilized by a negative zeta potential which prevents droplet coalescence upon random collisions of particles. The zeta potential is the overall charge a particle acquires in a specific medium. The magnitude of the zeta potential gives an indication of the potential stability of the colloidal system. If all the particles have a large negative or positive zeta potential they will repel each other and there is dispersion stability. If the particles have low zeta potential values then there is no force to prevent the particles coming together and there is dispersion instability. A dividing line between stable and unstable aqueous dispersions is generally taken at either +30 or -30mV. Particles with zeta potentials more positive than +30mV or more negative than -30mV are normally considered to be stable.

Zetasizer equipment is the device which determines the particle size, size distribution and zeta potential of nanoparticles. The overall negative charge (zetapotential) on the surface of synthesized Ag NPs was measured to be -40 mV indicating that the particles are highly stable.
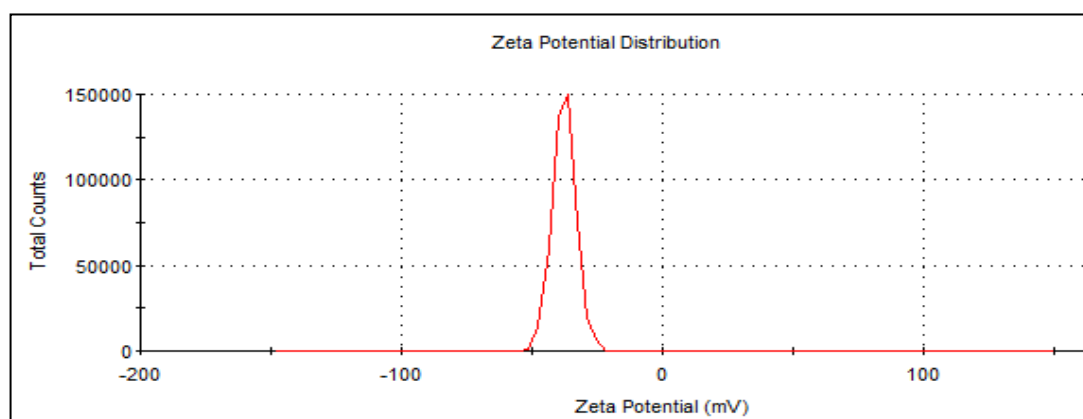
Figure 7.14. Zeta Potential of Hydrophilic Ag NPs

The formation of metallic Ag NPs was also confirmed by powder X-Ray diffraction (XRD) analysis. The crystal structure of this synthesized stable nanoparticles were identified on a Bruker D8 advance X-Ray diffractometer. The data are collected from $2\theta = 36 - 82^{o}$ at a scan rate of 1.5s per point. The Figure 7.15 shows a typical XRD pattern of Ag NPs obtained in an aqueous solution using gum arabic as dispersing agent and silver

nitrate as a silver precursor. All the reflection peaks can be indexed to face-centered cubic silver. The experimentally obtained pattern was identified through comparison with standard 4-0783 Silver pattern. XRD pattern shows characteristics peaks (at $2\theta = 38^{o}$, 65°, 78°) marked by their indices (111), (220) and (311) respectively.
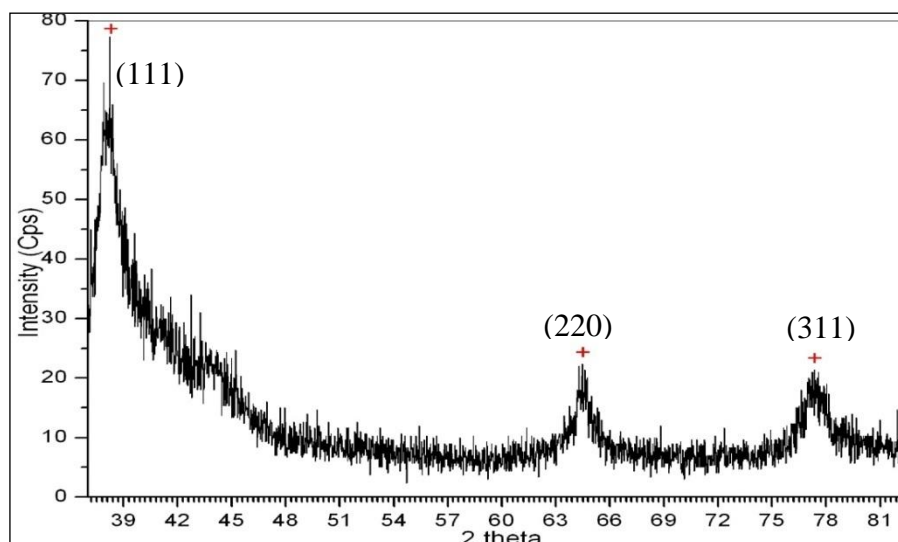
Figure 7.15. X-Ray Diffractogram of Hydrophilic Ag NPs

The standard analytical method for the determination of particle size is transmission electron microscopy (TEM). Accordingly, the colloidal Ag NPs were deposited onto a carbon support film which is fixed on a copper grid, followed by TEM investigation. The image is represented below in the Figure 7.16. From TEM image it is evident that the particles were well separated and have almost a narrow size distribution.
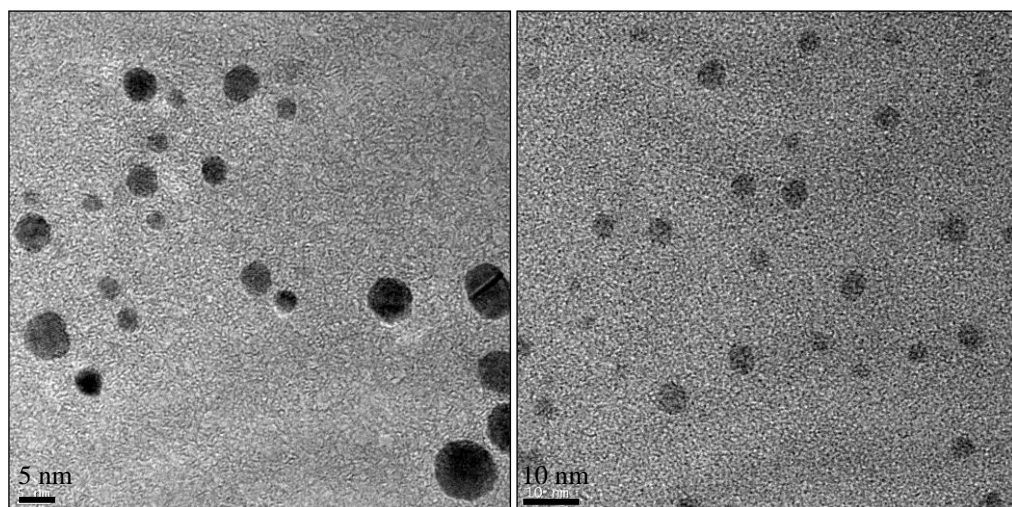
Figure 7.16. TEM images of Hydrophilic Ag NPs

Typically, a TEM micrograph contains images of several particles having different particle sizes. In order to establish a statistically meaningful histogram from which the average particle diameter and the size distribution can be deduced, one have to measure and count manually as many particles as possible from the TEM image. Figure 7.17 illustrates a case where the particle diameter for hydrophilic Ag NP is obtained as approximately 12 nm. As the particles in the TEM images are not readily recognizable due to the presence of a darker background, statistically only a small number of particles could be counted. That's why there is a difference between TEM and DLS results for average particle diameter of Ag NP.

Figure 7.17. Size Distribution from TEM pictures for Ag NP

7.7. SILVER NANOPARTICLES DISPERSED IN HEXANE

Hydrophobic Ag NPs dispersed in hexane were characterized by various equipments. Silver nanofluid having a black-brown color was analyzed to verify the presence of Ag NPs. The maximum absorbance peak was obtained at 436 nm, which was in the typical UV-VIS range indicating the existing of silver.
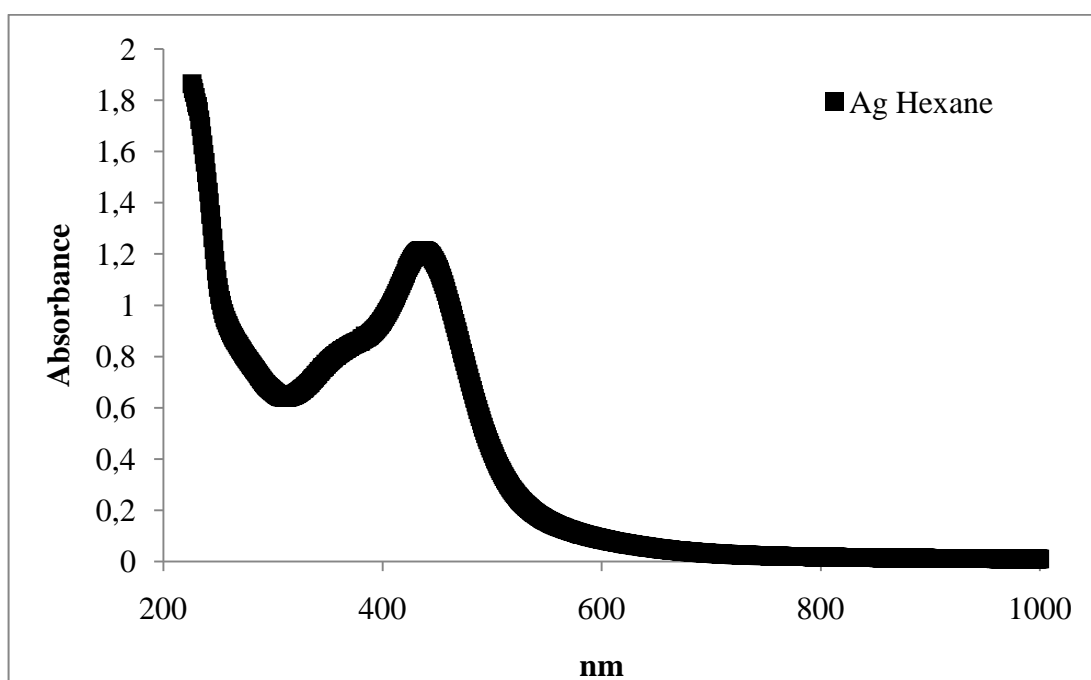
Figure 7.18. UV Spectrophotometric Analysis for Hydrophobic Ag NPs

Dynamic light scattering analysis was further performed to verify the UV analysis. The number average size distribution of hydrophobic Ag NPs dispersed in hexane was demonstrated in the Figure 7.19. The number averaged particle size was approximately 4.638 nm. The very small particle size is assumed to be coming from the presence of free surfactants in solution. According to intensity averaged particle size, the result is in coincidence with UV analysis that the particle size is in the applicable range.
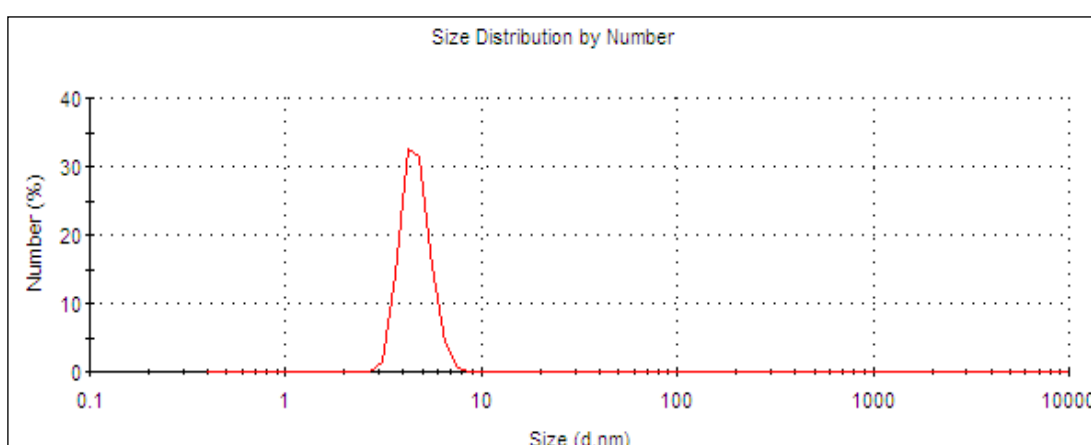
Figure 7.19. DLS Analysis for Hydrophobic Ag NPs

For hydrophobic Ag NPs Figure 7.20 shows a typical XRD pattern. All the reflection peaks indicate the presence of silver. The experimentally obtained pattern was identified through comparison with standard 4-0783 Silver pattern. XRD pattern shows characteristics peaks (at $2\theta= 38^{o}$, 65°, 78°) marked by their indices (111), (220) and (311) respectively. However, compared to the XRD result of hydrophilic Ag NPs, the crystallinity is lower in this case and the excess amount of surfactant or any other chemical in the synthesis suppresses the presence of silver.
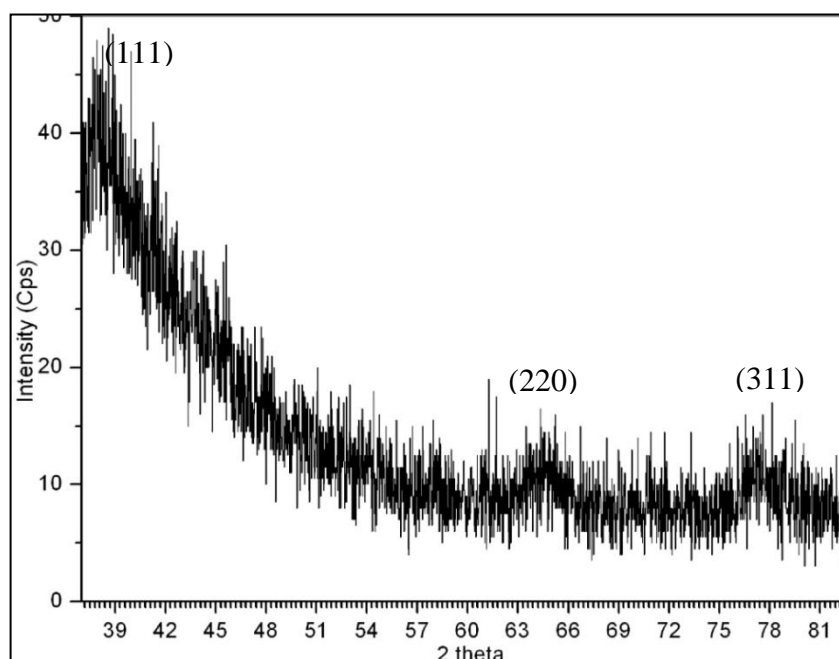
Figure 7.20. X-Ray Diffractogram of Hydrophobic Ag NPs

Besides the dynamic light scattering analysis, the particle size and stability are also investigated using the transmission electron microscopy (TEM). As described previously, the same sample preparation methods are applied and the obtained images are represented below in the Figure 7.21. Literally, the particles are well separated and have a narrow size distribution according to TEM images.
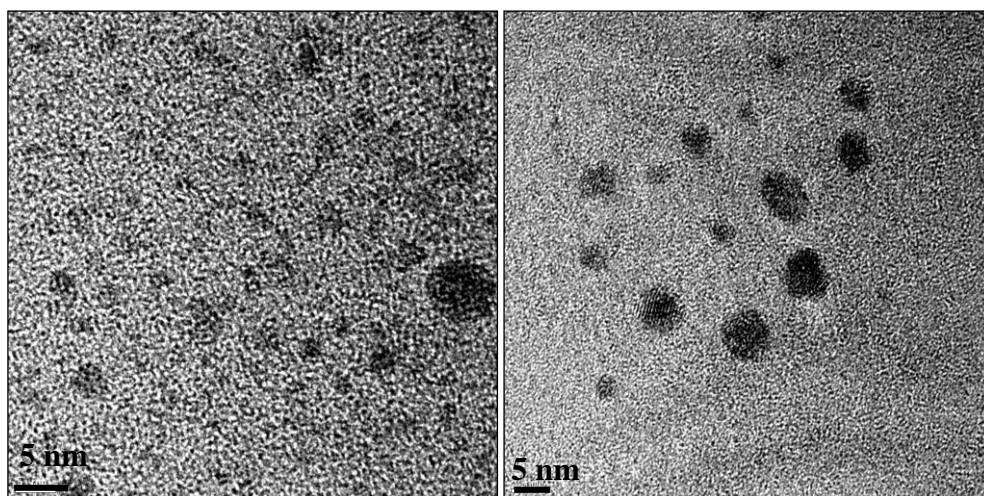
Figure 7.21. TEM images of hydrophobic Ag NPs

The size distribution analysis from TEM images is also performed for hydrophobic Ag NP. According to Figure 7.22 the particle diameter for hydrophobic Ag NP is obtained as approximately 3.71 nm. It is also valid for this type of particles that the particles in the TEM images are not readily recognizable due to the presence of a darker background and statistically only a small number of particles could be counted. That's why there is a difference between TEM and DLS results for average particle diameter of Ag NP.
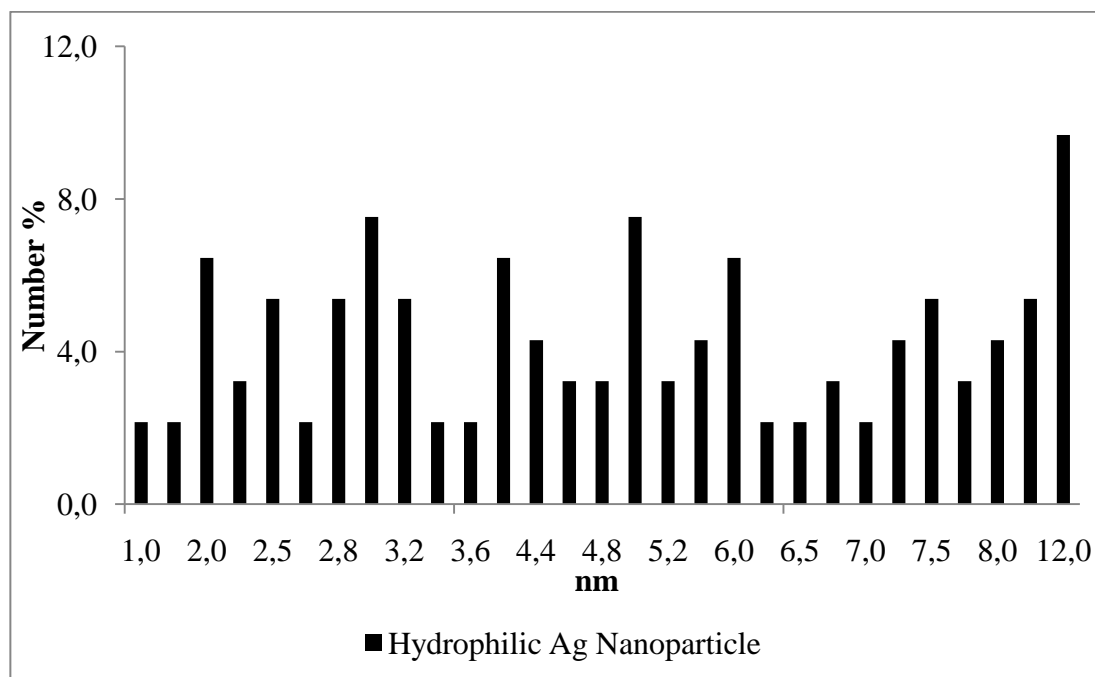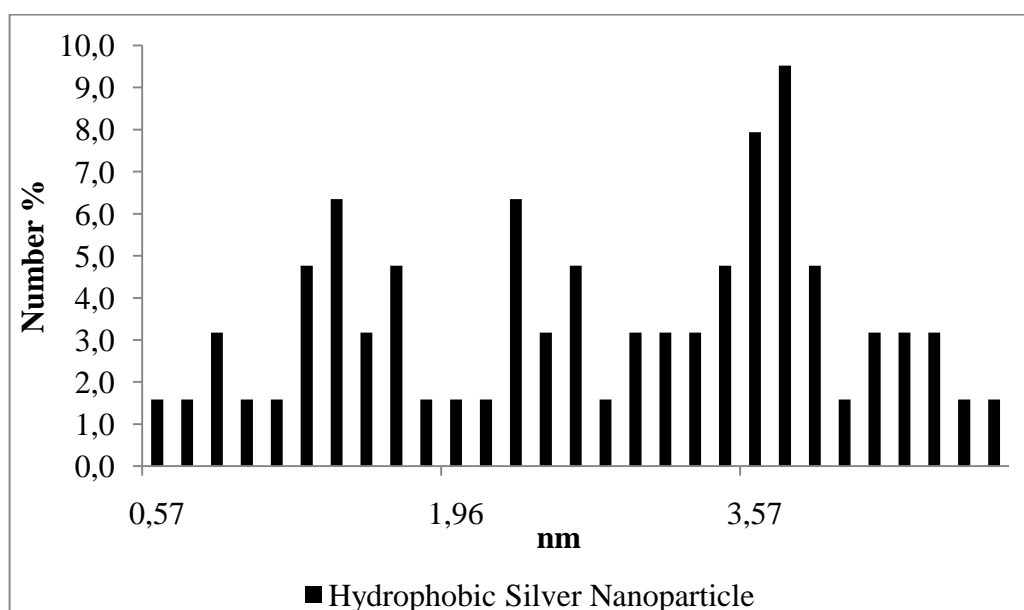

Figure 7.22. Size Distribution from TEM pictures for Ag NP

8. THERMOPHYSICAL PROPERTIES OF NANOFLUIDS

Magnetite and Ag NPs synthesized according to the previously described procedures in Chapter 5 were dispersed in various base fluids such as water, hexane and heptane. The temperature and particle loading effects were examined through the measurements of thermophysical properties as density, viscosity and thermal conductivity of synthesized hydrophilic and hydrophobic nanofluids using stated instruments. Experimental data was then compared with the values for corresponding base fluids to observe the presence of an enhancement or deterioration.

8.1. DENSITY

As previously mentioned, nanofluids can be used as replacements for commonly used heat transfer fluids. In order to evaluate the fluid dynamics and heat transfer performances of nanofluids, first the density must be known. In this study, density measurements were performed on different nanofluids containing magnetite (Fe_3O_4) and silver (Ag) nanoparticles dispersed in base fluids of water, hexane and heptane over a temperature range of $25^{o}C$ to $55^{o}C$ for several particle volume concentrations.

The measured results were compared with a widely used theoretical equation proposed by Pak and Cho [93] and good agreements between the theoretical equation and measurements were obtained for both nanofluids.

$$(8.1)$$

where   is the density of the nanofluid,   is the density of the particle,   is the particle volume fraction, and   is the density of the base fluid. [86]

8.1.1. Density Measurement of Silver Nanofluids

The general observation is that density increases linearly upon addition of nanoparticles, as the nanoparticles being added are of higher density than the base fluids. The synthesis method and the type of the synthesized nanoparticles either hydrophilic or hydrophobic do not affect the enhancements.

Ag NPs with a particle loading of 5.088 wt%, 2.83% increase is obtained when the particles are dispersed in hexane. On the other hand, with the same amount of nanoparticles dispersed in heptane 2.59% increase in density is achieved. As compared to those carrier fluids, 7.450 wt% of Ag NPs dispersed in water resulted in only 2.13% enhancement of density.

Besides the particle loading effect, temperature effect on density is also verified in all measurements following from Figure 8.1 through Figure 8.3 and generally density values are decreased with increasing temperature.

Figure 8.1. Density Enhancement for Ag NPs Dispersed in Water
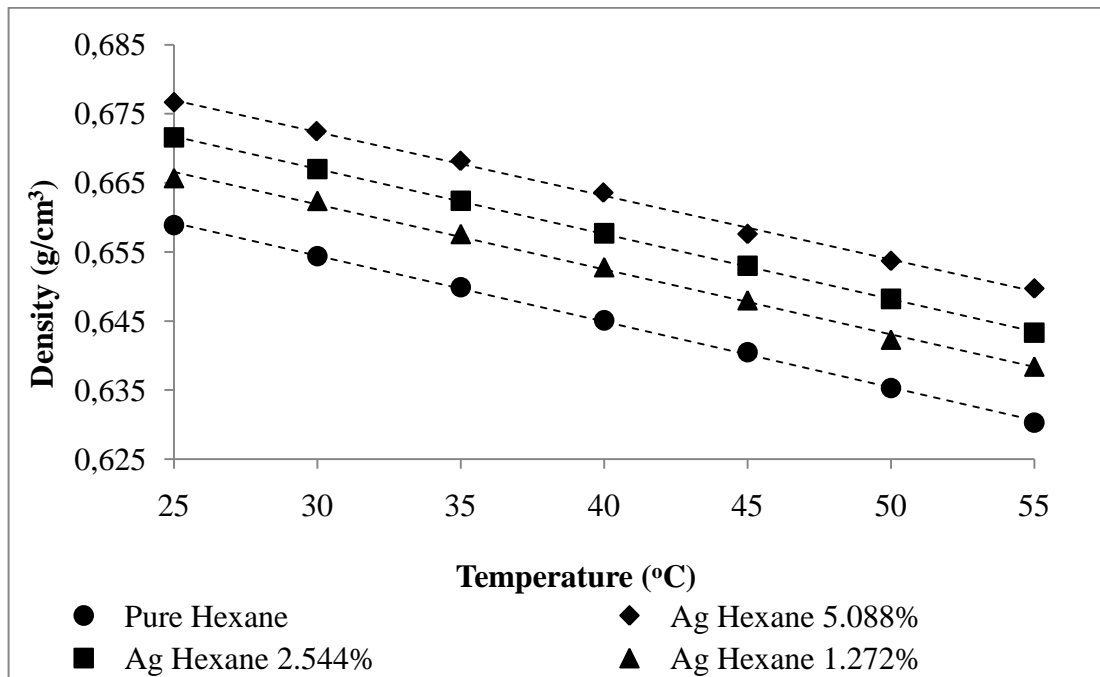
Figure 8.2. Density Enhancement for Ag NPs Dispersed in Hexane
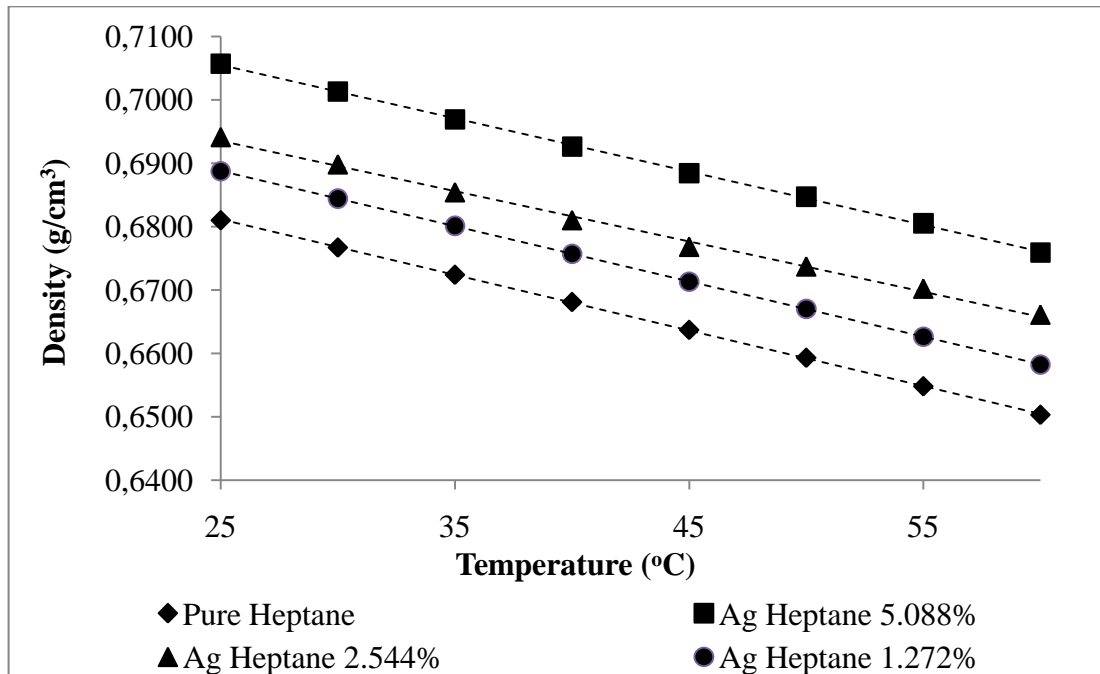
Figure 8.3. Density Enhancement for Ag NPs Dispersed in Heptane

The enhancement of density is further given as the comparison of different silver nanofluids in Figure 8.4. At 30°C, densities of hydrophobic and hydrophilic silver

nanofluids are selected and plotted against particle weight fraction. As a result, Ag NPs dispersed in hexane exhibit the highest enhancement compared to heptane and water.
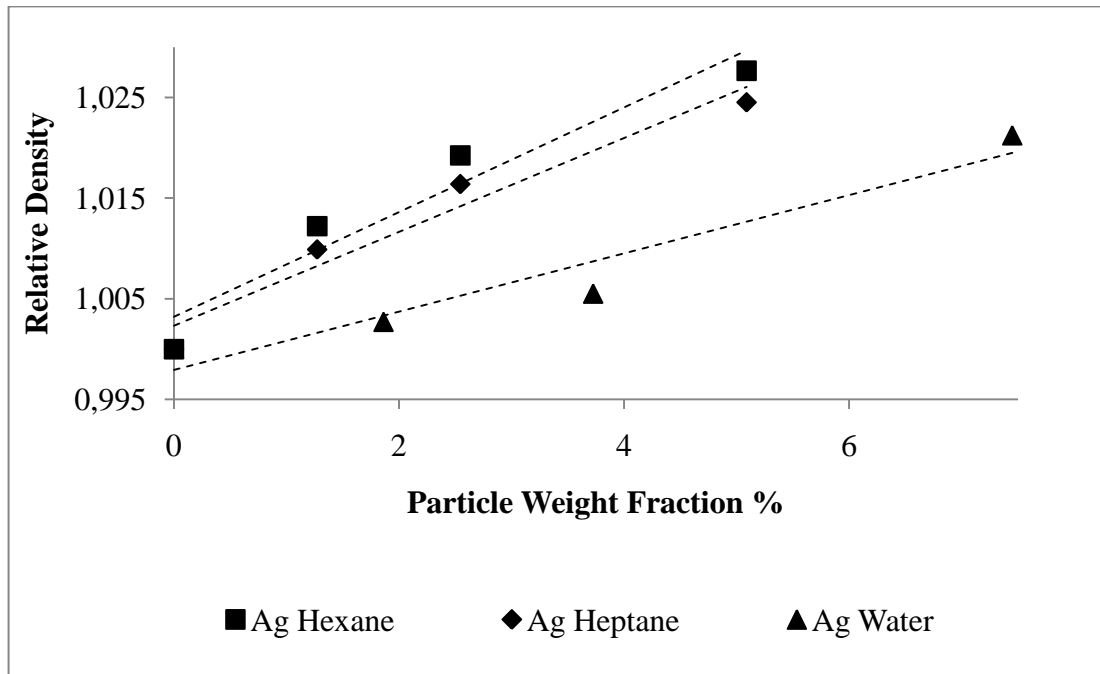
Figure 8.4. Relative Densities of Various Silver Nanofluids at Constant Temperature

It is also verified whether the measured density values for silver nanofluids matched with the theoretical values obtained from Pak and Cho formula. As shown in Figures 8.5 and 8.6, the general trend of density in terms of temperature and concentration is in good agreement between the experimental data and the theoretical results at all temperatures and concentrations.

For silver/heptane nanofluid of 5.088 wt%, the maximum deviation from Pak and Cho model is about 2.50% and the average deviation is 1.15%. For hydrophilic silver nanofluid of 7.450 wt%, the maximum deviation is 1.22% and the average is 0.85%. Unlike the closer agreement of silver/water nanofluid with the Pak and Cho equation, the density values of silver/hexane nanofluid show a little higher discrepancy with a maximum deviation of 2.53% and an average deviation of 1.02%. The highest percentage error between the experimental data and the theoretical model is observed for silver/hexane

nanofluid density value. Furthermore, generally the percentage deviation increases with increase in concentration and decrease in temperature for all three silver nanofluids.

Figure 8.5. Comparison of Density Values for Hydrophobic Silver Nanofluids

Figure 8.6. Comparison of Density Values for Hydrophilic Silver Nanofluid

8.1.2. Density Measurement of Magnetite Nanofluids

Densities of magnetite nanofluids containing various amounts of nanoparticles dispersed in water, hexane and heptane are also measured over a temperature range from 25°C 55°C. The general trend is again observed that the density increases with increasing concentration independent of specific synthesized nanoparticles.

Magnetite nanoparticles dispersed in heptane having a particle loading of 7 wt%, density enhancement is obtained as 7.86%. For magnetite nanoparticles dispersed in hexane with a particle loading of 1.8 wt%, the density improvement is 3.01%. On the other hand, 5.98 wt% of magnetite nanoparticles dispersed in water resulted in 4.41% enhancement of density.

Besides the particle loading effect, temperature effect on density is also observed in all measurements following from Figure 8.7 through Figure 8.9 and again density values are decreased with increasing temperature.
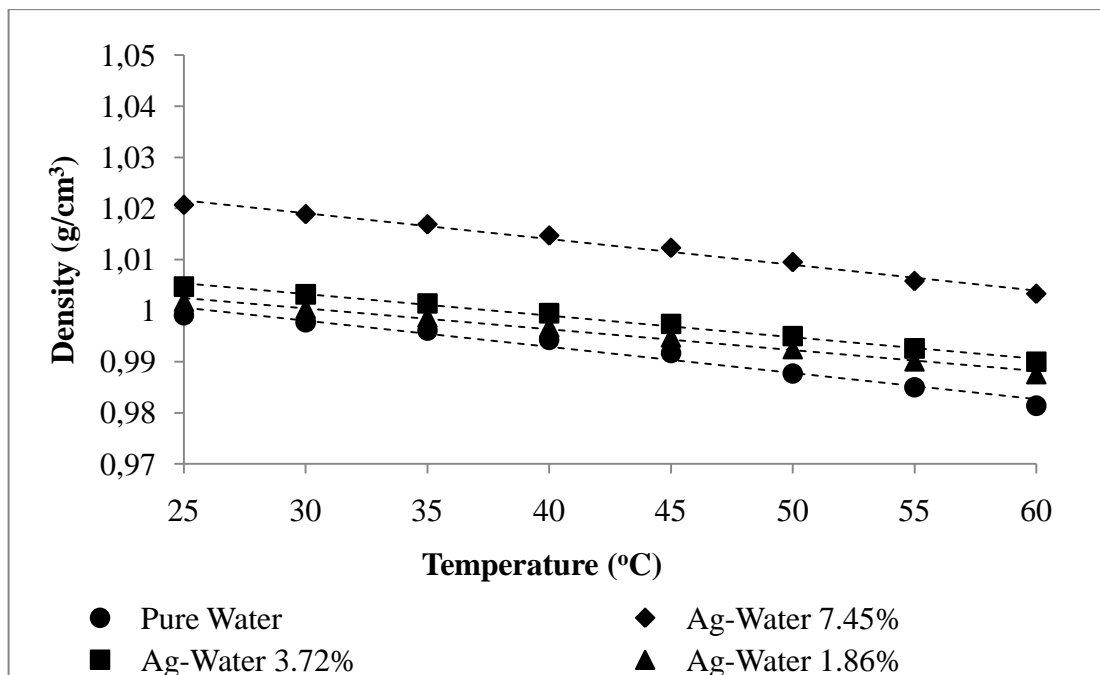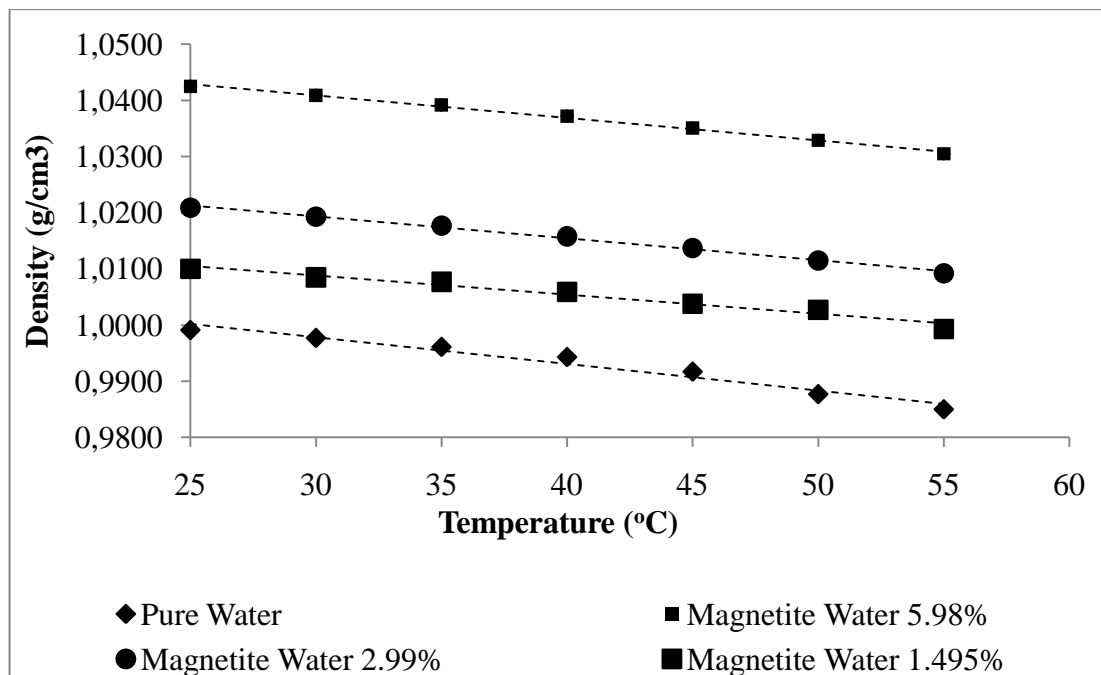

Figure 8.7. Density Enhancement for Magnetite Nanoparticles Dispersed in Water
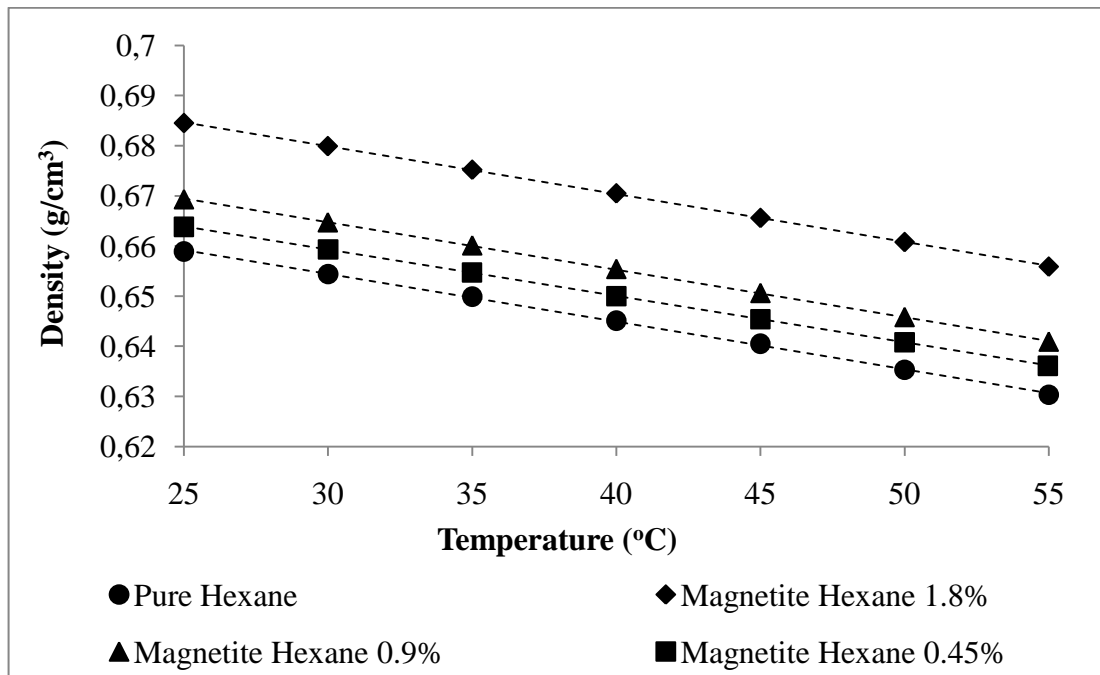
Figure 8.8. Density Enhancement for Magnetite Nanoparticles Dispersed in Hexane
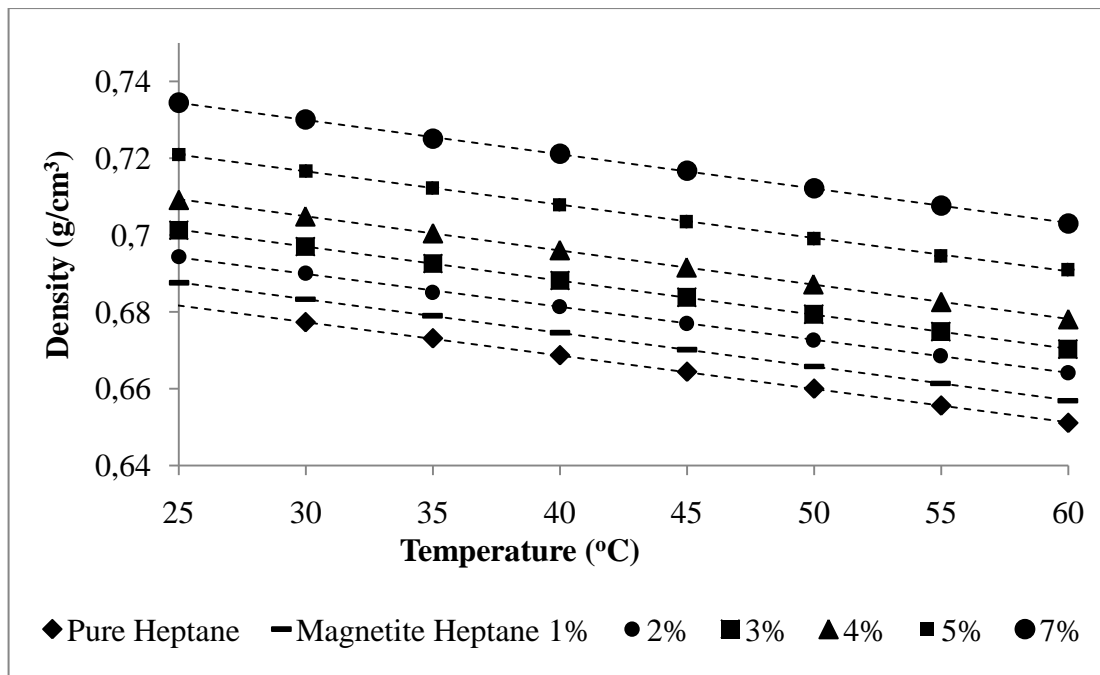
Figure 8.9. Density Enhancement for Magnetite Nanoparticles Dispersed in Heptane

In Figure 8.10, the enhancement of densities is compared for magnetite nanofluids in terms of relative densities at constant temperature of $30^{\circ}C$ against varying particle weight

fractions. As a result, magnetite nanoparticles dispersed in hexane exhibit the highest enhancement compared to heptane and water. To sum up, silver and magnetite nanoparticles dispersed in hexane exhibit the maximum density enhancement among the other base fluids. In designing equipments where density is a key parameter to be considered hexane should be selected for dispersing different kinds of nanoparticles.
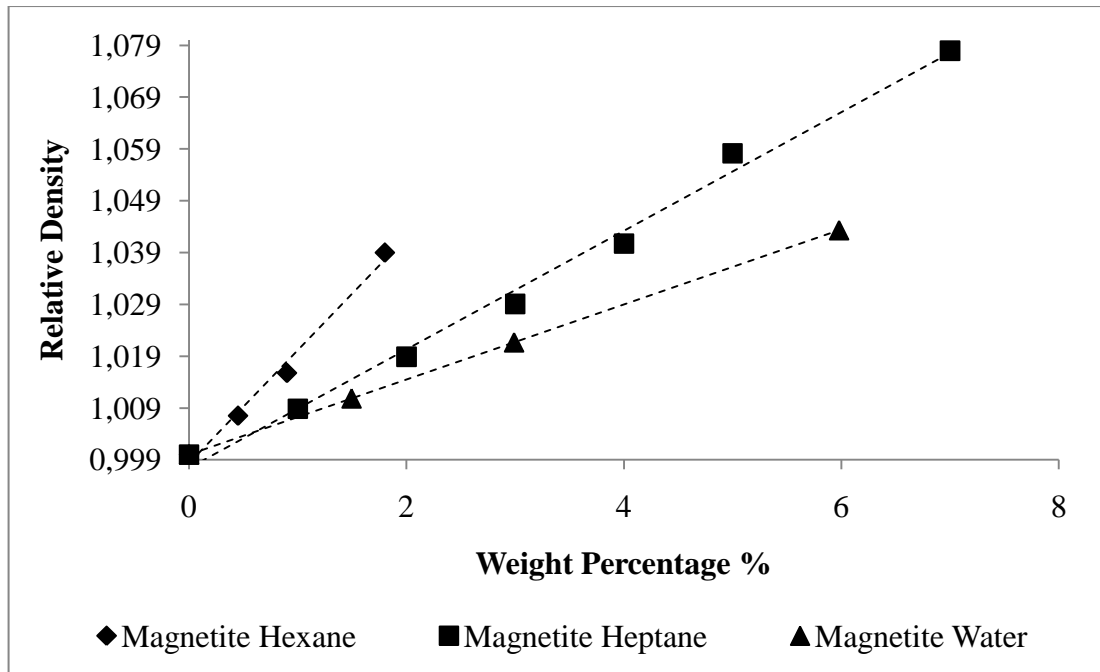
Figure 8.10. Relative Densities of Various Magnetite Nanofluids at Constant Temperature

The theoretical model by Pak and Cho shows also good agreement for magnetite nanofluids according to Figures 8.11 and 8.12 at all temperatures and concentrations. For magnetite/hexane nanofluid of 1.8 wt%, the maximum deviation is about 1.95% and the average deviation is 1.30%. For hydrophilic magnetite nanofluid of 5.98 wt%, the maximum deviation is 1.50% and the average is 0.42%. Unlike these two base fluids, the density values of magnetite/heptane nanofluid show a higher discrepancy with a maximum deviation of 4.20% and an average deviation of 2.37%. Furthermore, the percentage deviation increases with increase in concentration and decrease in temperature for all three magnetite nanofluids.
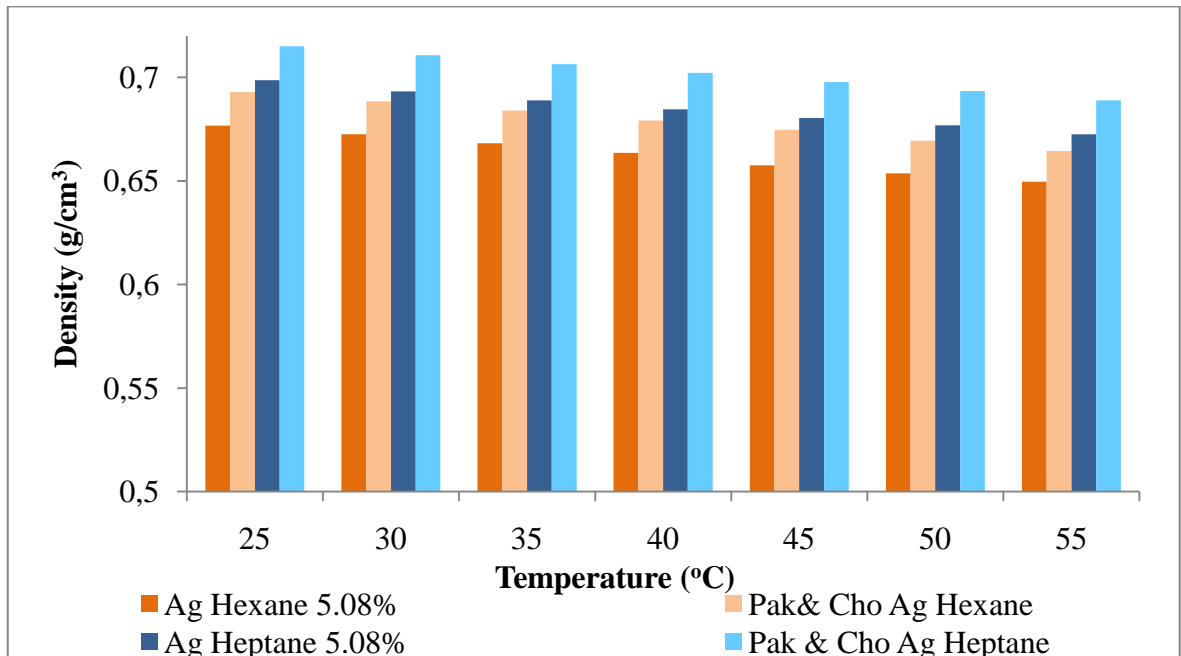
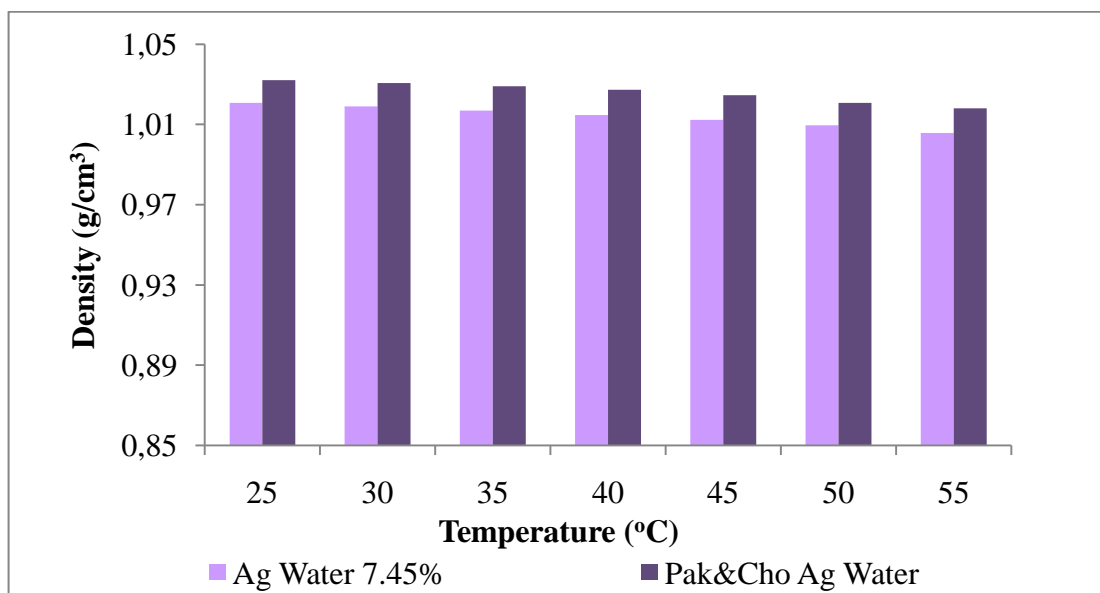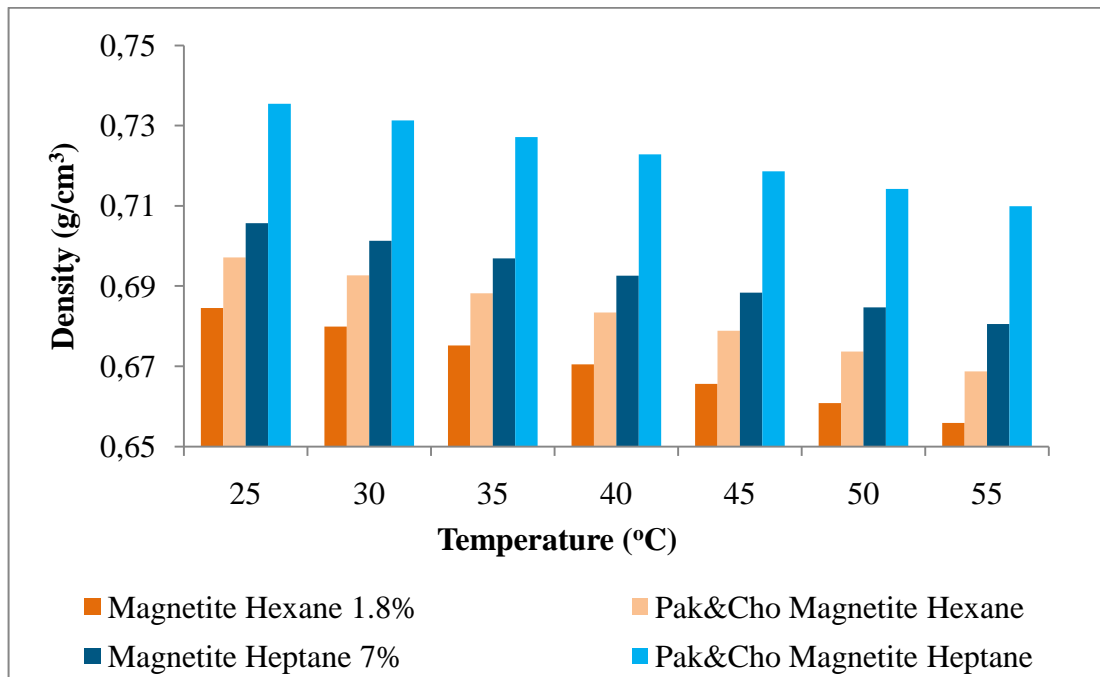Figure 8.11. Comparison of Density Values for Hydrophobic Magnetite Nanofluids
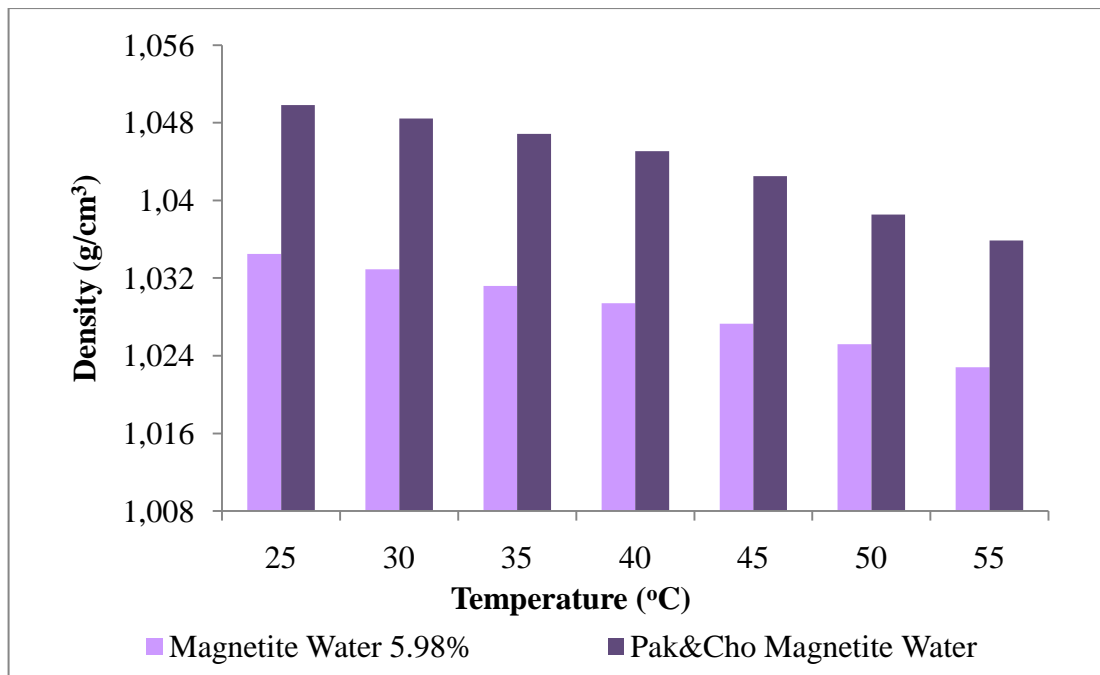
Figure 8.12. Comparison of Density Values with for Hydrophilic Magnetite Nanofluids

Moreover, the experimental data for both silver and magnetite nanofluids are compared with theoretical density values obtained from Pak and Cho model. As a general

trend, experimental values are lower than the theoretical density values for both cases. The type of the dispersed nanoparticles and the very high particle weight fractions can be attributed to this outcome. Although the model represents good agreement with experimental data, Pak and Cho developed it for nanofluids with lower concentrations. That's why the deviations increase with increase in particle concentration.

8.2. VISCOSITY

Regarding the thermal performance of nanofluids, the viscosity is as critical as thermal conductivity in engineering systems employing fluid flow. Pumping power is proportional to the pressure drop which is related to fluid viscosity. Large savings can be achieved if a large thermal conductivity increase can be achieved with a small volume fraction of nanoparticles. The fluid viscosity is therefore responsible for the strong temperature dependence of the conductivity enhancement in nanofluids.

Generally, the viscosity of nanofluids sharply increases with increasing the particle loading and becomes much higher than that of the base liquid. As the temperature is increased, the viscosity of base fluids is decreased, the Brownian motion of nanoparticles is increased, and consequently convectionlike effects are remarkably increased, resulting in increased conductivities.

In this study, the viscosity of several nanofluids (silver and magnetite nanofluids) are measured for temperatures ranging from room condition to $55^{o}C$ using a Brookfield viscometer.

8.2.1. Viscosity Measurement of Silver Nanofluids

Hydrophilic silver nanofluids dispersed in water and hydrophobic Ag NPs in hexane and heptane are measured over the temperature range of $25^{o}C$ to $55^{o}C$ represented in the Figures 8.13 through 8.15.

As expected, silver/hexane nanofluids with varying particle loadings from 1.27% to 5.09%, viscosities increase from 1.36% to 1.59%. Whereas for the same amount of Ag NPs

dispersed in heptane, the viscosity enhancements increase from 1.12 to 1.28%. For hydrophilic silver nanofluids with high particle weight fractions ranging from 1.86 to 7.45, the results in viscosity improvement vary from 2.02 to 4.12% respectively. As a result, the highest enhancement is obtained in silver/water nanofluids.
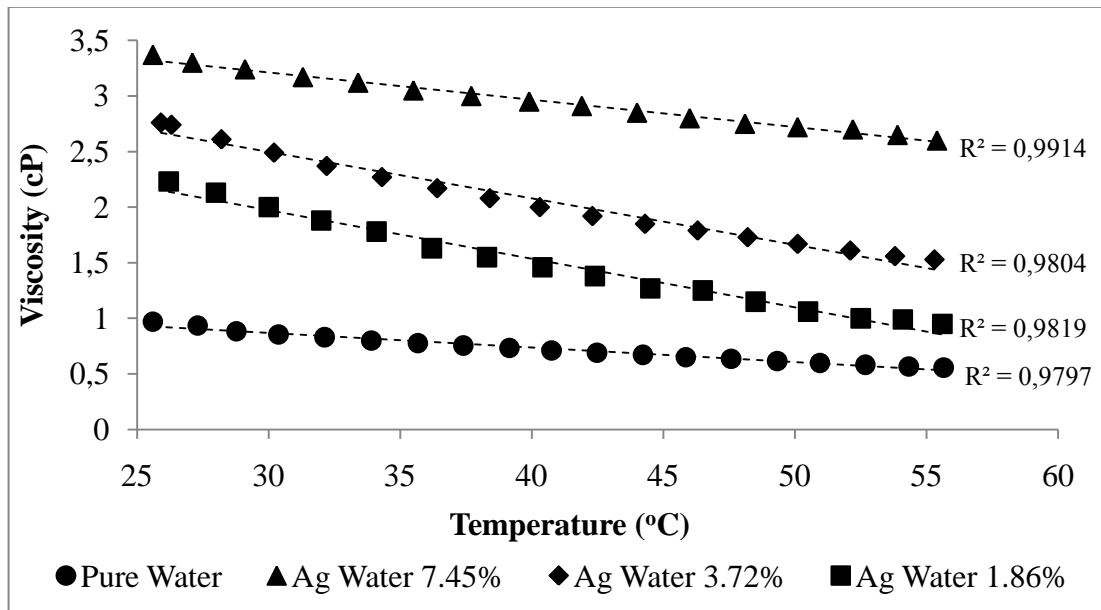
Figure 8.13. Viscosity Enhancement for Ag NPs Dispersed in Water
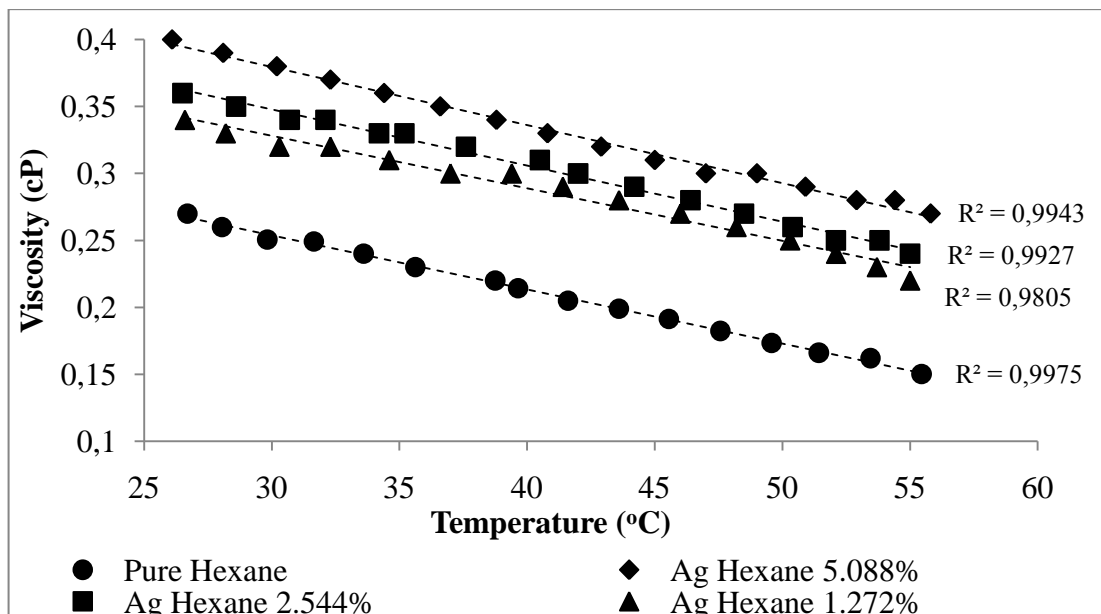
Figure 8.14. Viscosity Enhancement for Ag NPs Dispersed in Hexane
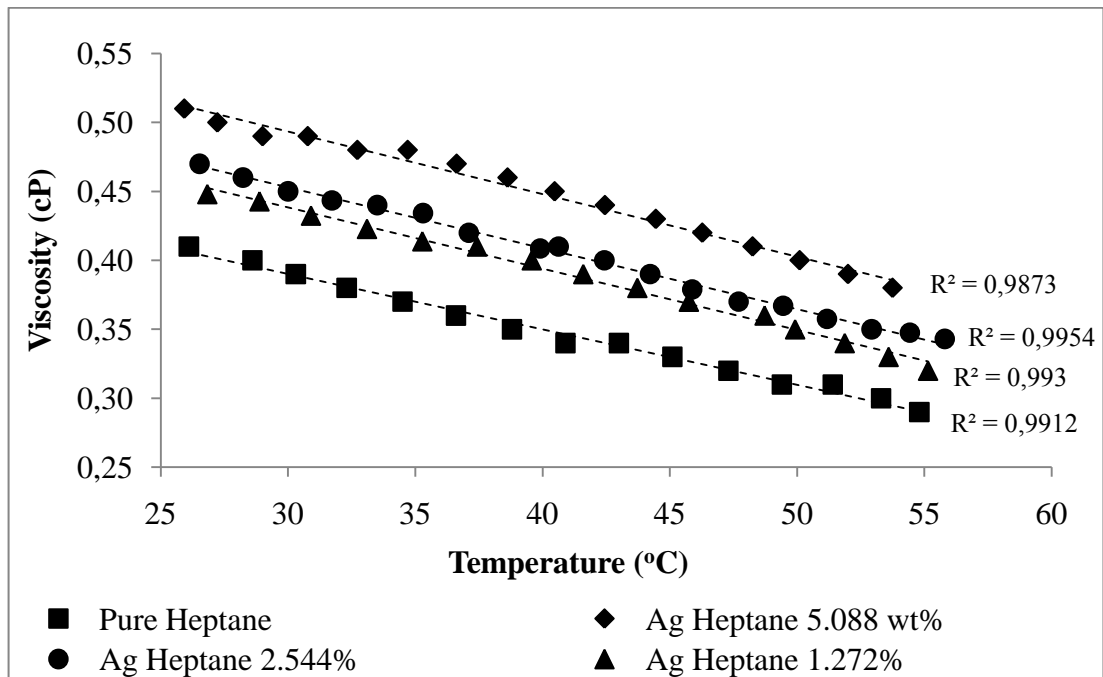
Figure 8.15. Viscosity Enhancement for Ag NPs Dispersed in Heptane

The viscosity results are expressed under the usual form of the viscosity and as well as relative viscosity defined as the 'nanofluid-to-basefluid' ratio of viscosities. As previously mentioned in density results, also viscosities at 30°C are plotted against the particle weight fraction. At constant temperature, the general trend for viscosity is observed. Viscosity decreased by increasing the weight fraction. Again the highest improvement is achieved in silver/water nanofluid. The main reason for this much high discrepancy between three nanofluids is the specific type of the synthesized hydrophilic Ag NP. The excess amount of surfactant in the synthesis results in high viscosities compared to the other two hydrophobic silver nanofluids. Silver/hexane nanofluid shows the maximum enhancement among hydrophobic silver nanofluids confirming the density results that hexane is a good solvent for dispersing nanoparticles.
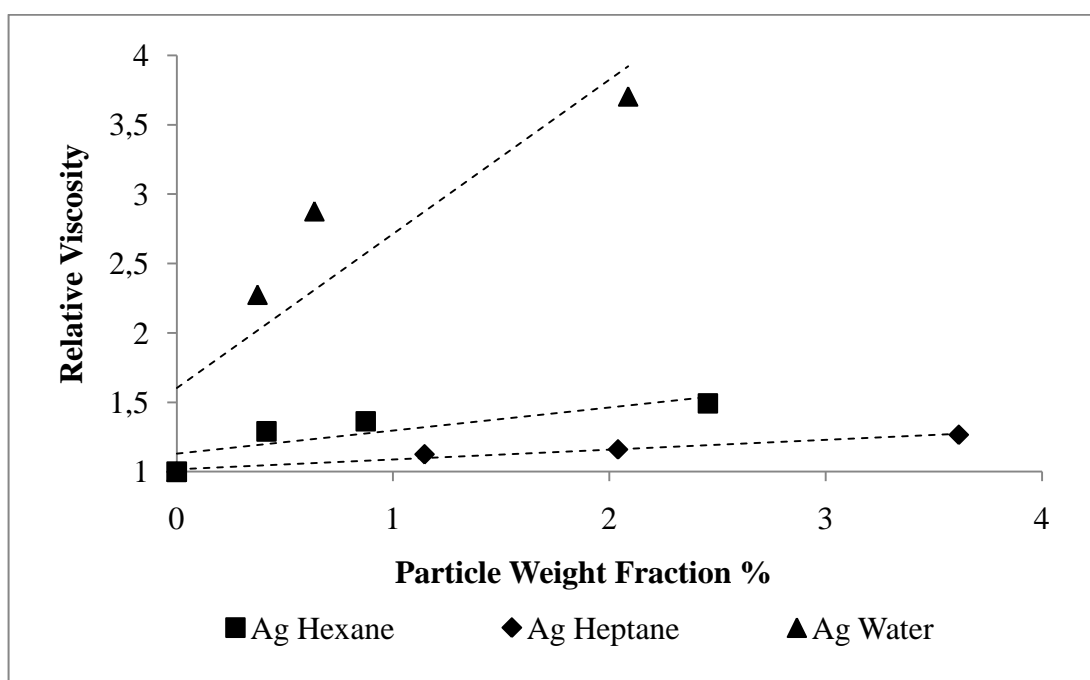
Figure 8.16. Relative Viscosities of Various Silver Nanofluids at Constant Temperature

8.2.2. Viscosity Measurement of Magnetite Nanofluids

Viscosities of hydrophilic magnetite nanoparticles dispersed in water are measured over the temperature range of 25°C to 55°C and represented in the Figure 8.17. 5.98 wt% of magnetite nanoparticles result in approximately 5% of viscosity enhancement.

The experimental viscosity results are represented in the Figure 8.18 for magnetite/hexane nanofluids with particle concentrations ranging from 1.8 to 0.45 wt%. The relative viscosities (——) at 30°C decrease from 1.49 to 1.29 for the given particle concentrations respectively.

With 1-3 wt% of magnetite/heptane nanofluid 6.5-12% of viscosity enhancement is obtained. As a result, the highest enhancement is obtained in magnetite/hexane nanofluids according to Figure 8.20, which is in perfect agreement with the previous results obtained for viscosity and density of silver nanofluid.
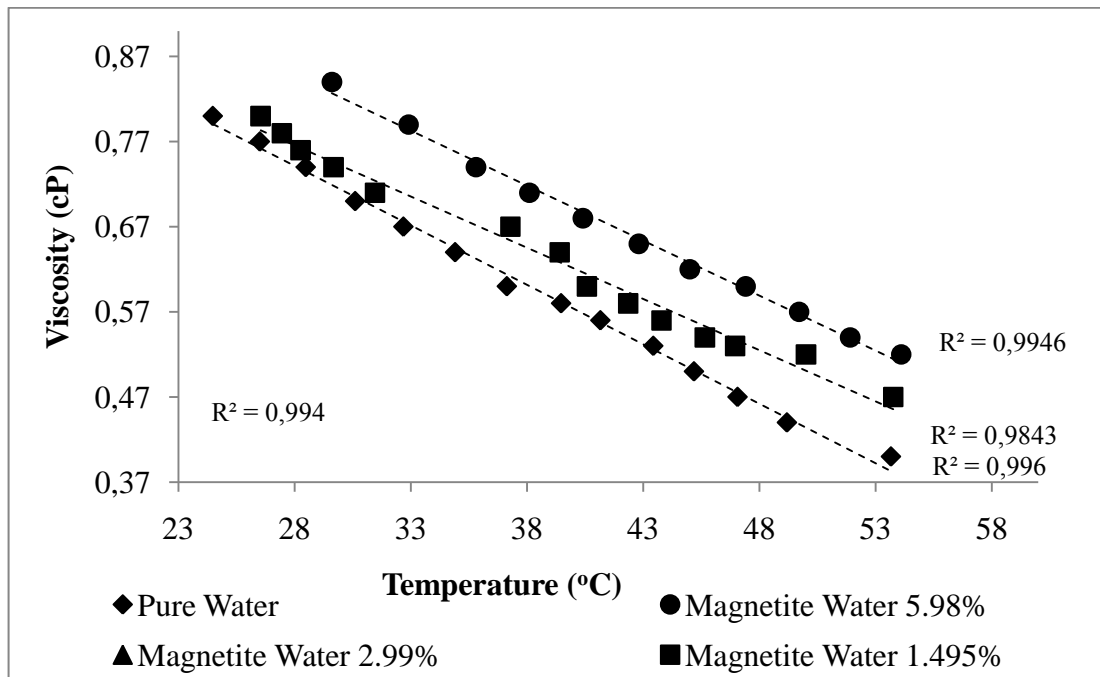
Figure 8.17. Viscosity Enhancement for Magnetite Nanoparticles Dispersed in Water
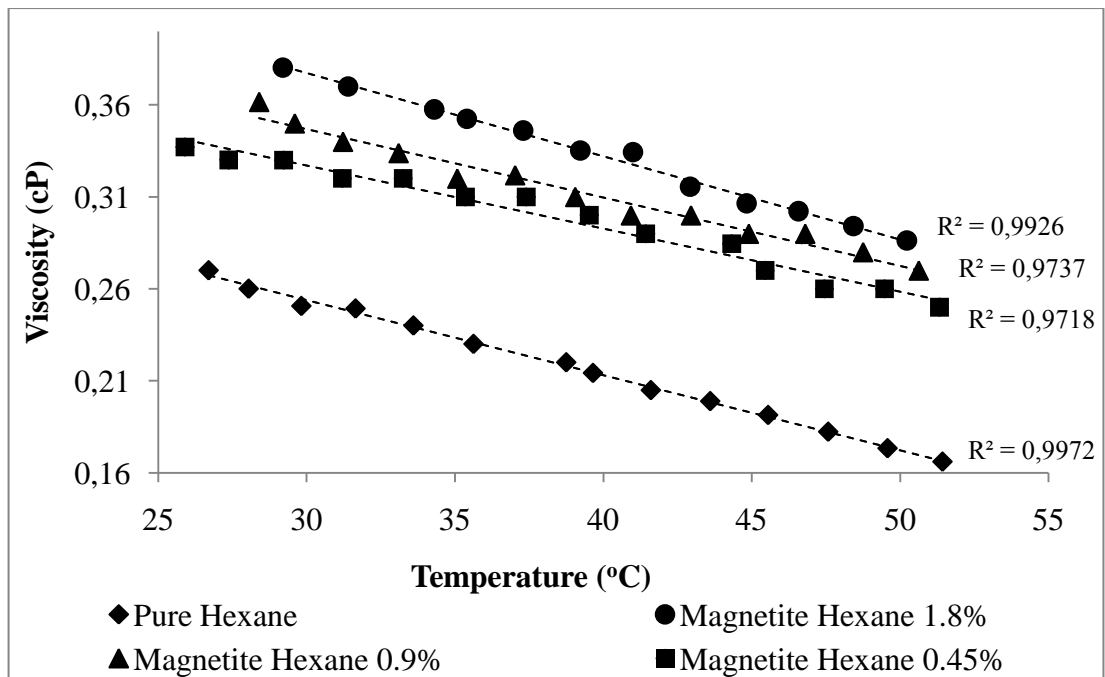
Figure 8.18. Viscosity Enhancement for Magnetite Nanoparticles Dispersed in Hexane
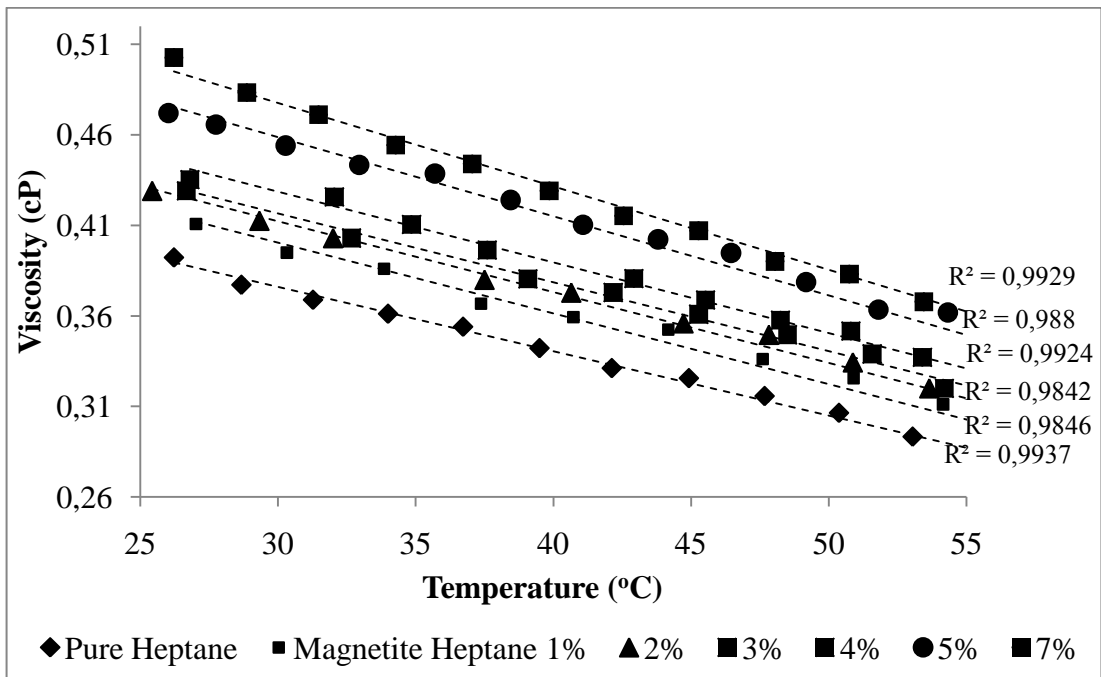
Figure 8.19. Viscosity Enhancement for Magnetite Nanoparticles Dispersed in Heptane
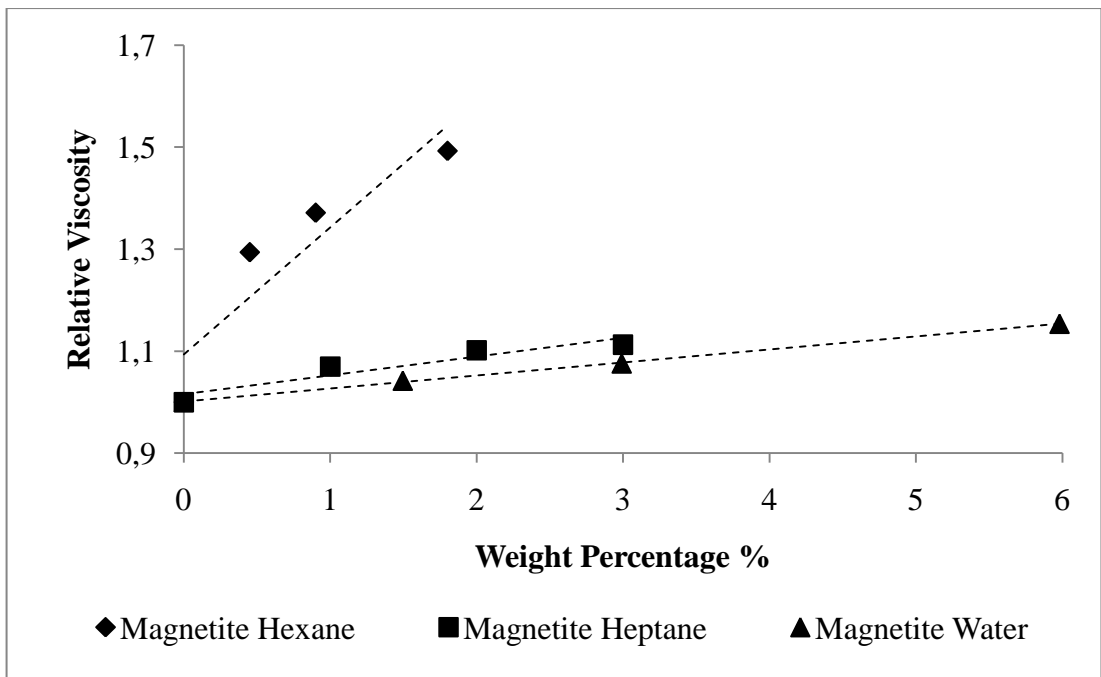
Figure 8.20. Relative Viscosities of Magnetite Nanofluids at Constant Temperature

To sum up, nanofluid viscosity increases considerably with increasing particle concentration, but decreases with temperature. The main reason for the first effect is that the increase in the amount of particles affects directly the fluid shear stress and the temperature effect is because of weak forces between nanoparticles. In fact, for silver and magnetite nanoparticles dispersed in hexane and heptane at all particle fractions, there exists a critical temperature beyond which the viscosities show unexpected results because of viscosity hysteresis. Hence, the viscosity experiments are performed between 25 and 55°C.

The highest viscosity enhancements are obtained for silver and magnetite nanoparticles dispersed in hexane. Comparing both nanofluids, for a similar particle fraction of 1.27% for silver and 1.8% for magnetite nanofluid, the relative viscosities are 1.29 and 1.49 respectively. This result is very reasonable in terms of the similarities in the type of the synthesis method, solvent and surfactant.

For the evaluation of experimental data, researchers have developed several models estimating the effect of particles on the viscosities of nanofluids. The basic equation was developed by Einstein and many other formulas were derived based on the pioneering work of Einstein. In order to compare the experimental data of this study with the correlations previously formulated, viscosities of silver and magnetite/hexane nanofluids at a particular temperature (25°C) and particle fraction are selected and the results are shown in the Table 8.1 and 8.2.

Table 8.1. Comparison of Experimental Viscosity Data for Silver/Hexane Nanofluid with Theoretical Models

Model	Formula	Theoretical Data (cP)	Experimental Data (cP)
Einstein	—	0.277283	0.40210
Brinkman	— ——	0.277298	0.40210

| Lundgren | — | — | 0.277304 | 0.40210 |
| Batchelor | — | | 0.277305 | 0.40210 |

Table 8.2. Comparison of Experimental Viscosity Data for Magnetite/Hexane
Nanofluid with Theoretical Models

Model	Theoretical Data (cP)	Experimental Data (cP)
Einstein	0.280632	0.40050
Brinkman	0.280717	0.40050
Lundgren	0.280752	0.40050
Batchelor	0.280757	0.40050

The theoretical models used to estimate particle suspension viscosities are generally based on the assumption of a linearly viscous fluid containing dilute, suspended, spherical particles. Einstein's formula was found to be valid for relatively low relative particle volume fractions   . Beyond this value, it underestimates the effective viscosity of the resulting mixture. Therefore, there are high discrepancies between the experimental and theoretical viscosity data.

8.3. THERMAL CONDUCTIVITY

As mentioned before, the bottleneck of slurries containing micron size particles can be eliminated suspending nanoparticles in traditional heat transfer fluids. It is found that the thermal properties of nanofluids are considerably more appealing than those of the base fluid itself. Using transient hot wire method, it is found that the thermal conductivities of these fluids show significant improvements. Small particle sizes and volume fractions of nanoparticles reduce the instability and sedimentation problems and result in tremendous increases in thermal conductivities of fluids. Due to these facts, thermal conductivities of

synthesized silver (Ag) and magnetite (Fe$_3$O$_4$) nanofluids are measured to observe their effect on enhancement or deterioration.

8.3.1. Thermal Conductivity Measurement of Silver Nanofluids

For the evaluation of nanofluid effective thermal conductivities, transient hot wire technique is used. Several measurements over a temperature range covering 25 to 55°C are carried out for the synthesized Ag NPs dispersed in various base fluids with several different particle fractions.

As expected, the effective thermal conductivity increases with nanoparticle fraction according to Figures 8.21 and 8.22. In the particular case for hydrophobic Ag NPs synthesized by the same method and dispersed in different base fluids, the particle loading and thermal conductivity is perfectly linear at all temperature ranges. For silver/hexane nanofluids, for particle weight fractions of 5.088 and 2.544%, approximately 2.81% and 1.42% increase in thermal conductivity are observed respectively. When the same Ag NPs are dispersed in heptane, 2.51% and 1.59% thermal conductivity improvements are measured at the same particle fractions respectively. Brownian motion of nanoparticles is one of the mechanisms contributing to the enhancement in thermal conductivity. Because the nanoparticles are in continuous motion in the fluid, they can transport heat to several points.

Hydrophilic Ag NPs synthesized via different route and dispersed in water with particle fractions varying from 7.45% to 1.86% give interestingly unusual results compared to hydrophobic fluids. Thermal conductivity of pure water indicates a slightly decrease with temperature; however the addition of nanoparticles does not result in enhancements in contrast to other base fluids. In this case, approximately 7% deterioration in thermal conductivity is obtained according to pure water data for a Ag NP fraction of 7.45%. The deterioration increases with particle concentration. As the particle concentrations increase, the thermal conductivities decrease. The trend of this deterioration will be explained in the next section in more detail.

Figure 8.21. Thermal Conductivity Enhancement of Ag NPs

Dispersed in Water

Figure 8.22. Thermal Conductivity Enhancement of Ag NPs

Dispersed in Hexane

Figure 8.23. Thermal Conductivity Enhancement of Ag NPs

Dispersed in Heptane

The experimental thermal conductivity results are also presented in relative effective thermal conductivity form, representing the ratio of effective thermal conductivities of the nanofluid with respect to the base fluid at the same temperature and particle fraction. The effect of base fluid, as previously mentioned, can be better observed through the Figure 8.24. Comparing the experimental results for hydrophobic silver nanofluids, silver/hexane sample indicates the highest enhancement although the two solvents are quite similar.
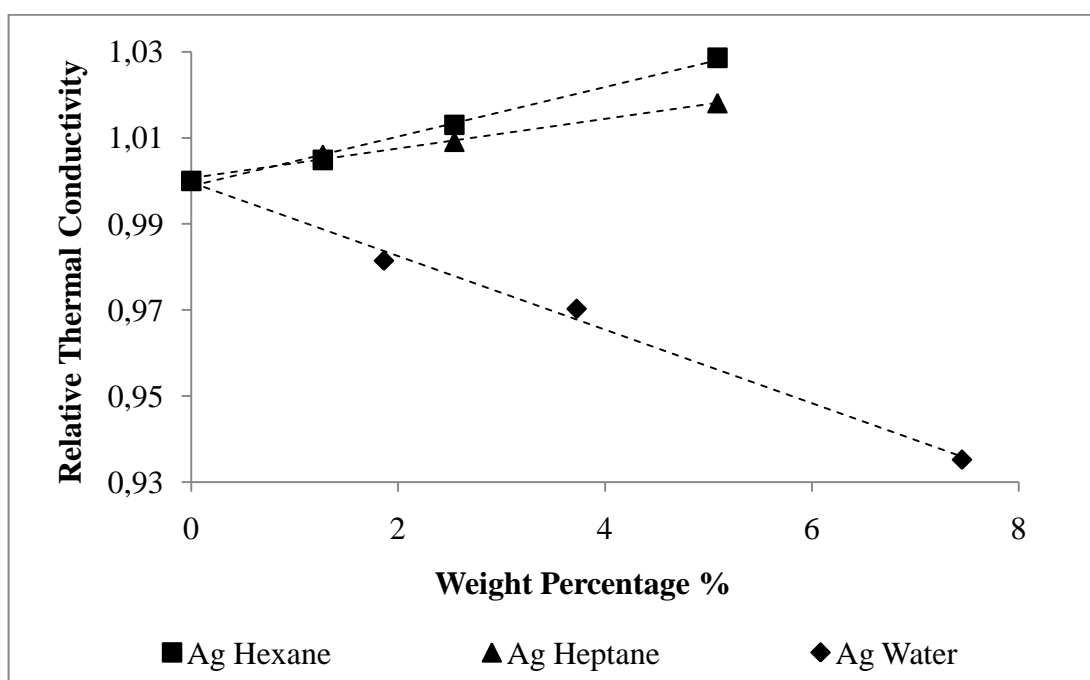
Figure 8.24. Relative Thermal Conductivities of Various Silver Nanofluids
at Constant Temperature

8.3.2. Thermal Conductivity Measurement of Magnetite Nanofluids

For the synthesized magnetite nanoparticles dispersed in base fluids water, hexane and heptane, several measurements are performed over a temperature range covering 25 to 55°C.

As in the case of hydrophobic silver nanofluids, the effective thermal conductivity increases with nanoparticle fraction according to Figures 8.25 and 8.26. In the particular case for magnetite/hexane nanofluids, for particle weight fractions of 1.8 and 0.9%, approximately 2.18% and 1.43% increase in thermal conductivity are observed respectively. For magnetite nanoparticles are dispersed in heptane, 4.80, 3.58 and 1.36 % thermal conductivity improvements are measured at the particle fractions of 7, 5 and 2 wt% respectively.

Hydrophilic Ag NPs synthesized via different route and dispersed in water with particle fractions varying from 5.98% to 1.495% give interestingly unusual results

compared to hydrophobic fluids as in the case of silver/water nanofluid. Thermal conductivity of pure water indicates a slightly decrease with temperature; however the addition of nanoparticles does not result in enhancements in contrast to other base fluids. In this case, approximately 34% deterioration in thermal conductivity is obtained according to pure water data for a Ag NP fraction of 5.98%. The deterioration follows through the particle concentrations. As the particle concentrations increase, the thermal conductivities decrease.
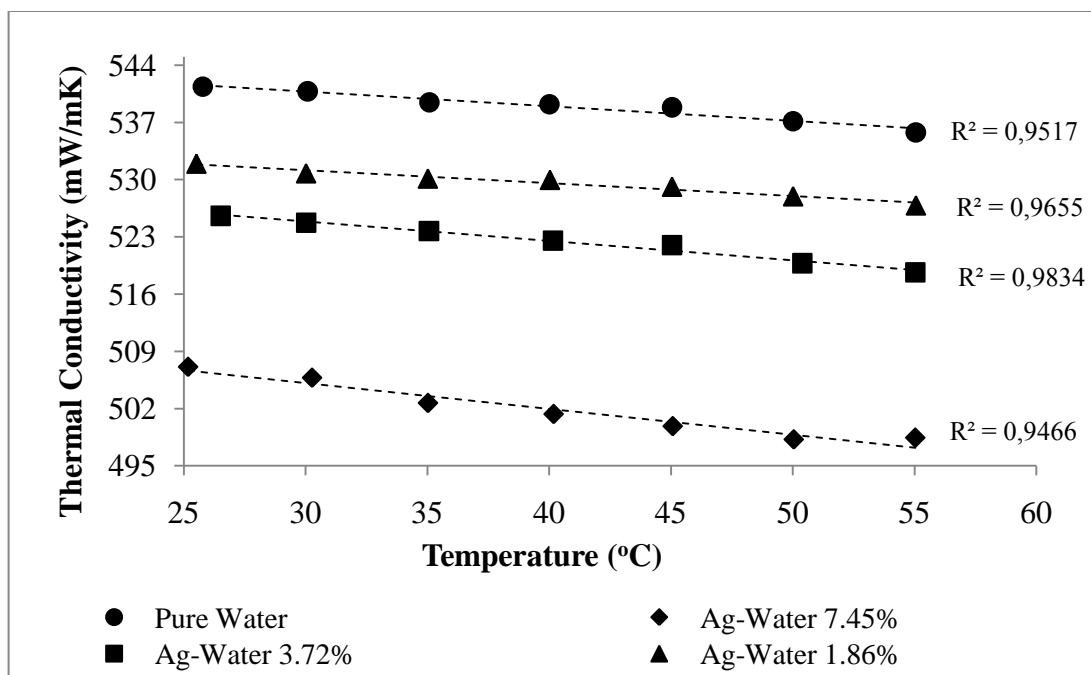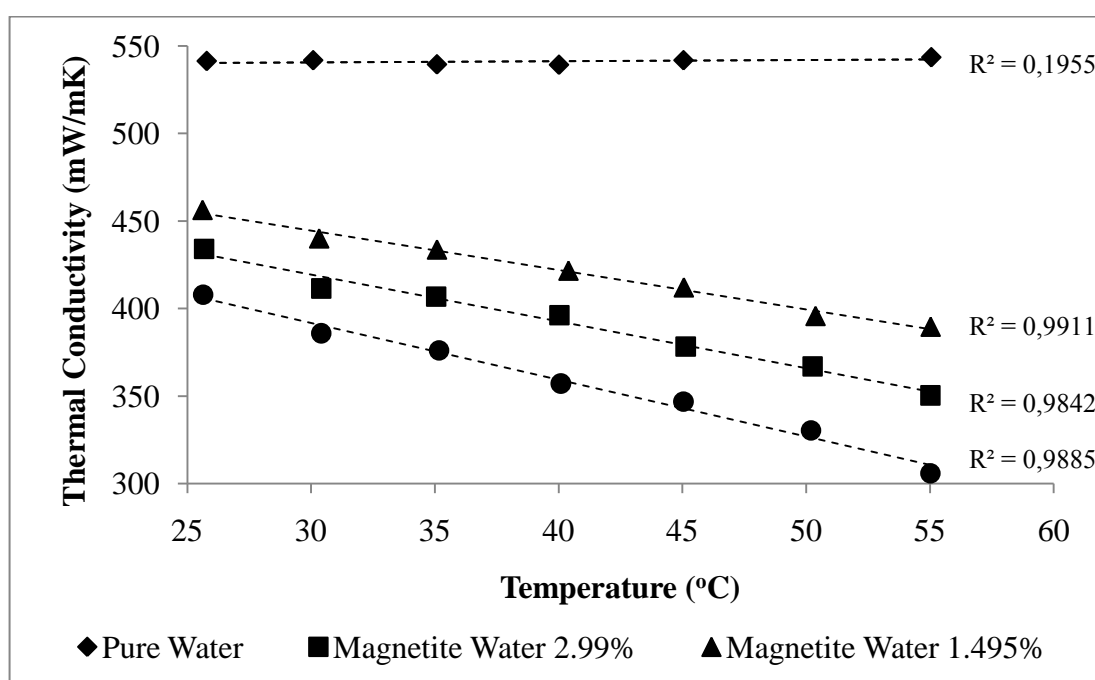

Figure 8.25. Thermal Conductivity Enhancement of Magnetite Nanoparticles Dispersed in Water
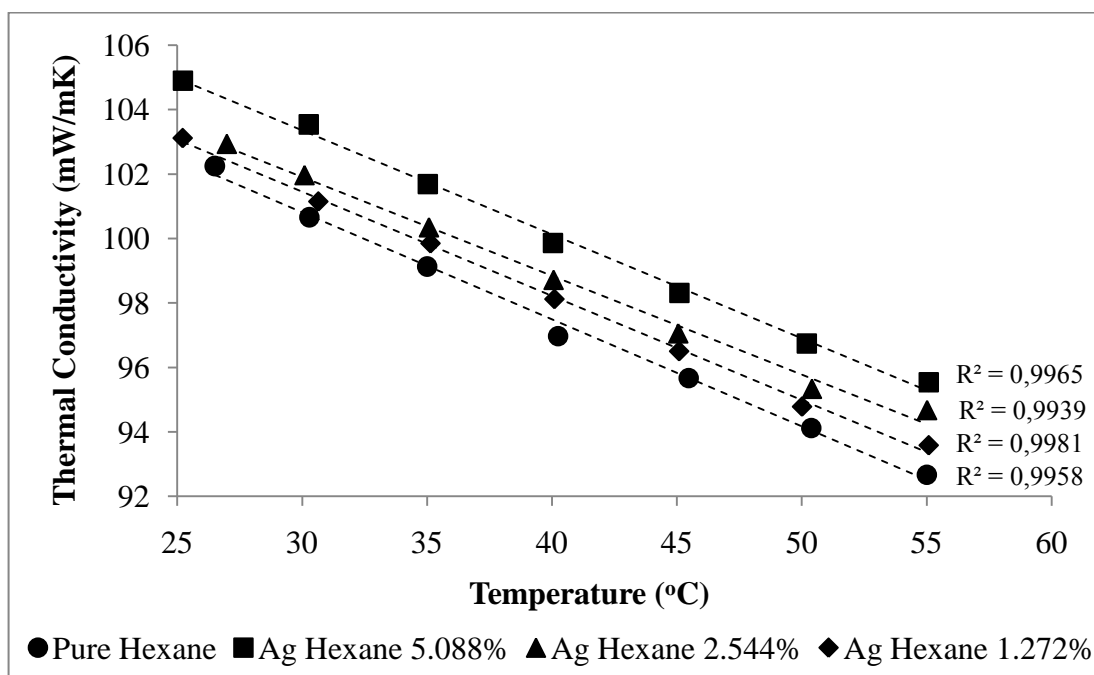
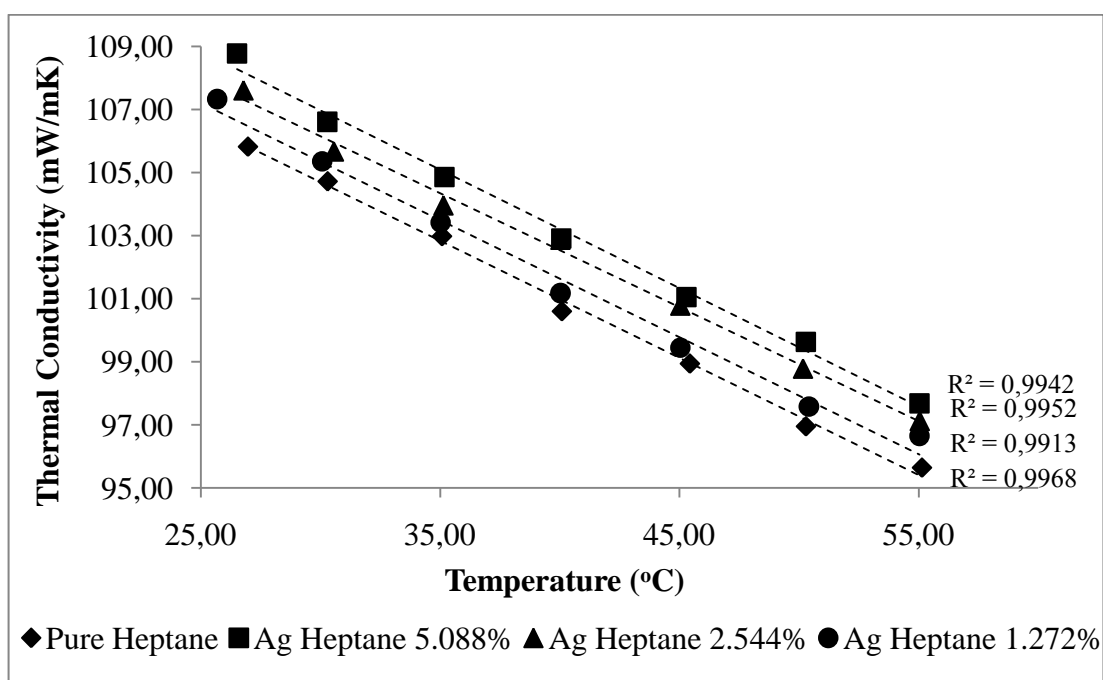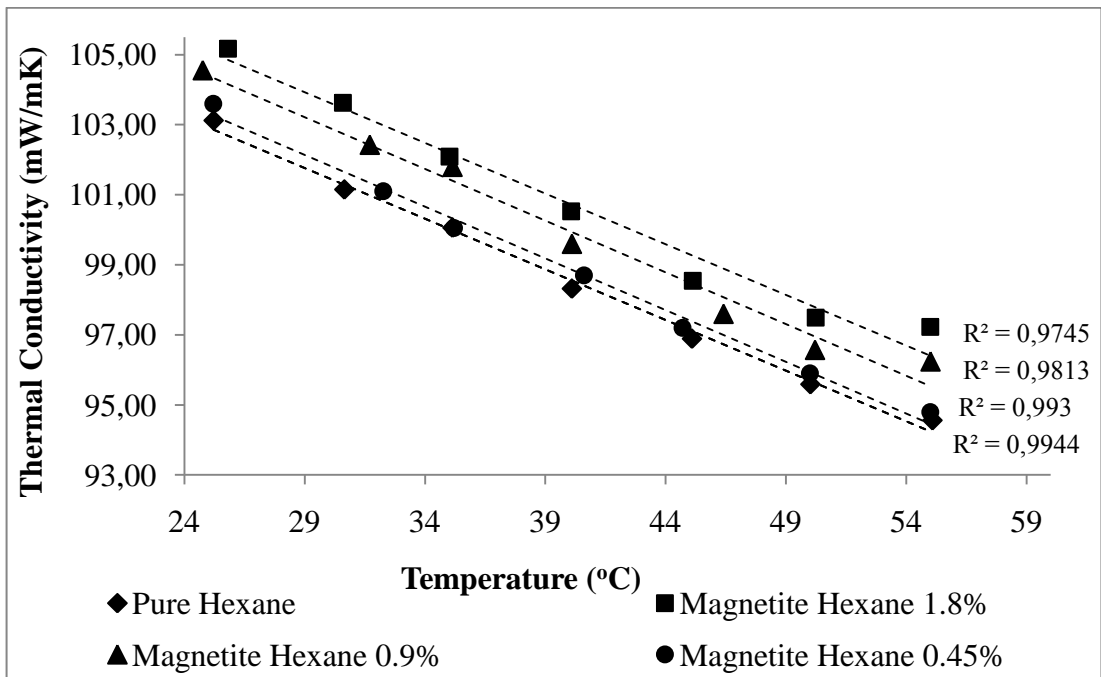Figure 8.26. Thermal Conductivity Enhancement of Magnetite Nanoparticles
Dispersed in Hexane
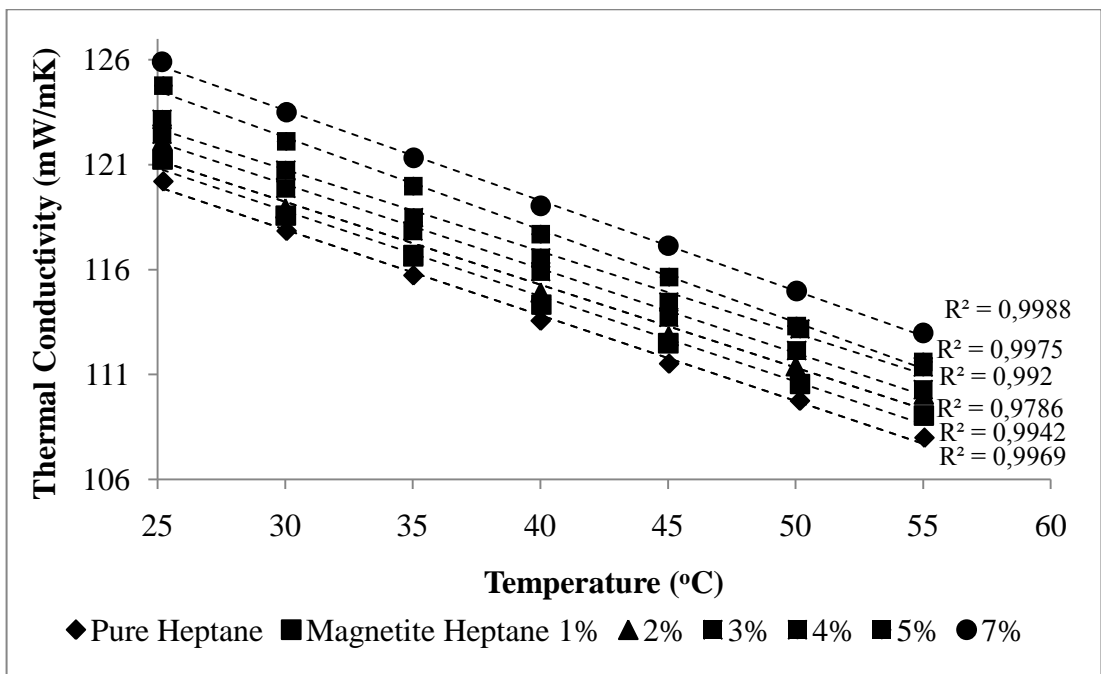
Figure 8.27. Thermal Conductivity Enhancement of Magnetite Nanoparticles
Dispersed in Heptane

The experimental thermal conductivity results are evaluated in terms of relative thermal conductivities in order to investigate the effect of base fluid in the Figure 8.28. Comparing the experimental results for hydrophobic magnetite nanofluids, magnetite/hexane sample indicates the highest enhancement. Magnetite/water nanofluid on the other hand represents a very high deterioration.
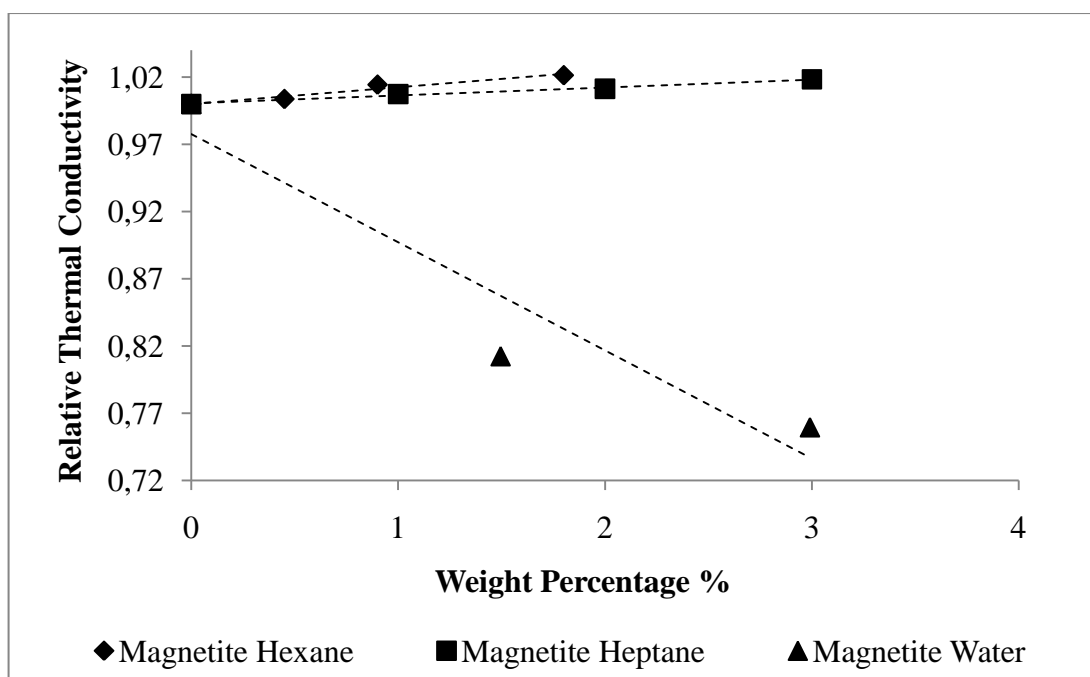
Figure 8.28. Relative Thermal Conductivities of Various Magnetic Nanofluids at Constant Temperature

The two synthesized types of nanoparticles are compared in terms of thermal conductivity enhancements. Comparing the slopes, magnetite/hexane nanofluid indicates the highest relative thermal conductivity among the other nanofluids. Hexane dispersed nanoparticles result in higher conductivities in contrast to heptane dispersed nanoparticles for magnetite and also for silver nanofluids. The reason is the thermal conductivity of base fluid itself. It is also stated in literature, that the thermal conductivity enhancement is lower for nanofluids where the thermal conductivity of the base fluid is higher. Hexane has a lower conductivity with respect to heptane, that's why the enhancements are higher in hexane nanofluids.
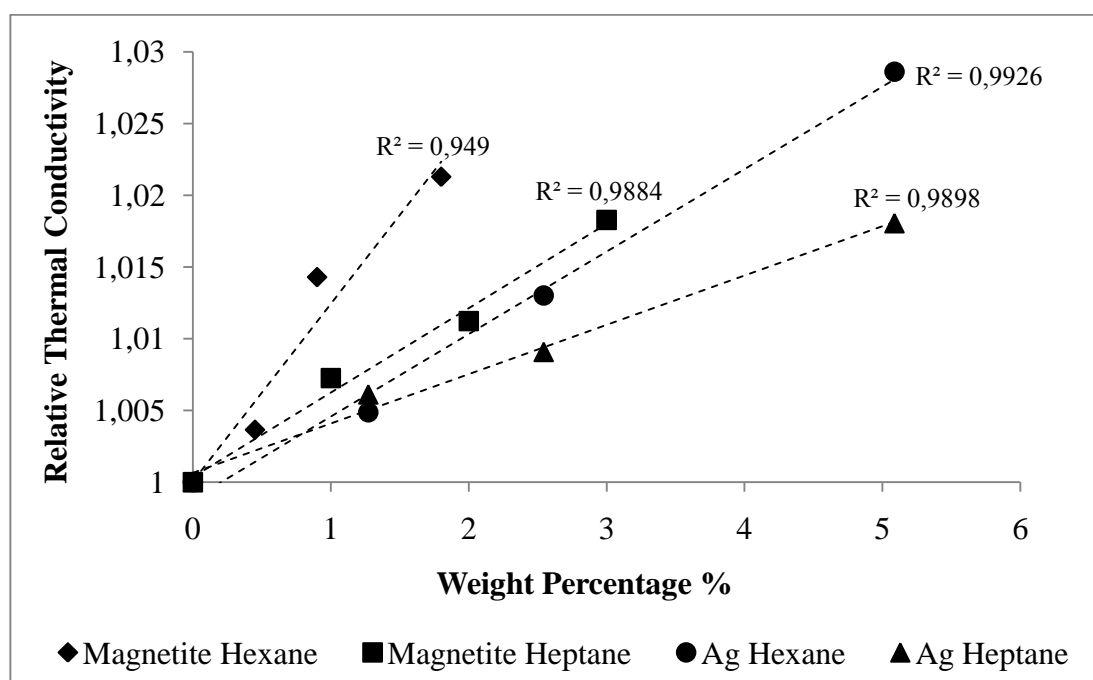
Figure 8.29. Comparison of Relative Thermal Conductivities of Various Hydrophobic Nanofluids

The deterioration in thermal conductivity for silver and magnetite nanoparticles dispersed in polar solvent water is attributed to several concepts. The main cause of this behavior can be the effect of viscosity. As previously stated in the viscosity measurement section, there is a high enhancement for silver/water nanofluid. The main reason is the presence and excess of stabilizing agent, gum arabic, which has a large size containing several sugar molecules. According to the synthesis route, namely Ag NPs are surrounded by gum arabic surfactant molecules to prevent the aggregation of nanoparticles.

As the size of the whole particle comprising surfactant and the nanoparticle is very large, the effect of conductivity through the liquid cannot be observed apparently. The large size of gum arabic molecules suppresses the thermal conductivity enhancement of nanofluids and results in decrease. However, in hydrophobic nanoparticle synthesis the hydrophobic surfactants oleic acid and/or oleylamine are aligned toward the hydrophobic solvent and as the surfactant sizes are not so big the thermal conductivity enhancements are more obvious. Moreover, according to Figure 8.30, as in the case of hydrophobic

nanofluids, magnetite containing nanofluid indicates more difference with respect to silver nanofluid.

Another concept to be determined in the deterioration of thermal conductivity is the presence of free surfactant molecules in the fluids. The tail groups of surfactants exposed to the mediums contain no charge and therefore electrostatic repulsion is not present in this case. However, charges on head groups of surfactant molecules cause repulsion and prevent collisions of nanoparticles resulting in deteriorated thermal conductivities. To study this assumption experimentally, free surfactant solutions in water were prepared and their thermal conductivities were measured. However, the conductivity results were surprisingly the same as that of pure water conductivity.

The last concept to be considered is concerned with the thermal conductivity measurement procedure. According to previous studies in literature, nanofluids containing electrically conducting particles are measured by transient hot wire method using Platinium wire which is coated by an insulating material such as Teflon. In our study, bare metal wire was used in the measurements which lead to ambiguous results in thermal conductivity. Some of the problems identified in the application of the ordinary transient hot-wire method to electrically conducting liquids are possible current flow through the liquid, resulting in measurement of heat generated in the wire and polarization of the wire surface.
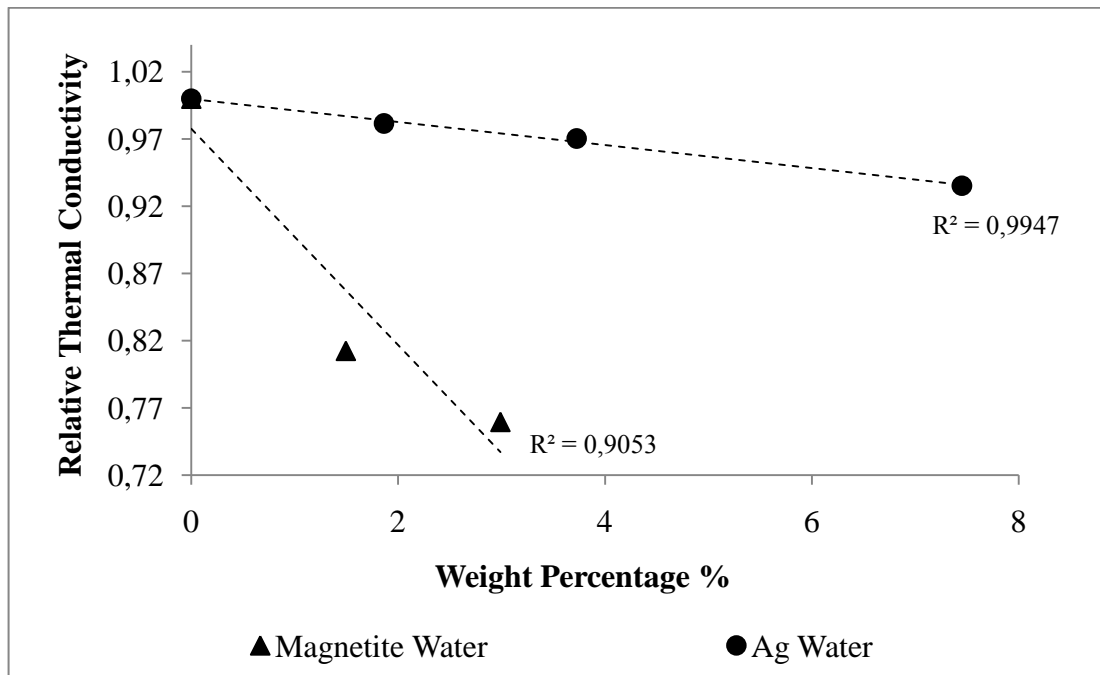
Figure 8.30. Comparison of Relative Thermal Conductivities of Various Hydrophilic Nanofluids

Generally, the need of explaining experimental data can be fulfilled by fitting them to existing theoretical models. From thermal conductivity experimental data it is already known that the thermal conductivity of nanofluids depends on several parameters including the thermal conductivity of base fluid, nanoparticle volume fraction and shape and temperature. Taking these parameters into consideration, the classical theory of thermal conductivity of fluids with suspended solid particles was developed by Maxwell assuming the nanoparticles to be spherical. However, the model is applicable for relatively large particles. A modified correlation is developed by Wasp indicating that the effective thermal conductivity of nanofluids relies on the thermal conductivity of the spherical particle, base fluid and the volume fraction shown in the Equation 8.1.

$$ \qquad\qquad\qquad $$ (8.1)

However, none of these correlations are currently reliable to predict the anomalous enhancement in thermal conductivity of nanofluids. To verify this, for silver and magnetite

nanoparticles dispersed in hexane and heptane the experimental data are compared with the Wasp model. According to Figure 8.31, the thermal conductivity results from Wasp model overestimate for the magnetite/heptane and hexane nanofluid.
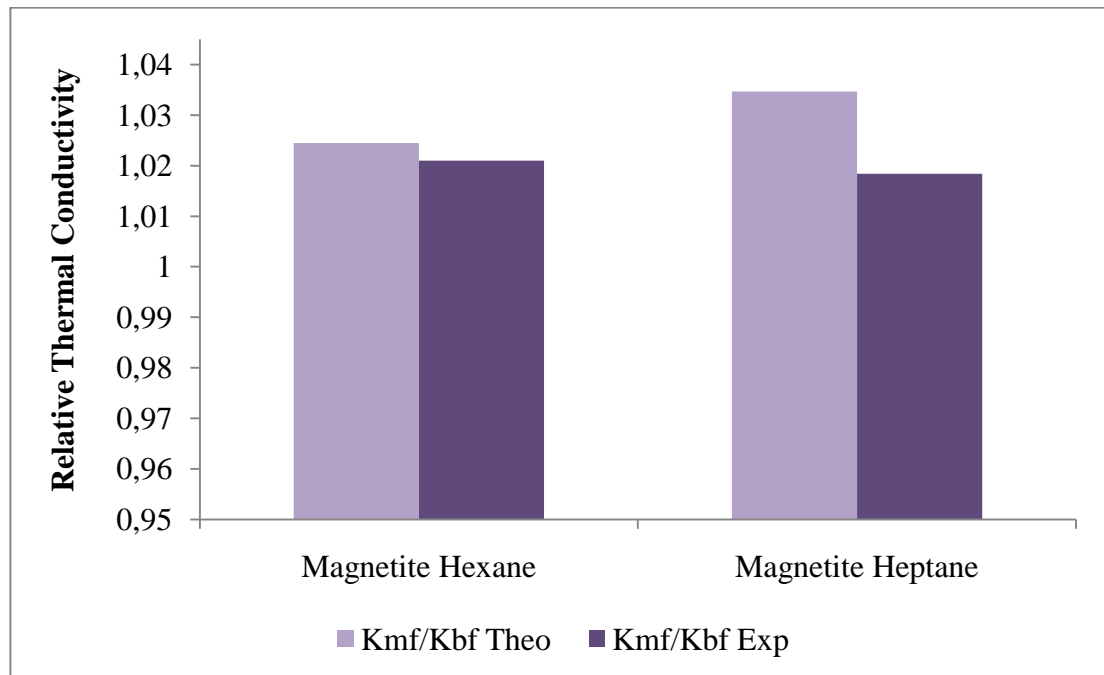
Figure 8.31. Comparison of Wasp model with Experimental Data
for Magnetite Nanofluids

According to Figure 8.32, the thermal conductivity results from Wasp model underestimate at both types of silver nanofluids hexane and heptane.
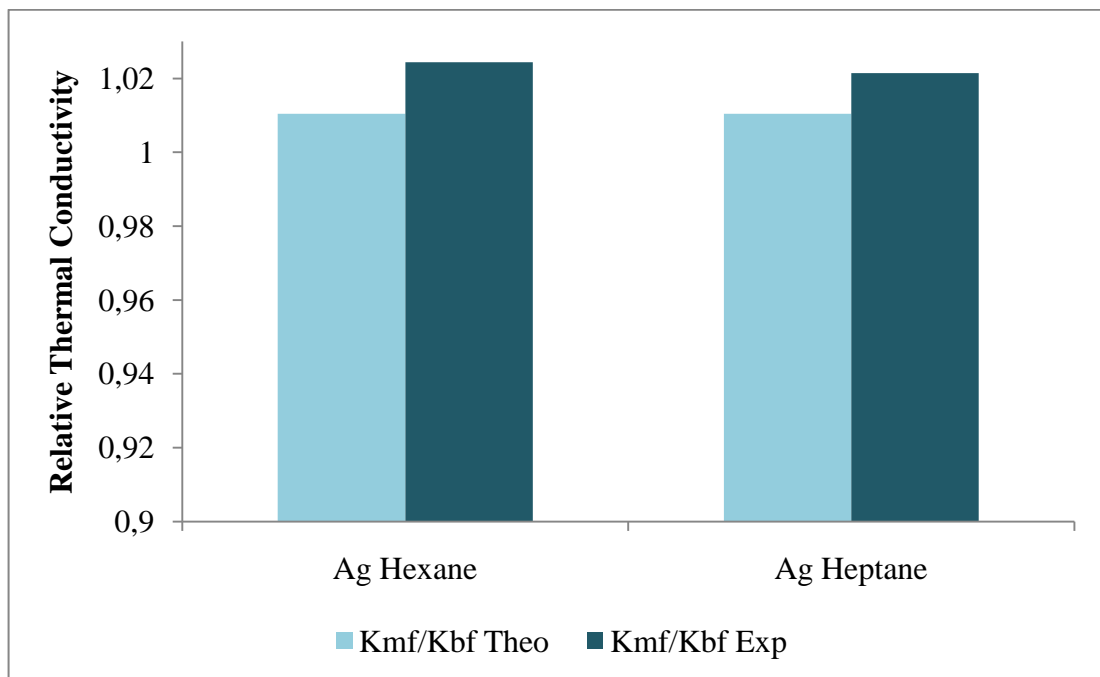
Figure 8.32. Comparison of Wasp model with Experimental Data
for Silver Nanofluids

9. CONCLUSIONS AND FUTURE WORK

The objective of this study is to demonstrate experimentally the mechanism of thermal conductivity enhancement of several fluids in the presence of silver and magnetite nanoparticles. As the traditional heat transfer fluids including water, engine oil and ethylene glycol fail to fulfill the requirements of industrial needs in terms of stability and flow properties, new kind of fluids are developed dispersing nanosized particles in these conventional fluids.

Dispersing these nanosized particles in conventional heat transfer fluids enhances the thermophysical properties to high extents. In order to obtain the most efficient results in heat transfer applications of these nanofluids, effective and successful synthesis methods should be applied. The synthesis methods and the surfactants surrounding the nanoparticles to prevent their aggregation and improve their stability must be selected very carefully.

In the present study, colloidal silver having the specific properties of high surface area and high electrical and thermal conductivity and in addition, magnetite nanoparticles with superparamagnetic properties were chosen to study the thermophysical property enhancements. Among the nanoparticle synthesis methods, mentioned in previous sections, the most applicable route is the chemical precipitation method. In this typical synthesis method used for magnetite and silver nanoparticles, metallic precursor molecules are reacted with several reducing agents in the presence of surfactants yielding stable nanoparticles. These synthesized particles are further dispersed in either polar or nonpolar solvents depending on their specific type.

These prepared nanofluids consisting of nanoparticles dispersed in base fluids represent interestingly different thermophysical properties with respect to that of the corresponding base fluids. In terms of density and viscosity, it was found that these properties are strongly temperature and particle concentration dependent. This behavior was investigated in more detail to understand mainly the effect of base fluid on the enhancement of thermophysical properties.

To achieve this, nanoparticles are dispersed in polar (water) and nonpolar (hexane and heptane) base fluids. According to experimental density and viscosity results, as the concentration increases, density and viscosity increases. However, at very low particle fractions this trend cannot be observed so apparently. From experimental data, silver and magnetite nanoparticles dispersed in hexane base fluid indicate the highest enhancements approximately for the same particle fractions. For viscosity, again the hexane nanofluids result in higher enhancements compared to other nanofluids.

Tabulated experimental data for density was also compared with the theoretical model proposed by Pak and Cho. The deviations between experimental and theoretical data were in acceptable ranges. The same procedure was applied also for viscosity analysis. Experimental data was matched with several models including Einstein, Brinkman and Lundgren. However, as the theoretical models are applicable only for very low particle fractions, the deviations were higher in viscosity.

Among the other thermophysical properties, thermal conductivity analysis is the most important part of this study. Transient hot wire method which eliminates the effects of natural convection was applied for measuring the thermal conductivities of several nanofluids. Like density and viscosity, thermal conductivity of nonpolar solvents such as hexane, heptane increases upon addition of nanoparticles. In other words, increasing particle concentration increases the thermal conductivity linearly dependent on the synthesized particle type and the base fluid. In contrast to that trend, dispersion of silver and magnetite nanoparticles in polar solvent, water in the case of this study represents an unexpected decrease in thermal conductivity. This deterioration of thermal conductivity of water can be attributed to the presence of free surfactants and the viscosities of nanofluids. Another reason is the measurement procedure of transient hot wire method and the use of uncoated Pt wire, which is not suitable for electrically conducting nanofluids. Therefore, this deterioration should be investigated in more detail in further studies. On the other hand, hydrophobic silver and magnetite nanoparticles dispersed in hexane result in the highest enhancement for thermal conductivity depending on the relative thermal conductivity analysis in this study. It can be concluded that the enhancement is higher in hexane based fluids than heptane due to the fact that the thermal conductivity of hexane base fluid itself is lower than heptane.

Except these parameters, the thermal conductivity enhancements of nanofluids are mainly affected by the particle size and clustering of the nanoparticles upon several studies in literature. Generally, thermal conductivities tend to increase with decreasing particle size. However, this effect cannot be observed in this study. As a future work, several nanoparticles should be synthesized having different particle sizes to observe the enhancement in thermophysical properties.

Experimental data of thermal conductivity for silver and magnetite nanofluids were compared with the theoretical model developed by Wasp as a modification for Maxwell model. However, these theoretical models fail to predict the thermal conductivities of nanofluids, as they do not consider the effect of particle size and nanolayer.

In this study, the aim to investigate the experimental thermophysical properties of hydrophobic and hydrophilic magnetite and silver nanofluids are fulfilled to some extent. Overall results indicate almost lower discrepancies with theoretical models however for polar solvents the results are quite distinctive from others therefore the analyses are not fully complete.

As a future work, the effect of magnetic field on thermal conductivity enhancement should be investigated for higher particle concentrations of magnetite nanofluids. The experimental setup should be arranged in a more convenient way to synthesize monodisperse and stable nanoparticles by controlling the reaction temperatures. Besides magnetite and silver, several nanoparticles can be synthesized at particle sizes covering small to very large size ranges in order to investigate the effect of particle size on the enhancement of thermophysical properties.

REFERENCES

1. Holman, J. P., *Heat Transfer*, 9th Edition, Mc Graw Hill, USA, 2002.

2. Geankoplis, C. J., *Transport Processes and Separation Process Principles,* 4th Editon, Pearson Education, New Jersey, 2003.

3. Çengel, Y. A., *Heat and Mass Transfer*, 3rd Edition, Mc-Graw Hill, Singapore, 2006.

4. Yu, W., D. M. France, J. L. Routbort and S.U.S. Choi, "Review and Comparison of Nanofluid Thermal Conductivity and Heat Transfer Enhancements", Heat Transfer Engineering, Vol. 29, No. 5, pp. 432-460, 2008.

5. The Engineering Toolbox, *The Thermal Conductivity of some common materials*, http://www.engineeringtoolbox.com/thermal-conductivity-d_429.html.

6. Lee, S., S.U.S. Choi, S. Li and J.A. Eastman, "Measuring Thermal Conductivity of Fluids Containing Oxide Nanoparticles", Journal of Heat Transfer, Vol. 121, pp. 280-289, 1999.

7. Chopkar, M., S. Kumar, D. R. Bhandari, P. K. Das and I. Manna, "Development and characterization of Al_2Cu and Ag_2Al nanoparticle dispersed water and ethylene glycol based nanofluid", Materials Science and Engineering: B, Vol. 139, Issues 2-3, pp. 141-148, 2007.

8. Choi, S. U. S. and J. A. Eastman, "Enhancing Thermal Conductivity of Fluids with Nanoparticles", ASME, New York, 1995.

9. Murshed, S. M. S., K. C. Leong and C. Yang, "Thermophysical and electrokinetic properties of nanofluids – A critical review", Applied Thermal Engineering, Vol. 28, pp. 2109 – 2125, 2008.

10. Van Hyning, D. L. And C. F. Zukoski, "Formation Mechanisms and Aggregation Behavior of Borohydride Reduced Silver Particles", Langmuir, Vol. 14, pp. 7034-7046, 1998.

11. Hwang, Y., H. S. Park, J. K. Lee and W. H. Jung, "Thermal conductivity and lubrication characteristics of nanofluids", Current Applied Physics, Vol. 6, Supplement 1, pp. e67-e71, 2006.

12. Chon, C. H. and K. D. Kihm, "Thermal conductivity enhancement of nanofluids by Brownian motion", Journal of Heat Transfer, Vol. 127, pp. 810, 2005.

13. Eastman, J. A., S. U. S. Choi, S. Li and L. J. Thompson, "Enhanced thermal conductivity through the development of nanofluids", Proceedings of the Symposium on Nanophase and Nanocomposite Materials II, Vol. 457, pp. 3-11, 1997.

14. Wang, B.-X., L.–P. Zhou and X.-F. Peng, "A fractal model for predicting the effective thermal conductivity of liquid with suspension of nanoparticles", International Journal of Heat and Mass Transfer, Vol. 46, pp. 2665-2672, 2003.

15. Patel, H. E., S. K. Das, T. Sundararajan, A. S. Nair, B. George, and T. Pradeep, "Thermal conductivities of naked and monolayer protected metal nanoparticle based nanofluids: Manifestation of anomalous enhancement and chemical effects", Applied Physics Letters, Vol. 83, pp. 2931-2933, 2003.

16. Zhu, H., C. Zhang, S. Liu, Y. Tang and Y. Yin, "Effects of nanoparticles clustering and alignment on thermal conductivities of Fe_3O_4 aqueous nanofluids", Applied Physics Letters, Vol. 89, pp. 023123-1-023123-3, 2006.

17. Mintsa, H. A., G. Roy, C. T. Nguyen and D. Doucet, "New temperature dependent thermal conductivity data for water-based nanofluids", International Journal of Thermal Sciences, Vol. 48, pp. 363-371, 2009.

18. Yang, B. and Z. H. Han "Temperature-dependent thermal conductivity of nanorod-based nanofluids", , Applied Physics Letters, Vol. 89, pp. 083111-1-083111-3, 2006.

19. Lu, An-Hui, E. L. Salabas and F. Schüth, "Magnetic Nanoparticles: Synthesis, Protection, Functionalization, and Application", Angewandte Chemie International Edition, Vol. 46, pp. 1222-1244, 2007.

20. Barron, A. R., *Introduction to Nanoparticle Synthesis*, USA, 2009.

21. Suneel, S. D., Nanotechnology, Schematic representation of the building up of Nanostructures, University of GITAM, India, http://www.gitam.edu/eresource/nano/NANOTECHNOLOGY/role_of_bottomup_and_topdown_a.htm, 2010.

22. Spinelnews, High Energy Ball Milling for Nanoparticle Synthesis, http://nanospinel.blogspot.com/2007/09/high-energy-ball-milling-for.html, 2007.

23. Holister, P., J-W. Weener, C. R. Vas and T. Harper, Nanoparticles, Cientifica, http://images.iop.org/dl/nano/wp/nanoparticles_WP.pdf, 2003.

24. Dahl, J. A., B. L. S. Maddux and J. E. Hutchison, "Toward Greener Synthesis", Chem. Rev., Vol. 107, pp. 2228-2269, 2007.

25. Li, L. And Ying-Jie Zhu, "High chemical reactivity of silver nanoparticles toward hydrochloric acid", Journal of Colloid and Interface Science, Vol. 303, pp. 415-418, 2006.

26. Song, K. C., S. M. Lee, T. S. Park, and B. S. Lee, "Preparation of colloidal silver nanoparticles by chemical reduction method", Korean Journal of Chemical Engineering, Vol. 26, No. 1, pp. 153-155, 2009.

27. Hiramatsu, H. and F. Osterloh, "A Simple Large Scale Synthesis of Nearly Monodisperse Gold and Silver Nanoparticles with Adjustable Sizes and with Exchangeable Surfactants", Chemistry of Materials, Vol. 16, No. 13, 2004.

28. Hu, Y., J. Ge, D. Lim, T. Zhan and Y. Yin, "Size-controlled synthesis of highly water-soluble silver nanocrystals", Journal of Solid State Chemistry, Vol. 181, pp. 1524-1529, 2008.

29. Yin, Y., Z. Li, Z. Zhong, B. Gates, Y. Xia and S. Venkateswaran, "Synthesis and characterization of stable aqueous dispersions of silver nanoparticles through the Tollens process", Journal of Materials Chemistry, Vol. 12, pp. 522-527, 2002.

30. Songping, W. and M. Shuyuan, "Preparation of ultrafine silver powder using ascorbic acid as reducing agent and its application in MLCI", Materials Chemistry and Physics, Vol. 89, Issues 2-3, pp.423-427, 2005.

31. Alvarez-Puebla, R. A. and R. F. Aroca, "Synthesis of Silver Nanoparticles with Controllable Surface Charge and Their Application to Surface-Enhanced Raman Scattering", Analytical Chemistry, Vol. 81, No. 6, pp. 2280-2285, 2009.

32. Dong, X., X. Ji and H. Wu, "Shape Control of Silver Nanoparticles by Stepwise Citrate Reduction", The Journal of Physical Chemistry C, Vol. 113, No. 16, pp. 6573-6576, 2009.

33. Lee, P. C. and D. Meisel, "Adsorption and Surface-Enhanced Raman of Dyes on Silver and Gold Sols", The Journal of Physical Chemistry, Vol. 86, pp. 3391-3395, 1982.

34. AL-Thabaiti, S.A., F.M. Al-Nowaiser and A.Y.Obaid, "Formation and characterization of surfactant stabilized silver nanoparticles: A kinetic study", Colloids and Surfaces B:Biointerfaces, Vol. 67, Issue 2, pp. 230-237, 2008.

35. Medina-Ramirez, I., S. Bashir, Z. Luo and J. L. Liu, "Green Synthesis and characterization of polymer-stabilized silver nanoparticles", Colloids and Surfaces B:Biointerfaces, Vol. 73, pp. 185-191, 2009.

36. Pillai, Z. S. and P. V. Kamat, "What Factors Control the Size and Shape of Silver Nanoparticles in the Citrate Ion Reduction Method?", Journal of Physical Chemistry B, Vol. 108, No. 3, pp. 945-951, 2004.

37. Wu, W., Q. He and C. Jiang, "Magnetic Ironoxide Nanoparticles: Synthesis and Surface Functionalization Strategies", Nanoscale Res Lett 3, pp. 397-415, 2008.

38. Encyclopedia of Science, Ferromagnetism, http://www.daviddarling.info/encyclopedia/F/ferromagnetism.html, 2009.

39. Nave, C. L., "Magnetic Properties of Solids", HyperPhysics, http://hyperphysics.phy-astr.gsu.edu/Hbase/tables/magprop.html, 2008.

40. Meyers, H. P., *Introductory solid state physics*, 2nd Edition, Taylor and Francis, 1997.

41. TerritorioScuola, Magnetic Nanoparticle Figure under applied magnetic field representation,http://www.territorioscuola.com/youtube/index.php?key=Ferrofluido &page=2.

42. Sun, S. and H. Zeng, "Size Controlled Synthesis of Magnetite Nanoparticles", Journal of American Chemical Society, Vol. 124, No. 28, pp. 8204-8205, 2002.

43. Hyeon, T., S. S. Lee, J. Park, Y. Chung and H. B. Na, "Synthesis of Highly Crystalline and Monodisperse Maghemite Nanocrystallştes without a Size-Selection Process", Journal of American Chemical Society, Vol. 123, pp. 12798-12801, 2001.

44. Vidal, J., J. Rivas and M. A. Lopez-Quintela, "Synthesis of monodisperse maghemite nanoparticles by the microemulsion method", Colloids and Surfaces A: Physicochemical Eng. Aspects, Vol. 288, pp. 44-51, 2006.

45. Chin, A. B. and I. I. Yaacob, "Synthesis and characterization of magnetic iron ozide and nanoparticles via w/o microemulsion and Massart's procedure, Journal of Materials Processing Technology, Vol. 191, pp. 235-237, 2007.

46. Wang, J., J. Sun, Q. Sun and Q. Chen, "One-step hydrothermal process to prepare highly crystalline Fe_3O_4 nanoparticles with improved magnetic properties", Materials Research Bulletin, Vol. 38, Issue 7, pp. 1113-1118, 2003.

47. Zheng, Y., Y. Cheng, F. Bao and Y. Wang, "Synthesis and magnetic properties of Fe_3O_4 nanoparticles", Materials Research Bulletin, Vol. 41, Issue 3, pp. 525-529, 2006.

48. Daou, T. J., G. Pourroy, S. Be´gin-Colin, J. M. Grene´che, C. Ulhaq-Bouillet and P. Legare´ et al., "Hydrothermal Synthesis of Monodisperse Magnetite Nanoparticles", Chem. Mater., Vol. 18,pp. 4399-4404, 2006.

49. Vijayakumar, R., Y. Koltypin, I. Felner and A. Gedanken, "Sonochemical synthesis and characterization of pure nanometer-sized Fe_3O_4 particles", Materials Science and Engineering A, Vol. 286, 2000.

50. Suslick, K. S., M. Fang, and T. Hyeon, "Sonochemical Synthesis of Iron Colloids", Journal of the American Chemical Society, Vol. 118, No. 47, pp. 11960-11961, 1996.

51. Pinkas, J., V. Reichlova, R. Zboril, Z. Moravec, P. Bezdicka and J. Matejkova, "Sonochemical synthesis of amorphous nanoscopic iron(III)oxide from $Fe(acac)_3$", Ultrasonics Sonochemistry, Vol. 15, pp. 257-264, 2008.

52. Day, M. M. And A. Carpi, "Density", Visionlearning, Vol. 1, http://www.visionlearning.com/library/module_viewer.php?mid=37, 2002.

53. Brookfield DV-III Ultra Rheometer for measuring viscosity and yield stress, http://www.brookfieldengineering.com/download/files/DV3Bro.pdf, 2007.

54. Masuda, H., A. Ebata, K. Teramae and N. Hishinuma, "Alteration of thermal conductivity and viscosity of liquid by dispersing ultra-fine particles", Netsu Bussei (Japan), Vol. 4, pp. 227-233, 1993.

55. Wang, X., X. Xu, S. U. S. Choi, "Thermal conductivity of nanoparticle-fluid mixture", Journal of Thermophysics and Heat Transfer, Vol. 13, pp. 474-480, 1999.

56. Ding, Y., H. Alias, D. Wen and A. R. Williams, "Heat transfer of aqueous suspensions of carbon nanotubes (CNT nanofluids)", International Journal of Heat and Mass Transfer, Vol. 49, pp. 240-250, 2006.

57. Kang, H. U., S. H. Kim and J. M. Oh, "Estimation of Thermal Conductivity of Nanofluid Using Experimental Effective Particle Volume", Experimental Heat Transfer, Vol. 19, pp. 181-191, 2006.

58. Kostic, M. and K. C. Simham, "Computerize, Transient Hot-Wire Thermal Conductivity (HWTC) Apparatus for Nanofluids", Proceedings of the 6th WSEAS International Conference on HEAT and MASS TRANSFER (HMT'09), http://www.kostic.niu.edu/WSEAS-HMT09-Paper10.pdf, 2009.

59. Hunter, R., *Introduction to Modern Colloid Science*, Oxford Science Publications, 2003.

60. Sartor, M., "Dynamic Light Scattering", University of California San Diego (UCSD),

http://physics.ucsd.edu/neurophysics/courses/physics_173_273/dynamic_light_scattering_03.pdf, 2006.

61. Malvern, "Dynamic Lights Scattering (DLS)"Zetasizer Nano Series, Mano317 User Manual, Issue 5, 2009.

62. Malvern, "Material Characterization- Dynamic Lights Scattering (DLS)", http://www.malvern.com/LabEng/technology/dynamic_light_scattering/dynamic_light_scattering.htm, 2009.

63. University of Nebraska-Lincoln, "TEM and SEM Electron Microscopy", http://www.unl.edu/CMRAcfem/em.htm, 2008.

64. Koninklijke Philips Electronics N. V., "Transmission Electron Microscopy", http://www.miplaza.com/materialsanalysis/projects/technicalnotessurfaceandthinfilm analysis/temtn.pdf, 2008.

65. The Official Web Site of the Nobel Prize, "The Transmission Electron Microscope", http://nobelprize.org/educational_games/physics/microscopes/tem/index.html, 2010.

66. FEI Company Tools for NanoTech, "Tecnai GF30 The benchmark for high performance nanoanalysis", http://www.nano.org.tr/files/tem/2007_07_TecnaiF2_30_ds.pdf, 2007.

67. Scintag Inc., "Basics of X-ray Diffraction", Chapter 7, http://epswww.unm.edu/xrd/xrdbasics.pdf, 1999.

68. Dinnebier, R. E. And S. J. L. Billinge, "Principles of Powder Diffraction", http://www.rsc.org/ebooks/archive/free/BK9780854042319/BK9780854042319-00001.pdf.

69. Dutrow, B. L. And C. M. Clark, "X-ray Powder Diffraction (XRD)", The Science Education Resource Center at Carleton College, http://serc.carleton.edu/research_education/geochemsheets/techniques/XRD.html.

70. Speakman, S. A., "Basics of X-Ray Diffraction Self-User Training for the X-Ray Diffraction SEF", http://prism.mit.edu/xray/BasicsofXRD.ppt#381.

71. Nelson, S. A., "X-Ray Crystallography", Tulane University, http://www.tulane.edu/~sanelson/eens211/x-ray.htm, 2010.

72. Magnetic Materials Chracterization techniques & instrumentation, "Magnetometers-Vibrating sample magnetometer (VSM)", http://www.nanomagnetics.org/instrumentation_and_characterization/VibratingSamp leMagnetometers_vsm.php.

73. SWT Physics Department, "Vibrating Sample Magnetometer", http://uweb.txstate.edu/~ab35/manuals/VSM/vsm.pdf, 2006.

74. William Reusch, *Visible & UV Spectroscopy*, Organic Chemistry On Line, 1999.

75. Stabinger, H., "Density Measurement using modern oscillating transducers", South Yorkshire Trading Standards Unit, 1994.

76. Anton Paar Unique Density and Concentration Meters, "DMA 4100 Product Specifications", http://www.uniontek.com.cn/images/antonapaar/%D7%CA%C1%CF-DMA-4100.pdf.

77. Anton Paar, "Operation Manual for Anton Paar DMA 4100", 2006.

78. Brookfield DV-III Ultra Programmable Rheometer Operating Instruction Manual, Brookfield Engineering Laboratories Inc., http://www.viscometers.org/PDF/Manuals/laboratory/DV-III%20Ultra.pdf.

79. PSL Systemtechnik, " Measuring of Thermal Conductivity with the Measuring System Lambda", http://www.psl-systemtechnik.de/thermal_conductivity.html?&L=1.

80. Enzel, P., N. Adelman, K. J. Beckman, D. J. Campbell, A. B. Ellis and G. C. Lisensky, "Preparation of an Aqueous-Based Ferrofluid   ", Journal of Chemical Education, Vol. 76, No. 7, pp. 943-948, 1999.

81. De Cuyper, M. and S. J. H. Soenen, "Cationic Magnetoliposomes", Methods in Molecular Biology, Vol. 605, Chapter 6, http://www.springerlink.com/content/u87mt87829r46306/fulltext.pdf, 2010.

82. Sun, J., S. Zhou, P. Hou, Y. Yang, J. Weng, X. Li and M. Li, "Synthesis and characterization of biocompatible Fe_3O_4 nanoparticles", Wiley InterScience, 2006.

83. Virender, K. S., Ria A. Yngard, and Yekaterina Lin, "Silver Nanoparticles: Green synthesis and their antimicrobial activities", Advances in Colloid and Interface Science, Vol. 145, pp. 83-96, 2009.

84. Lisensky, G., "Synthesis of Silver Nanoparticles", Materials Research Science and Engineering Center, University of Wisconsin, http://www.mrsec.wisc.edu/Edetc/nanolab/silver/, 2008.

85. Solomon, S. D., M. Bahadory, A.V. Jeyarajasingam, S. A. Rutkowsky, C. Boritz, and L. Mulfinger, "Synthesis of Silver Nanoparticles", Journal of Chemical Education, Vol. 84, pp. 322-325, 2007.

86. Vajjha, R. S., D. K. Das and B. M. Mahagaonkar, "Density Measurement of different nanofluids and their comparison with theory", Petroleum Science and Technology, Vol. 27, pp. 612-624, 2009.